Gels of Swellable Crosslinked Polymer Colloids for Lead Removal from Water

A thesis submitted to the University of Manchester for the degree of

Doctor of Philosophy

in the Faculty of Science and Engineering

Submitted December 2019

Syazwani Binti Mohd Zaki

School of Materials
The University of Manchester

TABLE OF CONTENTS

LIST OF TABLES

LIST OF FIGURES

LIST OF ABBREVIATIONS

AA	Acrylic acid
AAM	Acrylamide
AFM	Atomic force microscopy
AMPS	2-Acrylamido-2-methylpropane sulfonic acid
APS	Ammonium persulfate
BE	Binding energy
BL-CEA	Blend 2-carboxyethyl acrylate
Cd	Cadmium
CEA	2-carboxyethyl acrylate
CNT	Carbon nanotubes
COOH	Carboxylic acid group
CTAB	Cetyl trimethylammonium bromide
CTS-PAA	Chitosan-poly(acrylic acid)
Cu	Copper
DLS	Dynamic light scattering
DLVO	Derjaguin, Landau, Verwey and Overbeek
DMF	Dimethyl formamide
DMSO	Dimethyl sulfoxide
DN	Double network
DX	Double crosslinked
EGDMA	Ethylene glycol dimethylacrylate
EPA	Environmental Protection Agency

Fe_3O_4	Iron oxide
FTIR	Fourier transform infrared spectroscopy
GBL	γ-Butyrolactone
GF	Gel fraction
GMA	Glycidyl methacrylate
GO	Graphene oxide
HCI	Hydrochloric acid
H_2SO_4	Sulphuric acid
H_2O_2	Hydrogen peroxide
ICP-AES	Inductively-coupled plasma atomic emission spectroscopy
KE	Kinetic energy
K_2MnO_4	Potassium manganate
$KMnO_4$	Potassium permanganate
MAA	Methacrylic acid
MBAA	N,N-methylenebisacrylamide
MGs	Microgels
MMA	Methyl methacrylate
MW-CNT	Multi-walled carbon nanotubes
N_2	Nitrogen
$NaNO_3$	Sodium nitrate
NaOH	Sodium hydroxide
NC	Nanocomposite
NGs	Nanogels
OD	Optical density
PAA	Polyacrylic acid

PAM	Polyacrylamide
$Pb(NO_3)_2$	Lead nitrate
Pb	Lead
PE	polyelectrolyte
RGO	Reduced graphene oxide
rpm	Rotations per minute
SDS	Sodium dodecyl sulfate
SEM	Scanning electron microscopy
SF	Sol fraction
TEM	Transmission electron microscopy
TEMED	N,N,N',N'-Tetramethylethylenediamine
T_g	Glass transition temperature
UV-Vis	Ultraviolet–visible spectroscopy
WHO	World Health Organisation
XPS	X-ray photoelectron spectroscopy

LIST OF SYMBOLS

A	Hamaker constant
C	Concentration
C_0	Initial concentration
C_e	Equilibrium concentration
d_{coll}	Particle diameter in collapsed state
d_{swoll}	Particle diameter in swollen state
D	Translational diffusion coefficient
e	Charge
E	Modulus or compression modulus
G	Shear modulus
G'	Storage modulus
G''	Loss modulus
$G(\tau)$	Correlation coefficient functions
F	Force
h	Height
H	Distance between particles
I	Scattered light intensity
K	Boltzmann constant
k_d	Rate coefficient for initiator dissociation
k_p	Propagation rate constant
kt	Rate coefficient of termination
n	Number of random links

N_A	Avogadro constant
N	Number of network chains
N_p	Number of polymer particles
q	Adsorption capacity
q_e	Equilibrium of adsorption capacity
Q	Volume swelling ratio
R	Gas constant
R_p	Rate of propagation
t	Time
T	Absolute temperature
v_0	Molar volume of the polymer
v_1	Molar volume of the solvent
V_A	Van der Waals attraction energy
V_C	Volume in collapsed state
v_e	Number of effectively elastic chains
v_1	Molar volume of solvent
V_R	Electrostatic repulsive energy
V_S	Steric energy
X	Number of crosslinks
z	Valence
α	Particles radius of two spherical
γ	Shear strain
δ	Phase angle
ε	Strain
ε_B	Strain at break

σ	Shear stress
λ	Wavelength
ω	Angular frequency
ζ	Zeta potential
Ψ_0	Surface potential
Ψ_s	Stern potential
Ψ_d	Diffuse layer potential
η	Viscosity of medium
ϕ	Polymer volume fraction
τ	Delay time of time interval
π	Circular constant
χ	Flory-Huggins interaction parameter

THESIS ABSTRACT

In this thesis, a study of new pH-responsive double-crosslinked microgels/nanogels (DX MGs/ DX NGs) is conducted to investigate the properties and potential for lead (Pb) removal application. The first part of this study is about DX MGs from a new co-monomer, 2-carboxyethyl acrylate (CEA). An improvement in the ductility is desirable for biomaterials application. The ductility improvement of DX MGs with the presence of CEA was evident when compared to established DX MAA (MAA is methacrylic acid) gels (compressive breaking strain, 49.5%). The breaking strain obtained for DX CEA21 and DX CE28 gels were 58.24% and 62.3%. Mechanical properties are important parameter to evaluate the strength of these newly synthesised microgels (MGs) for specific application. Meanwhile, for a blend system (DX BL-CEA) the breaking strain obtained was 61.4%. Interestingly, the swelling behaviour of DX BL-CEA gel was in between that of DX CEA21 and DX CEA28. This behaviour shows that the swelling of the DX CEA gels can be tuned by blending of the two components.

The second part of the study is related to DX NG gels prepared using MAA. These MGs/NGs were synthesised by emulsion polymerisation. Thereafter, vinyl groups were introduced to the nanogels (NGs) through functionalisation with glycidyl methacrylate (GMA) by the reaction of carboxylic acid and epoxide group. The formation of DX NGs was obtained by free-radical polymerisation of vinyl groups on the surface of the NGs. The next part is associated with Graphene Oxide (GO) to prepare DX NGs composites with high modulus. Graphene oxide (GO) was exfoliated and well-integrated within the DX NG to produce DX NG/GO composite gels with outstanding mechanical properties. Given that only 0.2 wt.% of GO was present, the values of shear modulus showed remarkable enhancement for DX NG/GO (60.3 kPa)

compared with as-made gel, DX NG (10.2 kPa). From compression analysis, modulus values for DX NG/GO and DX NG are 82.4 kPa and 19.6 kPa, respectively.

Removal of Pb^{2+} from water by DX NG/GO hydrogels was investigated and the interaction between GO and NGs was studied. Adsorption isotherms were also constructed. Adsorption isotherms were measured to determine the maximum adsorption capacity of Pb^{2+} ions by the gels. The physical and mechanical properties of DX NG and DX NG/GO with and without Pb^{2+} were comprehensively studied to understand the effects of Pb as an additional crosslinker in the network structure of NGs. The effects of contact time and initial concentration of Pb^{2+} were explored. The maximum adsorption capacity obtained for DX NG/GO and DX NG were 254 ±15 mg/g and 204 ±17 mg/g. The GO role in capturing more Pb^{2+} ions was confirmed by XPS analysis. The effect Pb^{2+} uptake on the mechanical properties of the DX NG/GO and DX NG gels was investigated. The compression modulus values obtained for DX NG and DX NG/GO after 1000 ppm Pb uptake are 247 kPa and 336 kPa. For the breaking stress, the values obtained for DX NG and DX NG/GO after Pb uptake are 1045 kPa and 1273 kPa. These values are much higher than the as-made gels before Pb adsorption takes place. It is proposed that the network structure contained additional ionic crosslinker due to Pb^{2+} ions. The gels have good potential for Pb removal from wastewater. In this work, the main focus of removal is on Pb^{2+}.

DECLARATION

I declare that no portion of the work referred to in the thesis has been submitted in support of an application for another degree or qualification of this or any other university or other institute of learning.

Syazwani Binti Mohd Zaki

COPYRIGHT STATEMENT

ACKNOWLEDGEMENTS

Primarily, I would like to express my gratitude to The University of Manchester particularly the School of Materials for offering an opportunity and providing a comprehensive and conductive research environment with excellent facilities to complete my research project. I would like to acknowledge International Islamic University Malaysia (IIUM) and Ministry of Higher Education Malaysia (MOHE) for the scholarship and stipends.

There are many people earned my gratitude for their contribution on the completion of this PhD thesis Firstly, I am forever indebted to my PhD supervisor, Professor Brian Saunders. Thank you for the continuous support of my PhD study, for his patience, motivation, and immense knowledge. His guidance really helped me in the research and thesis writing. Professor Brian Saunders also continuously provided insightful discussions about research.

On top of that, special thank goes to all academic and technical staffs of School of Materials of University of Manchester for their advices and assistance in helping me in handling research facilities and analysing my samples. I also would like to express my appreciation to the technical staff from School of Earth and Environmental Sciences, Mr. Paul Lythgoe for being so supportive in helping me for ICP analysis. Same goes to Dr Nigel Hodson from Medical School and Dr Ben Spencer (XPS Research Officer) for helping me in analysing my samples. To my colleagues, Dr Amir, Dr. Nam, Dr. Hasif, Dr. Sharan, Dr. Cui, Dr. Melody Obeng, Dr. Wenkai Wang, Dr. Mu Chen, Rosie, James, Wayne, Dong, Hannah, Qing and Shanglin, thank you for the support and I gained a lot of from them. I feel so grateful for knowing all of you as my friend.

Special dedication goes to my dearest husband, Mohd Ridzwan and my beloved children, Wafiy Auzaie and Ayra Insyirah. Their courage, love, sacrifice and comforting efforts will always be remembered, fondly in good times and as encouragement in hard times. My warm gratitude also goes to my beloved parents and siblings for the support and prayer. Thank you to all my friends for their support throughout these years. Last but not least, I would like to extend my gratitude to everyone whom may have contributed in one way or another to make this thesis a reality, things that you do for me do not go unnoticed. Thank you.

CHAPTER 1 : INTRODUCTION

1.1 Motivation

Due to the industrial and economic growth, the production of a variety of compounds and chemicals also results of production of pollutants, many of which cause serious problems and risks for the environment and human health[1]. The serious threat of heavy metal ions such as cadmium (Cd), lead (Pb), nickel (Ni), and zinc (Zn) to the environment is of special concern worldwide. Heavy metals are considered as one of the most serious environmental problems and they are different based on their atomic weight, density and toxicity[2]. This heavy metal ions adversely affect the environment and living organisms[3]. Unlike organic wastes, heavy metals ions can be accumulated in the environment and living tissues, causing various diseases and disorders of living organisms even at a trace level[4]. Exposure to heavy metals has long-time effects on human well-being. Wastewater from electronic device manufacture, plating facilities and the production of electricity in nuclear power plants may contain considerable amounts of toxic and polluting heavy metals[5]. Among heavy metals, Pb has been given particular concern due to its highly toxic substance which lead to Pb poisoning. This Pb poisoning can cause serious ailment to human being especially in central nervous system and the gastrointestinal tract[6-7]. In fact, low levels (less than 0.1 ppm) of Pb exposure to young children specifically under the age of six can result in learning disabilities, attention deficit disorders, behavioural problems and kidney damage[8] (these can cause permanent adverse effects, particular affecting development of brain and nervous systems). Pb-based products have significantly increased ever since industrial revolution[9]. Pb has many different industrial, agricultural and domestic applications. It is currently used in the production of Pb acid batteries, ammunitions, metal products such as solder and pipes, and devices to shield X-rays[10].

An estimated 1.52 million metric tons of Pb were used for various industrial applications in the US in 2004. From that amount, Pb acid batteries production accounted for 83 percent, and the remaining contributed by various products such as ammunitions, oxides for paint, glass, pigments and chemicals, and sheet lead[2].

The removal of heavy metal ions from wastewater can be performed by physical and chemical methods such as adsorption, chemical precipitation, membrane ultrafiltration, chromatographic extraction, ion exchange and electrochemical techniques. However, adsorption emerged as the most cost-effective method to remove heavy metal ions compared with other existing methods and feasible in large scale production[8,11]. In the last several years, most studies have focused on the adsorption of heavy metal ions by various of traditional materials such as activated carbon[12], clay minerals[13-15], cellulose[16] and natural zeolites[17]. However, certain limitations exist to those materials such as tedious preparation, complex separation and poor-reusability[18-20]. Besides, another traditional synthetic adsorbent such as poly(sodium acrylate) and polyacrylamide have limitation such as poor bio-degradability[4]. Recently, composite hydrogels emerged as one of most effective ways in removing heavy metal ions due to its stability and improved mechanical properties. In general, a composite is obtained by combining two or more different materials. Ideally, the combined material is endowed with properties better to any of its components. An advantage of hydrogels is high-water content properties that permits more rapid ion penetration to combine with functional groups in the gels[21]. Composite hydrogels with incorporation of graphene have attracted tremendous attention among researchers due to this outstanding property. The versatility of graphene is associated to the properties that can be tuned to produce a broad new class of graphene-based materials.

1.2 Aims of thesis

There are three primary aims of this study. Firstly, to discover new MGs systems associated to lower glass transition temperature (T_g) monomer, 2-carboxyethyl acrylate (CEA). A primary concern is the consequences of CEA as co-monomer on the particle size as well as gel physical and mechanical properties. To date, there has been little discussion about CEA. Secondly, to synthesise NGs by emulsion polymerisation and to ascertain the effects of low loading GO in DX NG/GO in comparison to DX NG. The effect of GO on the physical and mechanical properties of the gels will be explored. Incorporation of GO as a filler is believed to improve Young's modulus and adsorption capacity of the gels for Pb^{2+} removal. Thirdly, the study seeks to investigate on Pb^{2+} removal by DX NG/GO and DX NG. The findings should make an important contribution to the field of adsorption of heavy metal ion by crosslinked gels. Another concern is the effects of Pb^{2+} uptake on the mechanical properties of the gels and to establish the mechanism for Pb^{2+} removal.

1.3 Survey of thesis

The research and development chapters are presented in three different chapters. The flow of this thesis started with literature review part that is presented in chapter 2. Chapter 2 begins by laying out the review on the background, fundamentals and theories related to this research work and was further discussed.

The third chapter is concerned with the newly synthesised MGs containing CEA. The MGs was synthesised by emulsion polymerisation method and following by vinyl functionalised step. The vinyl functionalised CEA MGs were used to prepare three doubly crosslinked MGs gels denoted as DX CEA21, DX CEA28 and a blend system that contained both CEA21 and CEA28. The mechanism of preparing the gels was summarised in Figure 1.1 and will be discussed in detail later.

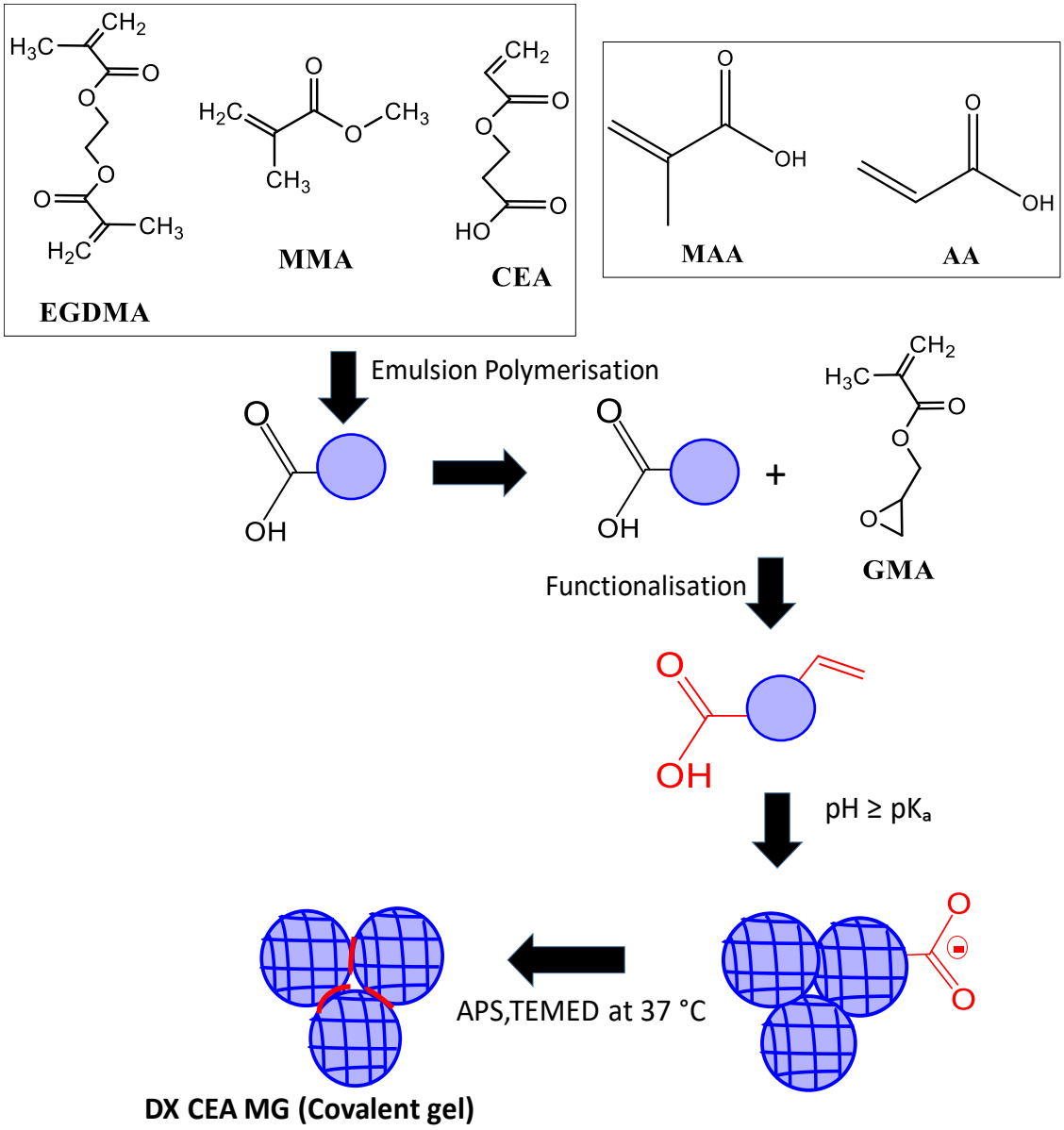

Figure 1.1: Schematic representation of the method used to prepare pH-responsive MGs and DX MGs. The particles were prepared by emulsion polymerisation. MGs were functionalised with GMA. The functionalised microgels was transformed to a physical gel (pH ≥ pK_a) and formed double-crosslinked gels in the presence of ammonium persulfate (APS) and *N*,*N*,*N*,*N*-tetramethylethylenediamine (TEMED) at 37°C. The structures of MAA and AA are shown for comparison.

Chapter 4 presents the findings and discussion on MAA-based NGs system that was prepared by emulsion polymerisation and followed by functionalisation with GMA as elaborated in Chapter 3. In this chapter, GO was prepared by Hummers method and incorporated into NGs to form DX gels. The covalent composite gel was formed by free-radical reaction in the

presence of initiator (APS) and TEMED. A comparison between DX NG/GO and DX NG is discussed. Figure 1.2 summarised the details of method used to prepare DX NG/GO.

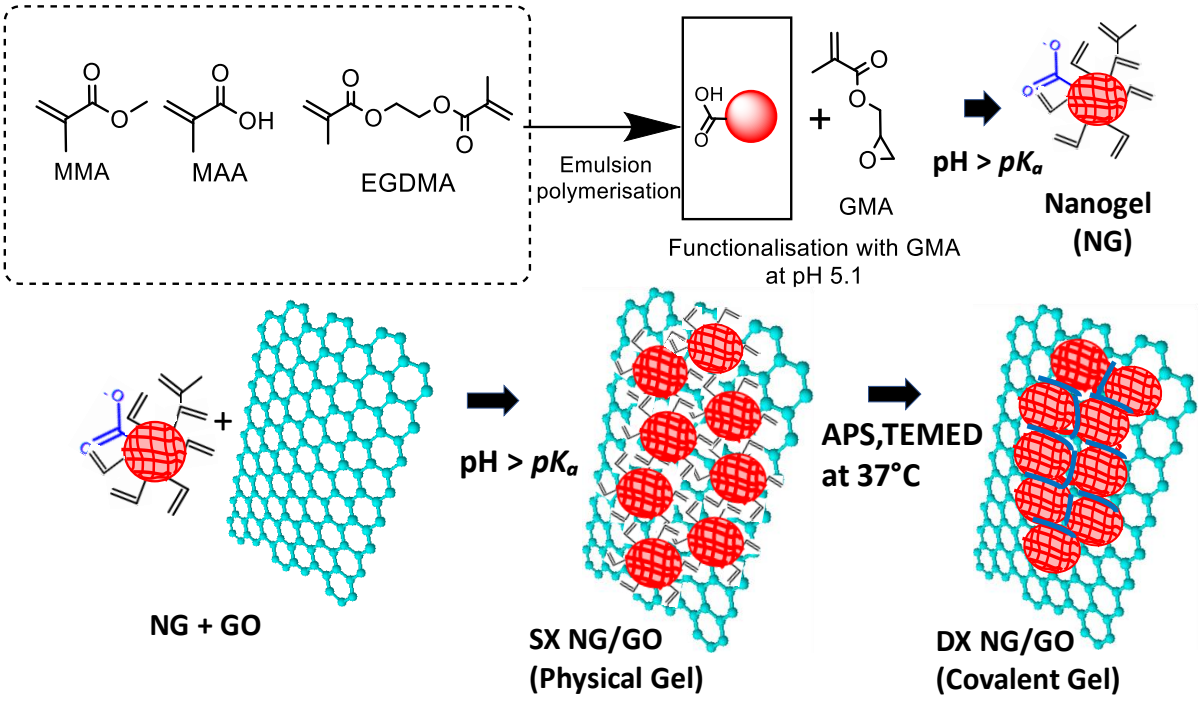

Figure 1.2: DX NG/GO composites were prepared using concentrated dispersions of vinyl-functionalised NG particles mixed with GO. The NGs underwent pH-triggered swelling at pH values greater than their pK_a to form a physical gel. The latter was transformed into covalent gel by free-radical coupling between surface vinyl groups of neighbouring NGs with ammonium persulfate (APS) and *N,N,N′,N′*-tetramethylethylenediamine (TEMED). The covalent linkages at the periphery of the NG particles are indicated in blue.

Chapter 5 analyses the findings associated to Pb^{2+} removal by DX NG and DX NG/GO gels. Adsorption experiments was conducted at various Pb^{2+} initial concentration. In this chapter, adsorption isotherm model for both systems were proposed. From this adsorption isotherm model, maximum adsorption capacity for Pb^{2+} was generated. Besides, this chapter also further discusses on the mechanical properties of DX NG and DX NG/GO after Pb adsorption. The mechanism of Pb^{2+} removal in Figure 1.3 was proposed and further discussed.

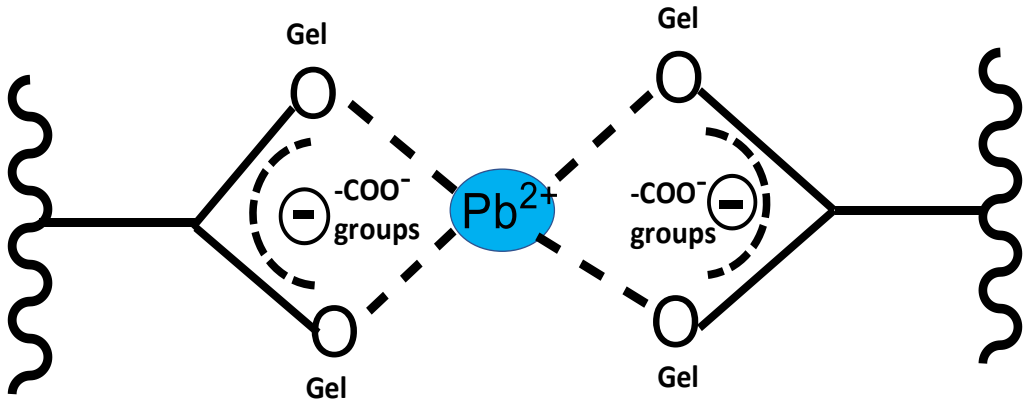

Figure 1.3: Proposed mechanism for Pb^{2+} adsorption by complexation between Pb^{2+} and $–COO^{–}$ groups.

The final chapter gives the brief summary of the conclusions and identified the areas for further research.

CHAPTER 2 : LITERATURE REVIEW

This chapter aims to explain to the reader about the background and theoretical understanding associated to pH-responsive MGs/NGs, DX NGs/MGs, DX gels with composite, graphene and heavy metal ions removal. This chapter will cover the background and theoretical aspects for Chapter 3 to 5.

2.1 Hydrogels

Hydrogels are important class of materials due to is three-dimensional network structure with ability to absorb large amount of water while maintaining their stability. Hydrogels can be divided into two categories, synthetic and natural hydrogels. Synthetic hydrogels contain hydrophilic network and shows better performance such as elevated mechanical strength[22]. Examples of excellent monomers to form synthetic hydrogel are acrylic acid (AA) and acrylamide (AM). Hydrogels are prepared by synthetic polymers using chemically polymerisation process. Hydrogels can be designed to exhibit architectures and property that responsive towards environment conditions such as pH, ionic strength, light, temperature, solvent or magnetic field[23]. The stimuli-responsive hydrogels hence can be used in various applications such water treatment, biomedical and sensor[24]. Several strategies have been explored to increase the response of the gel dynamics such as reducing gel size and producing a microporous gel structure to increase the contacting surface area between polymer and solvent[25]. Micro and nanosized hydrogels are faster in responding to environmentally triggered changes in swelling and molecules binding due to their higher interfacial area[26-27]. MGs and NGs will be further reviewed in the next subtopics.

2.2 Nanogels and microgels

A few different terms are used for MGs, including microsphere, microbead, nanogel, and mini gel for larger particles. NGs are crosslinked polymer colloids with a swollen diameter of between 20-100 nm[28]. The elastic moduli of microgels/nanogels is in the range of 0.1-100 kPa[29]. An increased in surface area for NGs has an advantage in necessitating the application of dispersion forces to maintain colloidal stability during their synthesis[27]. Besides, MGs and NGs are faster in responding to changes in the environment such as pH, ionic strength, electric field than their macroscopic or bulk counterparts[24,30]. Figure 2.1 shows the average size of pH responsive polymers with different structures[31].

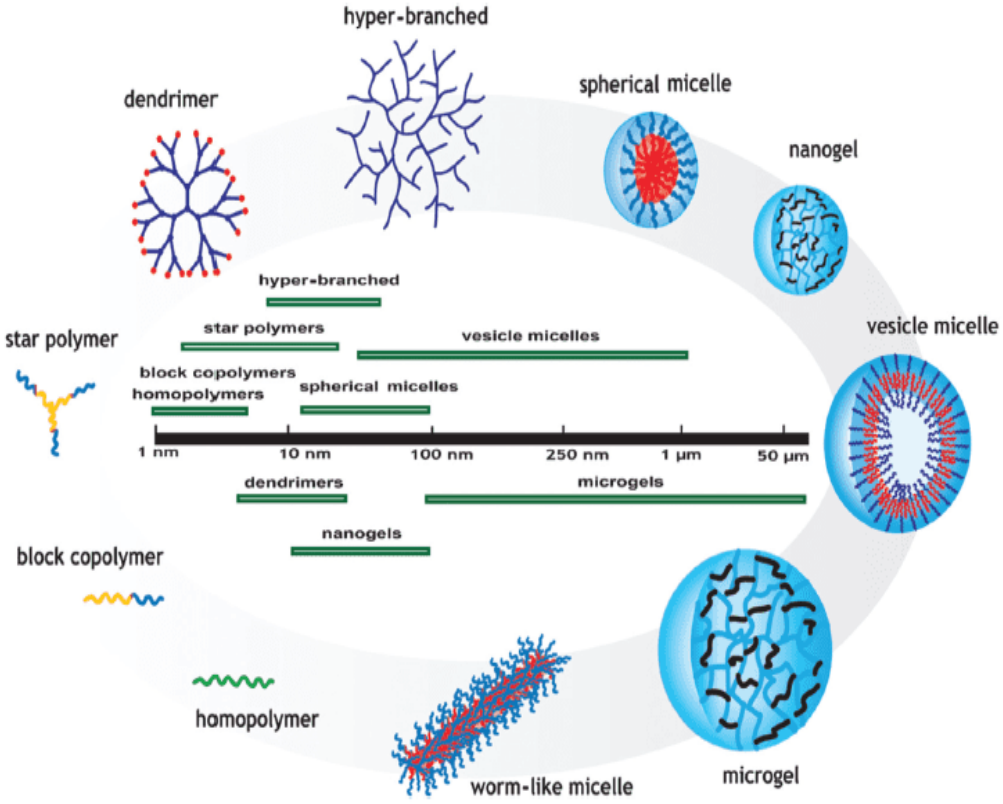

Figure 2.1: Average size of pH responsive polymers with different structures[31].

2.2.1 Chain and step polymerisation

There are two main types of polymerisation namely as chain polymerisation and step polymerisation. Chain polymerisation process involves low molar mass molecules of monomer with C=C double bond and reacts with a free-radical as discussed below. For step polymerisation, the process involved the reaction of pairs of functional groups on the monomers (bifunctional groups to link one molecule at one time) and is not discussed further because it is not used in this study.

2.2.2 Free-radical polymerisation

Free radical polymerisation is a chain type polymerisation. A monomer that can undergo free-radical polymerisation must be able to accept a radical from an initiating species and transfer that radical to another monomer to create a polymer chain. Figure 2.2 shows several monomers that meet the requirement. A free radical is generated from the decomposition of an initiator[32]. Free radicals are able to attack the relatively reactive C=C bond, resulting in incorporation of the monomer in the growing chain and generation of a larger free radical. These reactions produce long chains quickly[33]. Free-radical polymerisation consists of three phases namely; initiation, which begins the chain growth; propagation, which increases the size of the polymer molecule; and termination, which ends the growth of the molecule[32]. By using free-radical polymerisation, two or more vinyl monomers can be co-polymerised together so that the repeat units from all monomers occur in the same polymer chain[34].

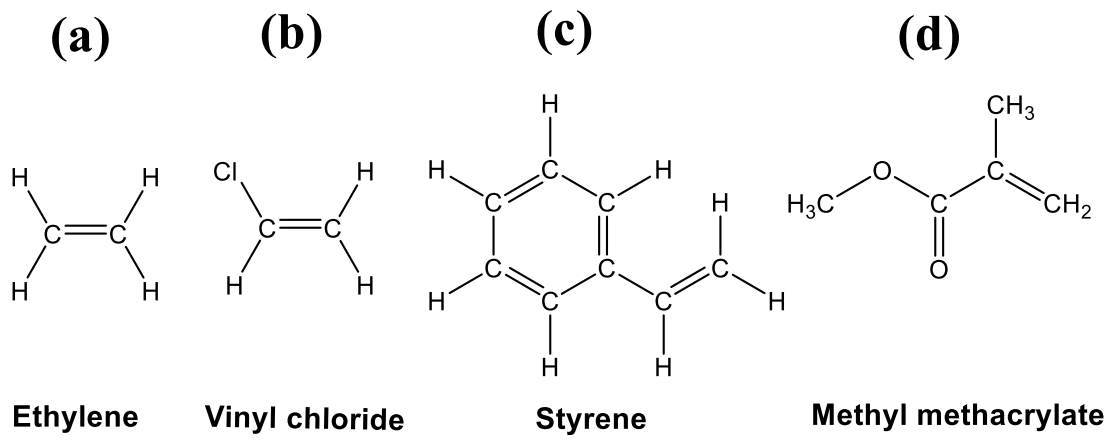

Figure 2.2: Examples of monomers that can undergo free-radical polymerisation.

2.2.2.1 Initiation

Initiation has two steps involved, firstly is the formation of free radical and secondly is the addition of the first monomer[33] (Figure 2.3). The initiator concentration, temperature and nature of other molecules are factors that affect the rate of radical formation[34]. During initiation, a free radical attacking the double bond (also known as π bond) of a monomer and transfers a high energy radical electron to the end of the monomer. Free radicals are converted into monomer radicals by addition of initiator radical to monomer molecules and into polymer radicals by further addition of monomers[35].

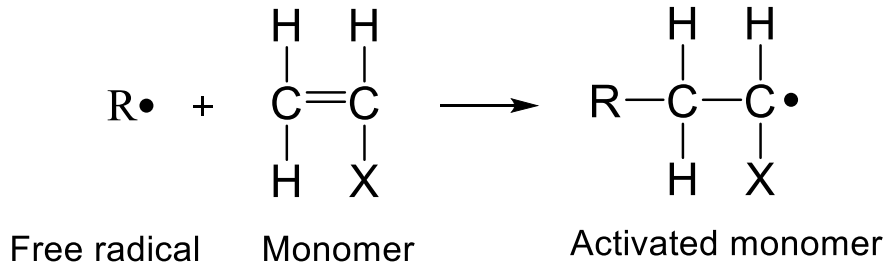

Figure 2.3: Initiation step in free-radical polymerisation[33].

2.2.2.2 Propagation

During propagation, a free radical unit at the end of growing polymer unit reacts with the added monomer and leading to longer chain radical. This reaction may then repeat itself many times This is the propagation or growth stage (Figure 2.4)[32].

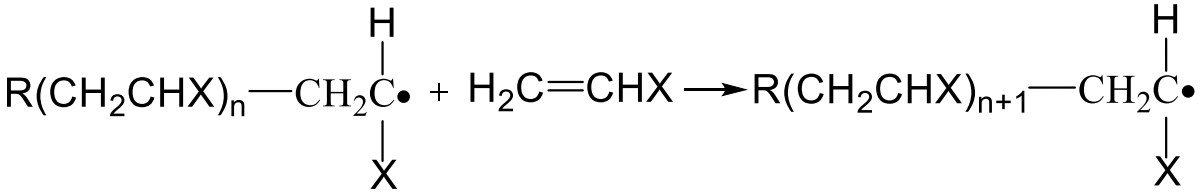

Figure 2.4: The propagation step in free-radical polymerisation[32].

2.2.2.3 Termination

Termination is the final step in conventional free-radical polymerisation. This process can proceed via two routes: 1) combination and 2) disproportionation. For combination, two active radicals react together to form a single bond. For disproportionation, two active radicals react via hydrogen removal and lead to the formation of two reaction products[32]. Figure 2.5 shows the termination step of combination and Figure 2.6 shows disproportionation between growing radicals[10,34].

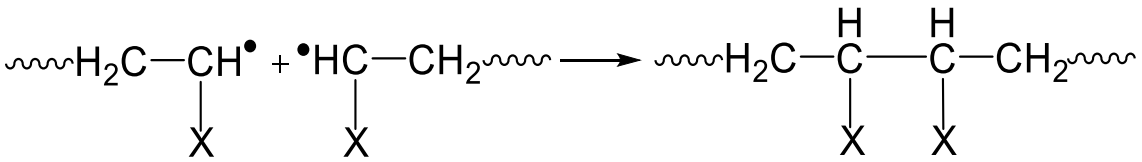

.

Figure 2.5: Mutual combination of two growing radicals for final termination[34].

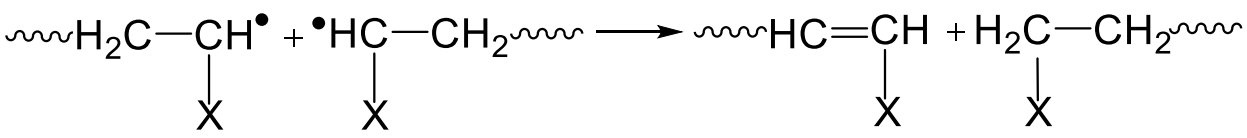

Figure 2.6: Disproportionation between growing radicals for termination step[34].

2.2.3 Emulsion polymerisation

Emulsion polymerisation is the most popular route for the preparation of vinyl-based pH responsive MGs systems because of well-controlled particle size, distribution, and structure and employs free-radical polymerisation methodology[36]. The method is water-based polymerisation and is extensively used to control the thermal, viscosity, and environmental problems of polymer industry[37]. The use of water during the process makes this an environmentally friendly process in comparison to the use of volatile organic solvents. More than 13 million tonnes of polymer dispersions in water are prepared by free-radical emulsion polymerisation each year[38]. From this amount, 11 million tonnes are sold and used as polymer dispersions and the remaining two million tonnes of polymers are produced via emulsion polymerisation[38]. Emulsion polymerisation systems are composed of monomer, initiator, water and surfactant that are stirred together in the reaction vessel[38-40].

The mechanisms of particle nucleation in emulsion polymerisation may include micellar, homogeneous, droplet, or combinations of these. In emulsion polymerisation, the number of particles that are generated is influenced by the polymerisation rate. The polymerisation rate is controlled by temperature, initiator and surfactants concentrations[39]. The polymer particle size and distribution are dependent on the polymerisation rate. Narrow size distributions are achieved when all the particles nucleate in a relatively short time and then grow uniformly. The surfactant is employed to stabilise the droplets through the formation of micelles[41] and providing sites for particle nucleation. The selection of water soluble surfactant can be used as

efficient stabiliser of colloidal systems and to control the morphology and polymer particles size[42].

The simplified emulsion polymerisation process is shown in Figure. 2.7. The system consists of three types of particles: monomer droplets, inactive micelles (polymerisation is not occurring) and active micelles (polymerisation are occurring). In emulsion polymerisation process, when the concentration of surfactant exceeds critical micelle concentration (CMC), the excess of surfactant molecules facilitates the formation of colloidal small cluster known as micelles. Typical micelles have dimensions of 2–10 nm, with each micelle containing 50–150 surfactant molecules[37]. The growing chain migrates to the micelles and diffuse into them and cause the polymerisation to occur in these stabilised droplets. In a typical emulsion polymerisation system, the monomer droplets are much larger than the monomer-containing micelles. Usually, monomer droplets have diameters in the range of 1–100 μm as it depends on the stirring rate. Due to smaller total surface area of the droplets, monomer droplets do not compete efficiently with micelles in capturing radicals produced in the solution. The micelles are favoured as the reaction site due to their high monomer concentration than the monomer in the solution. This permits the nucleation of new polymer particles when initiator radical formed through reaction between free radicals of initiator and monomer present in the water phase, enter the monomer-swollen micelles[43].

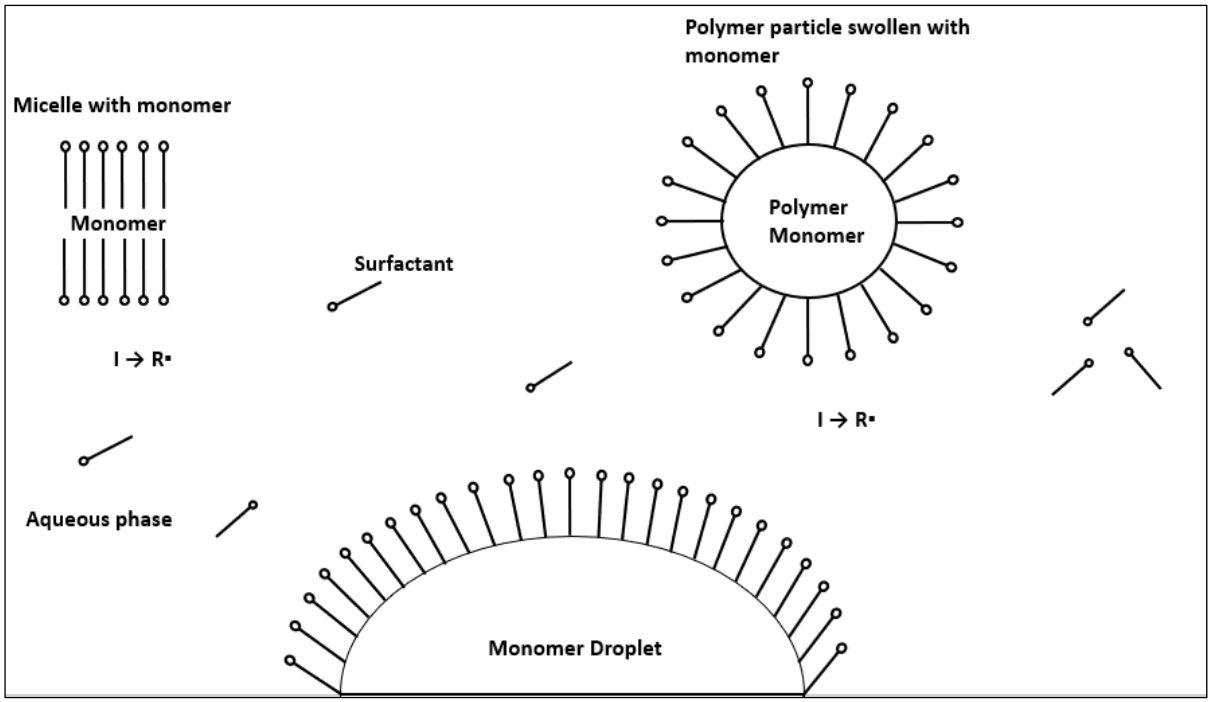

Figure 2.7: Simplified of emulsion polymerisation process[37]. A surfactant molecule is shown as ○— to indicate one end (○) is polar or ionic and the other end (—) is nonpolar.

Figure 2.8 shows a typical emulsion polymerisation mechanism[40]. It is divided into three stages. The nucleation of particles occurs in Interval I. In this stage, the nucleation of growing particles is initiated by radical oligomers. Interval II shows particle growth is propagated when the dissolved monomer reacts with growing chains inside activated micelles and that resulted in monomer droplets shrink and monomer diffuses into the growing particles[34]. The rate of polymerisation is constant. Equation 2.1 below shows the rate of polymerisation (R_p):

$$R_p = \frac{k_p \bar{n} N_P c_M}{N_A} \tag{2.1}$$

Where, k_p is the propagation rate constant in the particle, $\bar{n}$ is the average radical number per particle, N_P is the number of polymer particles per unit volume latex, and N_A is Avogadro's number. In the final stage as shown in Interval III, there are no monomer droplets left because the remaining monomer is in the polymer particles. Additionally, the radical numbers per

particle can be increased because of the high viscosity within the particles near the end of the polymerisation[38].

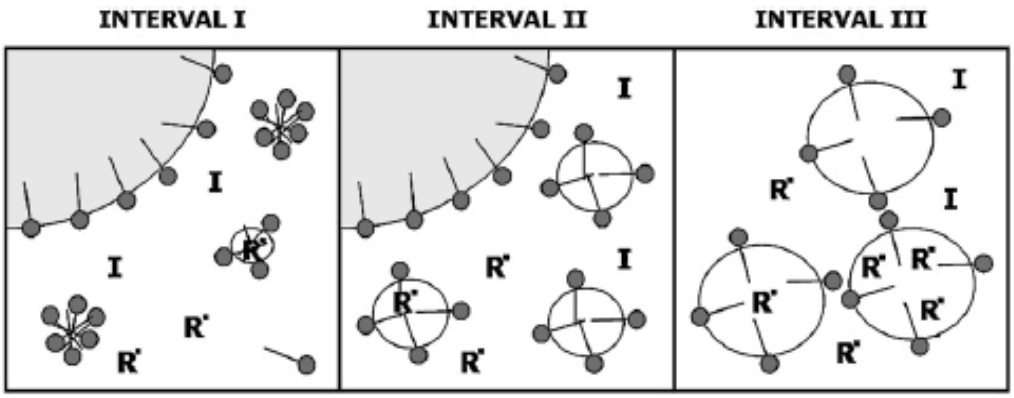

Figure 2.8: The three intervals of a typical emulsion polymerisation reaction, showing surfactant molecules (●—), large monomer droplets, micelles, radicals (R•), initiator (I) and surfactant-stabilised latex particles[40].

2.2.4 DLVO theory

The colloidal stability of charge particles is explained by this classical Derjaguin–Landau–Verwey–Overbeek (DLVO) theory. It explains the interaction between the two approaching particles. According to this theory, the colloidal stability of particles suspension is determined by repulsive electrostatic interaction and attractive van der Waals attraction[44-45]. Electrostatic repulsion between particles serves as a barrier for aggregation and if it is strong enough with respect to van der Waals attraction will result in stable suspension[45]. The prediction of DLVO is depicted in Figure 2.9. Electrostatic repulsion and van der Waals attraction become stronger when the particles are brought close together[46]. The colloidal stability depends on the height of the repulsive barrier with respect to the energy of particle collisions. If the particle collides with sufficient energy to pass the repulsive barrier, they will fall into the deep potential energy minimum[47].

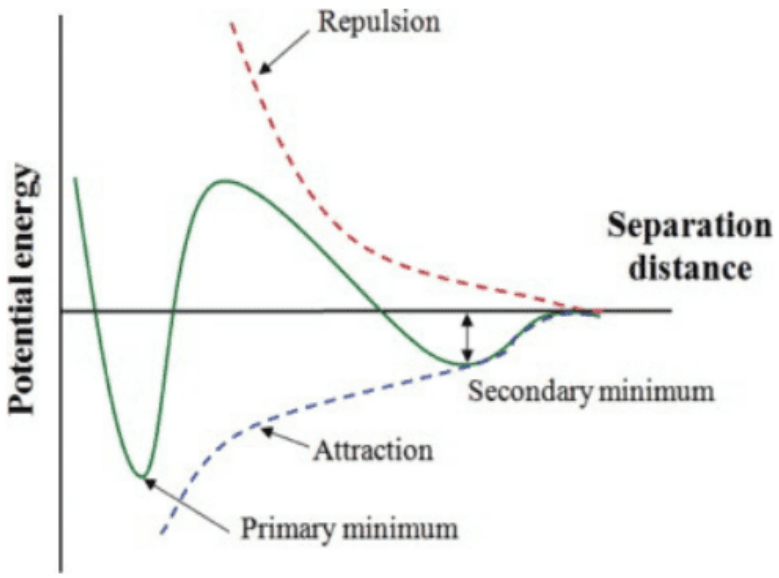

Figure 2.9 : Interaction potential energy as a function of intermolecular distance[46].

2.2.4.1. The electrical double layer

Understanding of electrostatic colloidal stabilisation is obtained using the electric double layer. The electric double layer is formed by an ionic cloud for surface charge particles induced by electrical potential[48-49] (Figure 2.10). An ionic cloud of thickness is characterised by the double layer thickness ($1/\kappa$) forms by mobile ions generated around the colloidal particle when immersed in an electrolyte solution. The concentration of counter ions (electrolyte ions with opposite charges with the particles charges) becomes much higher that co-ions (electrolyte ion with same charges as the particle charges) due to Coulomb interaction between electrolyte ions and particle surface charges.

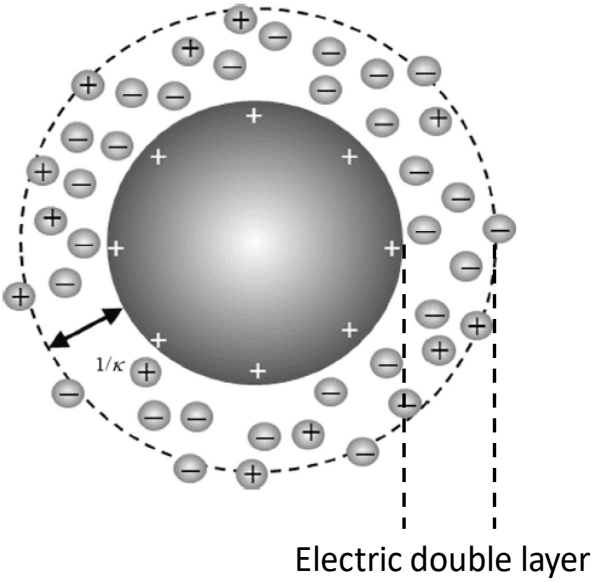

Figure 2.10: Electrical double layer of thickness (1/κ) around a spherical charged particle[48].

Figure 2.11 depicts the details of the electric double layer[46]. The double layer screens the electric surface charge. The net electric charge in this screening diffuse layer is equal in magnitude to the net surface charge but has the opposite polarity. As a result, the complete structure is electrically neutral. The stern layer is the inner region. The outer part of the screening layer is called the diffuse layer. The surface charge ions are fixed to the surface and immobile. In contrast, the Stern plane ions, in principle, retain some degree of freedom.

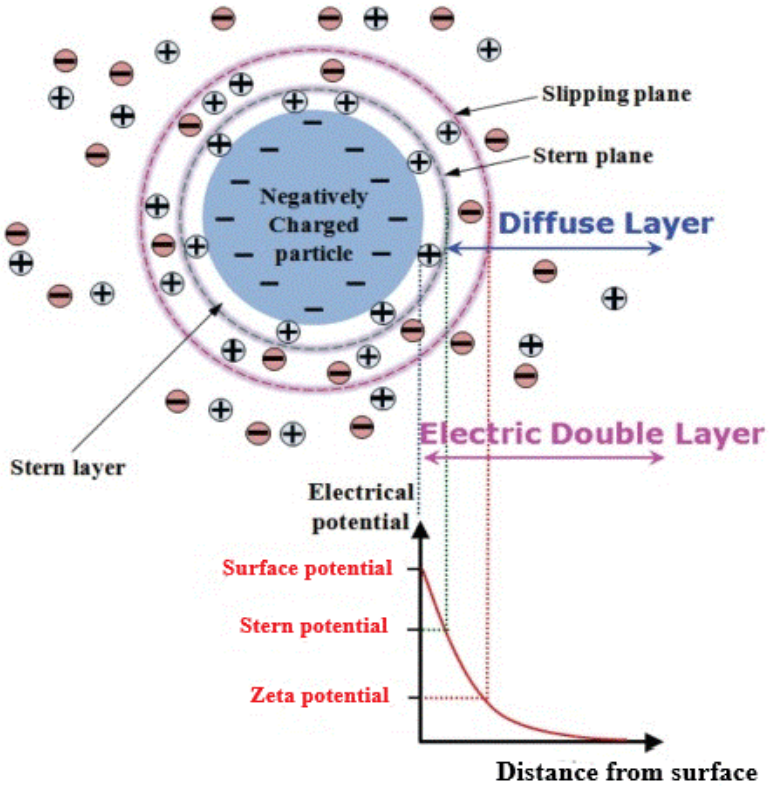

Figure 2.11: Depiction of the electric double layer[46].

The surface potential (Ψ_0) decays exponentially with increasing distance from the surface. The value for $1/\kappa$ indicates the distance at which electrostatic interactions are significant. This changes as a function of electrolyte concentration. The value for κ (m^{-1}) is the Debye screening parameter and is given by equation 2.2 for a symmetrical electrolyte[50];

$$\kappa = 0.329\, x\, 10^{10}(\, cz^2)^{0.5} \qquad (2.2)$$

Where c is the concentration (mol dm^{-3}) of the electrolyte and z is the charge number. This indicates that electrolyte concentration can influence the thickness of diffuse layer. When two particles move towards each other, their diffuse parts of electric double layer may overlap, and a repulsive force is generated. The repulsive interaction energy (v_R) for two spherical particles can be calculated using equation 2.3[51]:

$$v_R = 2\pi\varepsilon a\psi_d^2 exp^{-kh} \quad (2.3)$$

Where ε is the dielectric constant of medium, a is the radius of the particles, Ψ_d is the diffuse layer potential and H is the distance between spheres. According to equation 2.2 and 2.3, it can be concluded that the repulsive force between particles can be altered by changing the concentration of electrolyte or the surface potential.

2.2.4.2 Van der Waals forces

The attractive intermolecular forces called the van der Waals forces are acting due to interactions between the fluctuating dipoles when two molecules are approaching each other. In solving the problem of electrostatic interaction of the charged surfaces separated by an ionic interlayer, the boundary conditions are first of all determined by the charging mechanism[46]. Integration of all the van der Waals interactions between two molecules over the two spherical particles of radius (α), separated by a distance (H) (Figure 2.12)[48].

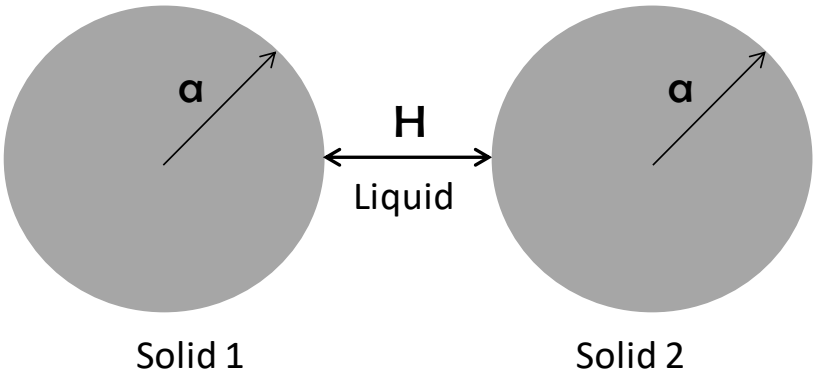

Figure 2.12: Van der Waals interaction between two particles[48].

The van der Waals attraction energy, V_A, is derived in the following equation:

$$V_A = -\frac{A}{6}\left(\frac{2r^2}{(S^2+4rS)} + \frac{2r^2}{(S^2+4rS+4r^2)} + ln\left[\frac{(S^2+4rA)}{(S^2+4rS+4r^2)}\right]\right) \quad (2.4)$$

where $S = \mathrm{H}/\alpha$. The negative sign in equation 2.4 indicates the attractive nature of the interaction between two particles and A is the Hamaker constant with magnitude $10^{-19} \sim 10^{-20}$ J. When the separation distance between two equal sized spherical particles is smaller than the particle radius, i.e., $\mathrm{H}/\alpha << 1$, the simplified version of equation 2.4 can be obtained:

$$V_A = -\frac{A\alpha}{12H} \quad (2.5)$$

2.2.5 Colloidal stability

Colloidal stability is an important property for nanoparticle dispersions. If the colloidal stability is unstable, the dispersed phase particles tend to aggregate[52]. To prevent aggregation and floc formation, a potential barrier must be developed between two particles. These forces involve two repulsive forces: (1) Electrostatic forces due to the presence of electric charges on particle surface; (2) Steric forces due to hydrophilic macromolecules on particle surface[53]. The steric interaction between two surfaces appears when polymer molecules attach at some points on a surface and suspend into the solution. Steric stabilisation can impart the colloidal stability of MGs dispersion and arising from swollen polymer chains that comprise the particle[54-55]. As shown in Figure 2.13, electrosteric mechanism is a combination of electrostatic and steric stabilisation.

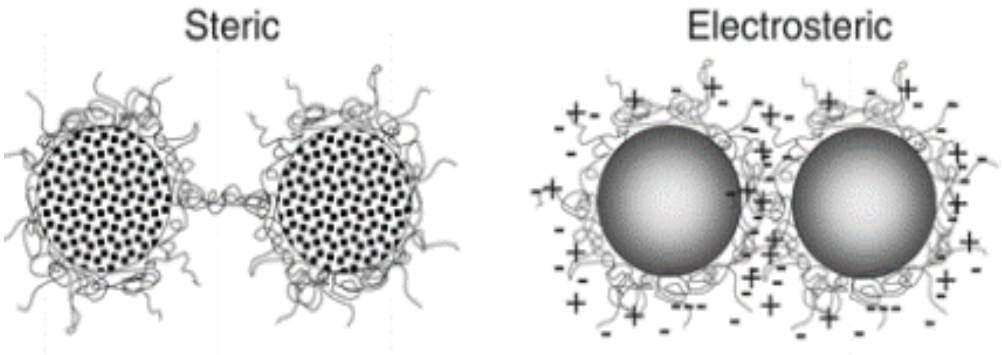

Figure 2.13: Two general mechanisms that impart colloidal stability[54].

For sterically stabilised systems the total interaction energy can be written as in equation 2.6 and potential energy diagrams is depicted in Figure 2.14b with entry into a deep primary minimum made virtually impossible by the steric interactions[51]. Figure 2.14a depicted typical DLVO interaction, the electrostatic barrier exists when the double layer repulsion exceeds the van der Waals attraction:

$$V = V_R + V_s + V_A \tag{2.6}$$

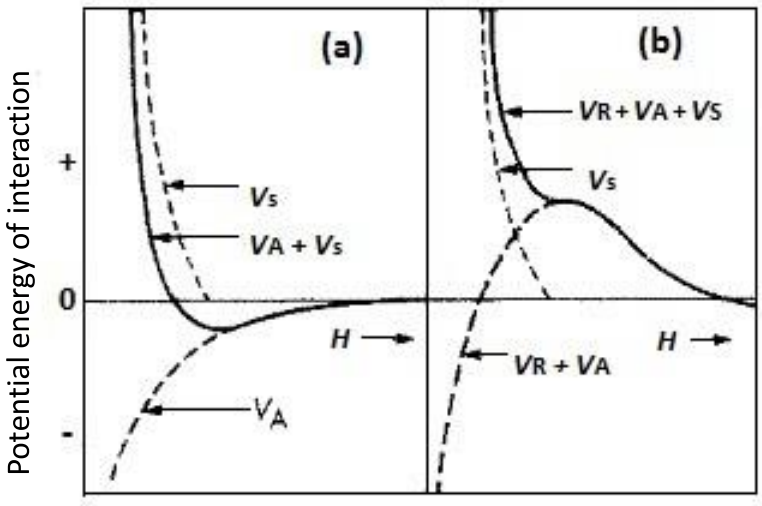

Figure 2.14: Schematic interaction energy diagrams for sterically stabilised particles[51]: (a) in the absence of electric double layer repulsion ($V = V_A + V_S$), (b) with electric double layer repulsion ($V = V_R + V_A + V_S$). R= repulsion, A= attraction; S = steric.

2.2.6 pH-responsive microgels

Stimuli responsive MGs can undergo phase transitions or morphology changes under a number of parameters such as temperature, pH, ionic strength, electrolyte concentration and light[31]. These MGs have ability to swell and de-swell in response to the changes highlighted above[56]. pH-responsive MGs are polyelectrolytes that have acidic or basic groups bonded to the polymer chains[57]. Generally, pH-responsive MGs are composed of weak polyelectrolytes with carboxylic, phosphoric or amino functional group (acid or basic)[58]. Additionally, certain functional groups may serve the complexation of metal ions opening a platform for new applications such as the template-based fabrication of hybrid materials or separation and purification technologies[59].

The pH for the onset of for swelling transitions of MGs can be determined from the apparent dissociation constant (pK_a). This transition of MGs from collapsed state to swollen state occurs in a range close to the pK_a ionisable groups. Ionisation begins at the apparent pK_a of polymer and the present of electrostatic repulsion of the same charges results in a drastic swelling of MGs in the network. Upon the completion of ionisation of ionisable groups, the swelling extent stops. At this point, further increase in pH values only increases the ionic strength. In addition, the pH range of the phase transition can be controlled based on the selection of ionisable moiety with a pK_a that corresponding to the desired pH or can be executed by incorporating of hydrophobic moieties into the polymer backbone[53].

The pK_a of anionic polyelectrolyte is higher than the free monomers because of the polyelectrolyte effect that generated due to an increase in K_a value and results in RCOOH groups being positioned adjacent to the segments of a polymer chain[53]. To further elaborate, a high segment density of RCOO− groups opposes formation of more RCOO− groups within

the particle due to electrostatic repulsion. The explanation above is supported with equilibrium reaction in equation 2.7 as shown below:

$$RCOOH + H_2O \rightleftharpoons RCOO^- + H_3O^+ \quad (2.7)$$

The dissociation of carboxylic acid group is based on the equilibrium above and leads to the swelling of MGs at high pH. Formation of blocks of carboxylic acid containing monomers within the MGs results in an increase of effective pK_a. It was reported that the value of pK_a for poly(NIPAM) MGs containing carboxylic acid co-monomers has been shown to be dependent on the distribution of these groups throughout the particles[53]. Another possible reasons for a positive shift of the pK_a are hydrophobic segments, associative crosslinking and ion-solvation[53]. The ion solvation is a medium effect associated to the position of acid dissociation equilibrium and hence the solvation of carboxylate anion depends on the properties of the medium at monolayer surface and should affect the pK_a of acid group[60].

2.2.7 Swelling of microgels

The swelling of MGs is generated by the difference of chemical potential inside and outside of the network associated to electrostatic repulsion and osmotic pressure in an equilibrium state. The swelling theory of MGs is based on Flory's theory as shown in equation 2.8. The polymer volume fraction is denoted as ϕ_2 and the value of $\phi_2 = 1$ in the collapsed state.

$$\phi_2 = \left\{ \frac{X v_1}{V_c(\frac{1}{2} - X_{12})} \right\}^{3/5} \quad (2.8)$$

X is the number of crosslinks, V_c is collapsed network volume, v_1 is the molar volume for solvent, X_{12} is Flory's solvent polymer interaction parameter, and $\frac{X}{V_c}$ is the average crosslink number density in the collapsed particle.

Non-crosslinked polymer segments are represented by B; whereas, A is the di-functional crosslinked segments. The mole fraction of crosslinked segment (X_A) is usually less than 0.1. It is assumed that molecular weight of segment A and B is same and therefore introduces two moles of crosslinking units as shown in equation 2.9;

$$\frac{X}{V_c} = \frac{2X_A\ \rho_B}{M_B} \tag{2.9}$$

where M_B and ρ_B are the molecular weight and density of the B segments, respectively. Equation 2.9 is substituted in equation 2.8 by assuming $\rho_B = 1$ to obtain equation 2.10. From equation 2.10, the polymer volume fraction is proportional to crosslink density.

$$\phi_2 = \left\{\frac{2X_A\ V_1}{M_B\ (0.5 - X_{12})}\right\}^{\frac{3}{5}} \tag{2.10}$$

2.3 Double crosslinked microgels.

The mechanical properties of hydrogels can be significantly improved by introducing the double network (DN) associated with strong interpenetrating network entanglement and contrast structure[61-62]. In DN structure, the first network is tightly crosslinked to rigid polyelectrolyte whilst the second network loosely crosslinked interpenetrating structure the first network. The improvement in DN is owing to the network and entanglement. DN hydrogels has major limitation due irreversible and permanent bond breakage of the first network at high strain. Hence chemically linked DN hydrogels are not able to recover efficiently from damage and lose most of its mechanical properties[63].

In 2011, hydrogels were prepared by crosslinking of concentrated MGs using free-radical chemistry reported by Liu et.al[64]. In his work, doubly crosslinked term was used to describe two types of crosslinking known as intra-particle crosslinking and inter-particle crosslinking. Intra-particle crosslinking is referring to single crosslinked (SX) particles while interparticle crosslinking is associated to the formation covalent crosslinking between vinyl groups and particles at the peripheries. These MGs particles were functionalised with GMA (to introduce the vinyl groups) and the inter-linking of neighbouring MGs in the physical gel state enable formation of covalent gel. GMA is a versatile candidate for functionalisation with MGs due to epoxide chains that can react with numerous types of nucleophiles, including carboxylates, alcohols, amines, thiols, and azides[65-66,67-69]. Besides, no additional monomers were required for preparing the DX MGs. These DX MGs crosslinked MGs retains its shape in the water because of covalently inter-linked MGs particle.

Previous work related to CEA is associated with polyampholyte hydrogels that were formed from mixtures of [2-(acryloyloxy)ethyl] trimethylammonium chloride (TMA) and CEA and triethylene glycol dimethacrylate (TEDGMA) was added as a crosslinker[70]. These hydrogels were fully characterised as a function of cross-linker density and monomer ratio. The purpose of this hydrogel is for protein adsorption. The monomers were dissolved in the solvent containing ethylene glycol, ethanol and NaOH. Then, the polymerisation was initiated with the addition of APS solution, followed by the addition of sodium metabisulfite (SMS). Then, the polymerisation solution was mixed homogeneously and transferred into a mould. The reaction was allowed to proceed at 60°C for 1 hour, thereafter the apparatus was removed from the oven and allowed to cool for 3 hours to reach room temperature. These hydrogels were demonstrated to have a high swelling capacity, and hydrogels with higher cross-linker densities were found to have greater mechanical properties.

Lane et.al highlighted that construction of DX MGs has improved the ductility and elasticity of MGs[71]. In his work, MGs existed as pre-formed hydrogels which independently of any other polymer phase and were not dispersed within the hydrogel matrix. Consequently, this established method of DX offers considerable versatility compare to conventional polyelectrolyte hydrogels. The preparation of DX MG using free-radical polymerisation is depicted in Figure 2.15 below[72]. The novelty of the MGs approach here is that it converts a fluid dispersion to physically gelled MGs particles, which then transform into a permanent covalent network of pH-responsive MGs. Irreversibly crosslinked gel are obtained from this method[64].

.

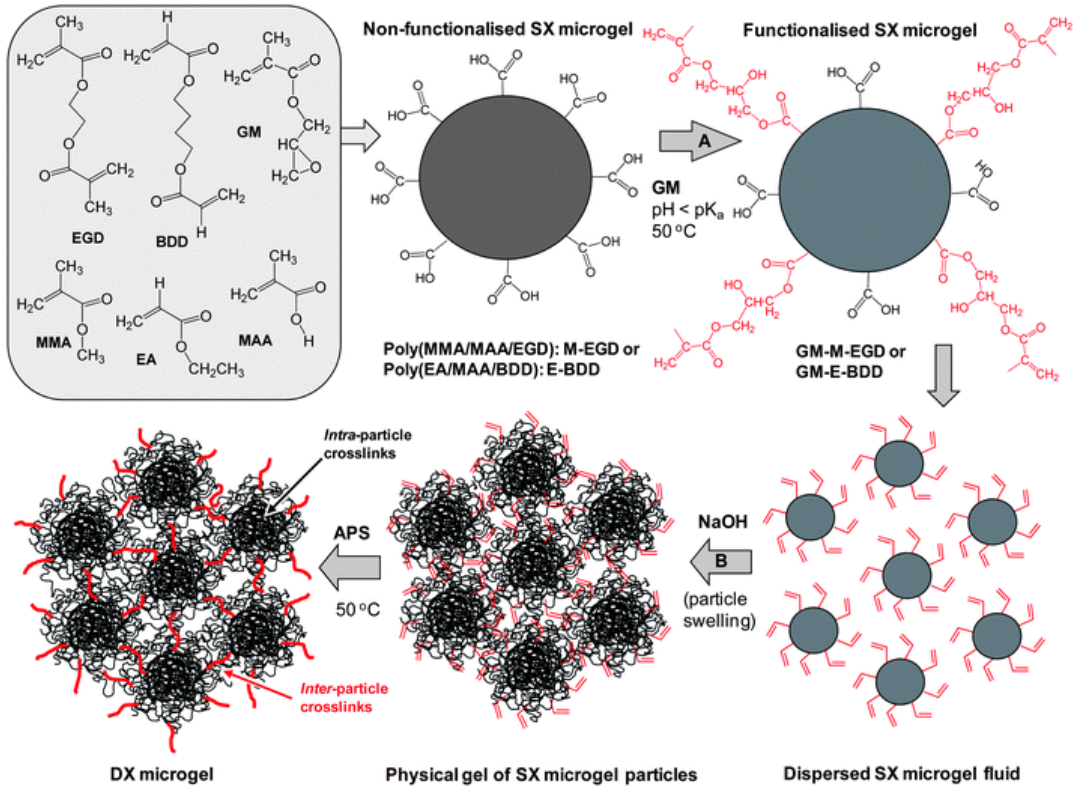

Figure 2.15: Preparation of DX MGs by free-radical polymerisation[72]. SX is referring to single crosslinked MGs.

In Figure 2.16, the example of PGMA functionalised with rhodamine-B through acid–epoxy reaction is shown[73]. The epoxide group possesses high reactivity and has an ability to enter into a range of chemical reactions due to the deformation of valency angles and shortening of C-C bonds[74]. In addition, the presence of three membered ring can be unlocked by various nucleophiles in addition reaction[75]. Co-polymerization is also possible with other acrylate or methacrylate monomers to further diversify the range of structures and applications of the final materials[66].

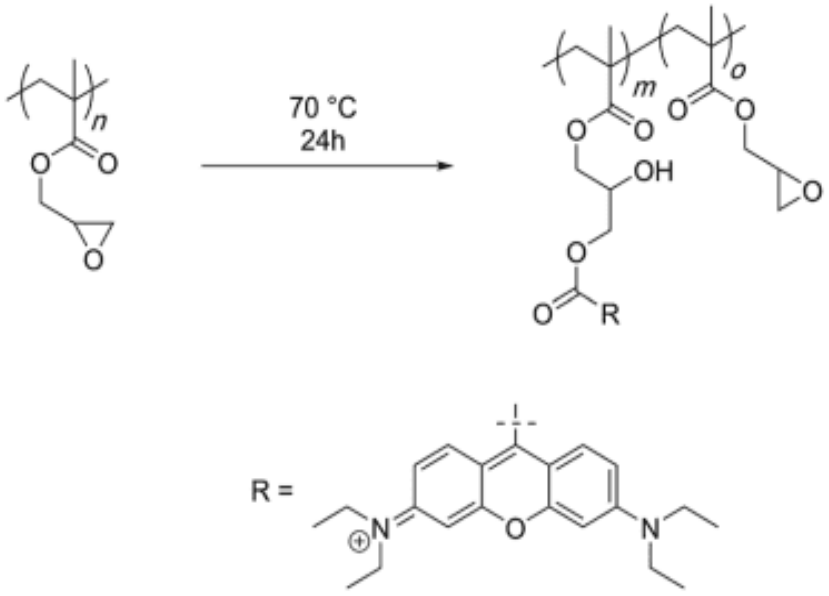

Figure 2.16: Oxirane ring-opening reaction of PGMA with rhodamine-B[73].

The structures associated to MGs network is shown in Figure 2.17. The mechanical properties of the gels such as elasticity and ductility are depending on $M_{c(ave)}$ values which referring to mean molar mass of the elastically effective chains. In Figure 2.17(b), in the presence of crosslinking in the network structure, the value of $M_{c(ave)}$ should decrease at the surface boundary. For DX MG network structure as shown in Figure 2.17(c), in the overlap region which corresponding to the crosslinking network, the value of $M_{c(ave)}$ is meant to be lowered than the interior region. Therefore, the mechanical properties of DX MGs are affected by

effective volume fraction of this phase. It worth noting that the difference in $M_{c(ave)}$ values significantly affect the mobility of the dissolve molecules in DX MGs structure[76].

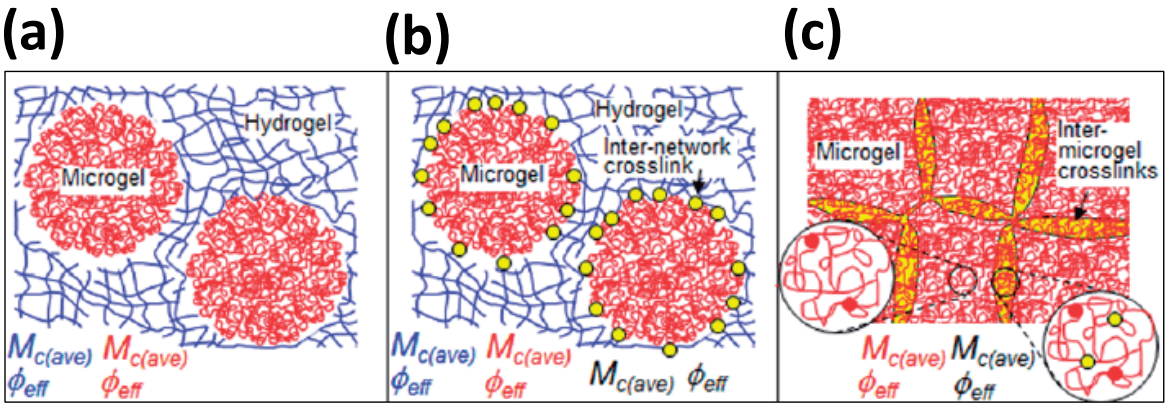

Figure 2.17 : Depiction of hydrogel containing MGs structures[76]; (a) MGs filled hydrogel ; (b) MGs reinforced hydrogels; (c) DX MGs

2.3.1 Rubber elasticity theory; elasticity of gels

Rubber elasticity means the capacity to sustain large deformation and followed by complete recovery. The theory of elasticity according to Flory means that properties are retained after deformation due to crosslinking chains that produce highly elastic and interconnected network[77]. Materials that exhibit rubber like properties must satisfy three requirements; the presence of long chain molecules which have high degree of flexibility. Secondly, weak secondary forces between molecules and thirdly formation of three dimensional network[78]. Rubber elasticity theory is related to molecular effects on the strain hardening which resulted in the change of elastic behaviour. The relationship of molecular weights between crosslinks and rubbery modulus has been applied to calculate molecular weight between crosslinking (MGs) as shown in equation 2.11:

$$G = NkT = \frac{\rho RT}{M_c} \qquad (2.11)$$

Where N is the number of network chains per unit volume, ρ is the physical density of the polymer, R is the gas constant, T is the temperature[79]. From equation 2.11, it is predicted that the value of G should increase with T and slope of strain hardening regions goes up when M_c decreases.

2.4 Double-crosslinked microgels with composite

Development of composite hydrogels is a demand for today's materials due to certain flaws of conventional hydrogels in terms of poor mechanical properties, poor recovery and insufficient functionality that hinders its practical application in biomaterials and environmental. Mechanical property enhancement of hydrogel composite is obtained owing to an improvement in the network structure. Incorporation of composite into the hydrogels structure significantly enhance functional groups amount making the hydrogel has excellent responses in various environments[80]. In addition, high water content of hydrogels allows more rapid ion penetration to interact with functional units of the gels[21]. As this research work is focusing on the heavy metal ions removal, the improvement of mechanical strength of hydrogel and various functional groups by incorporation with GO is relevant[22, 81]. The existence of functional groups aids the adsorption process and enhance the uptake. In recent years, the development of advanced or hybrid NGs with multifunctionality and novel properties has been of interest in many research fields ranging from materials science to nanomedicine[82-84]. This diversity in applications exists because these nanocomposites can be designed in various forms, such as thick and thin membranes, uneven sheets, hollow tubes, and bellows (see Figure 2.18)[80].

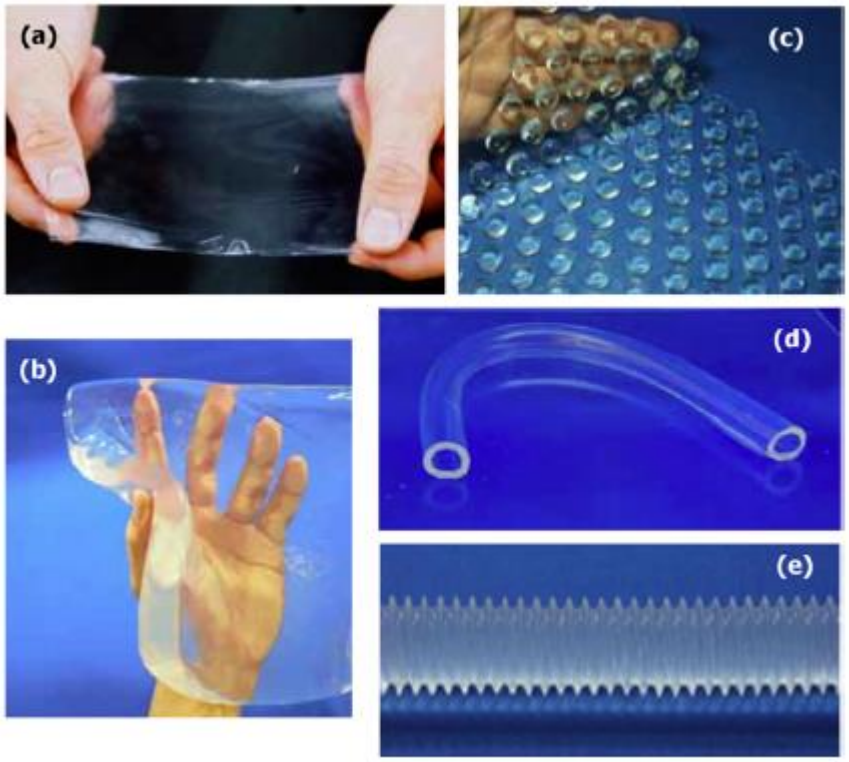

Figure 2.18: Various shapes of nanocomposite hydrogels[80]: (a) thin film, (b) sheet, (c) uneven sheet, (d) hollow tube, and (e) bellows.

A study of physical and DX MG hydrogels containing GO was reported by Cui et.al[85]. In that work, the effect of GO concentration (between 0.1 to 1.0 wt.%) on gel properties was studied. Monomers of MMA, MAA and the crosslinker, EGDMA were used as a matrix in the formation of composite MGs. In 2013, highly elastic and super stretchable GO/ polyacrylamide (GO/PAM) hydrogels were established by Cong et.al[86]. In that work, exceptional mechanical behaviour was triggered by synergistic effects of GO and Ca^{2+} ions. That hydrogel was synthesised by in situ polymerisation of acrylamide (AM) monomers in a mixture of $Ca(NO_3)_2$ and GO dispersion using N,N-methylenebisacrylamide (MBAA) and ammonium persulfate (APS) as the crosslinker and initiator, respectively[85,86]. They investigated the effect of GO, Ca^{2+} and crosslinker on hydrogel properties. The toughness and stretchability of GO/PAM hydrogels depended on their microstructures and crosslinking mechanism. Highly

elastic and super stretchable hydrogel were generated by the synergistic effect of Ca^{2+} induced three-dimensional GO crosslinking network, chemically crosslinked PAM network and inter-twined hydrogen-bonding network (see Figure 2.19)[86].

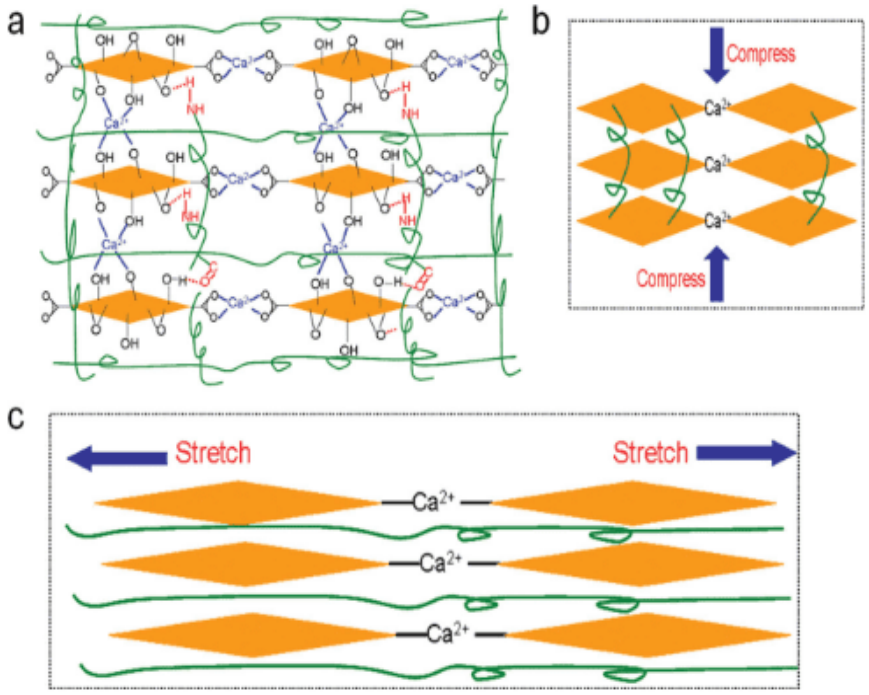

Figure 2.19: Schematic models of the GO/PAM composite hydrogel[86]; (a) Types of crosslinking networks in the hybrid hydrogel including Ca^{2+} coordination-induced GO network; (b) Compression model for GO/PAM hydrogel; (c) Stretch model for GO/PAM hydrogel.

In 2002, Haraguchi and Takehisa introduced nanocomposite (NC) hydrogels[87]. They used dimethylacrylamide, TEMED, APS and laponite. Interestingly in that work, no crosslinker was added as laponite itself acted as a multifunctional crosslinking agent. These hydrogels had low turbidity and remarkably high ductility (yield strains > 1000%) compression analysis (see Figure 2.20)[88]. The nanocomposite gel is denoted as NC3 and this gel exhibits a monotonic increase in stress with increasing strain. Whilst for comparison, OR gels (conventional organic, crosslinked, polymeric hydrogels) underwent brittle fracture at very low (10 ± 30%) elongations. It was also observed that the large elongation of NC gels was almost completely

reversible, and the recovery obtained was more than 98% of the total deformation. That thin cylinders could be stretched, and knots tied in them without macroscopic fracture. The laponite platelets were exfoliated and acted as crosslinking points, and this was in part attributed to the presence of TEMED. These hydrogels were termed rubbery polymeric hydrogels because they showed extraordinarily large and reversible extensions[76].

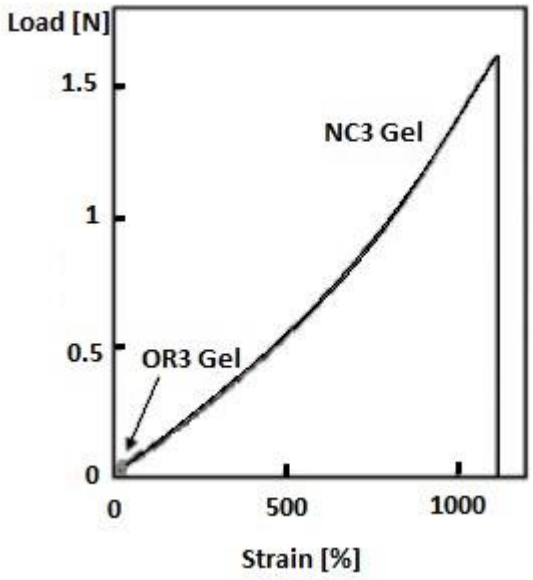

Figure 2.20: The stress-strain curve of nanocomposite (NC3) gel. The data for conventional gel (OR3) gel is also shown for comparison[88].

Previous work conducted by Sun et.al was corresponding to organic–inorganic composite hydrogel with excellent adsorption performance for methylene blue removal[89] (Figure 2.21). In that work, MAA was grafted on hemicellulose chain and the acid-treated multi-walled carbon nanotubes (MW-CNTs) were embedded in the hydrogel through physical effects. This hemicellulose-g-poly(MAA)/carbon nanotube (CNT) composite hydrogel was used as an absorbent for methylene blue removal. Incorporation of CNT in the hydrogel network resulted in an improvement of mechanical performance and heat resistant properties. The interaction between polymer chains and inorganic particles enhanced with increasing amount of multi-

wall carbon nanotube loading which also resulted in smaller pore size of the gel[89]. However, CNT has several limitations such as it could form large agglomerations in the water or hydrogels due to hydrophobicity of the structure and CNT dispersion in the hydrogels remains as a great challenge due to strong van der Waals attraction[90].

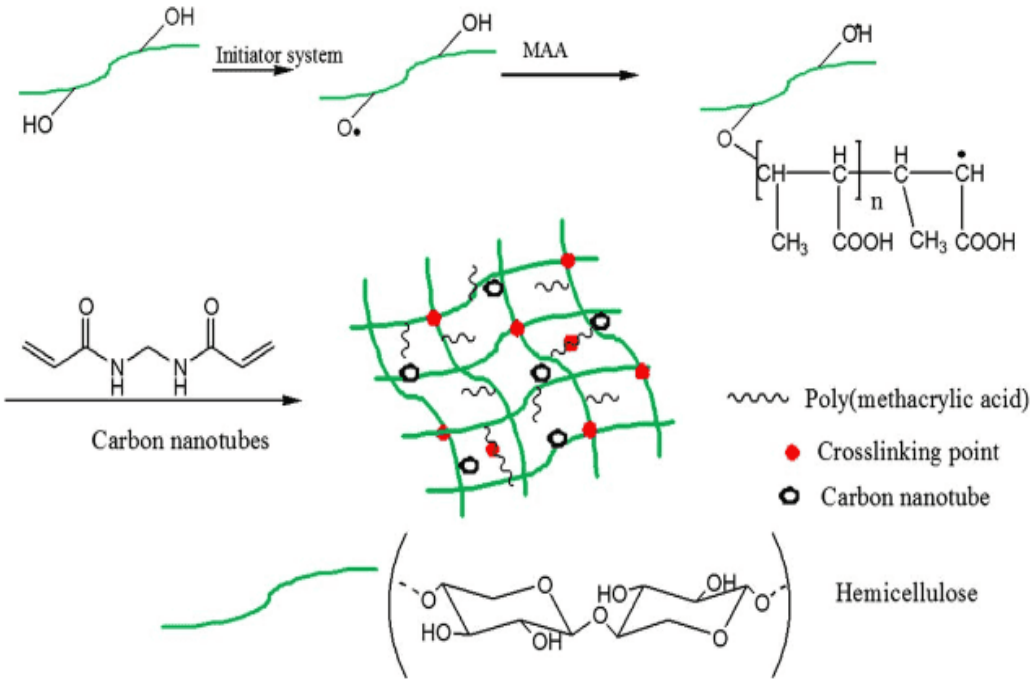

Figure 2.21: The preparation of hydrogel of hemicellulose-g-poly(MAA)/CNT[89].

2.4.1 Graphene

Graphene is two-dimensional, which can be single or few-layer sheets of carbon atoms. It has attracted tremendous attention and research interest due to the unique hexagonally packed flat structure and remarkable properties. Graphene is a one of the most famous sp^2 nanocarbons group besides fullerene and carbon nanotubes[91]**.** Graphene has such remarkable properties such as high modulus value (~ 1 TPa), ultimate mechanical strength (130 GPa), mechanical stiffness up to 1030 GPa, comparable thermal conductivity (3000-5000 W/(m.K)) to single-walled carbon nanotubes and a very high electrical conductivity up to 6000 S/cm[92-93]. Besides,

graphene also hold extremely high surface area (2630 m^2/g) and excellent gas permeability[94]. Other forms of graphene-related materials including graphene oxide (GO), reduced graphene oxide, and exfoliated graphite, have been reliably produced in large scale[86]. Figure 2.22 shows illustration of GO and functionalised graphene[80].

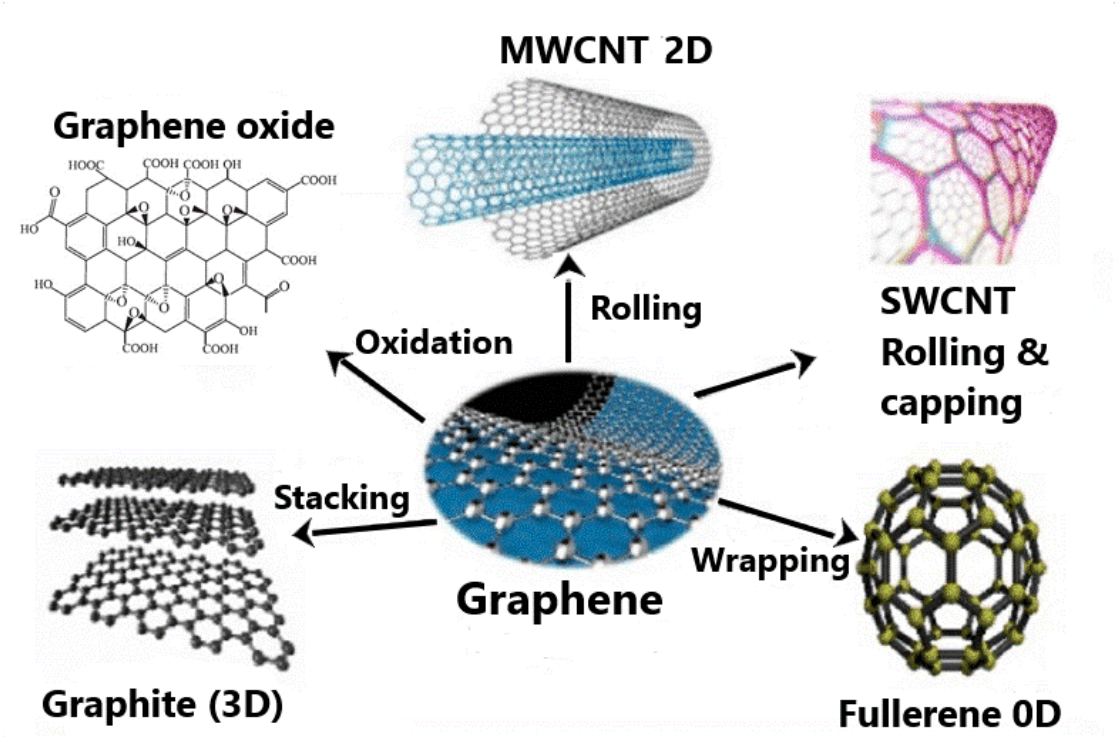

Figure 2.22: Illustration of graphene, GO or functionalised graphene and 3D (graphite, silicate, $BaTiO_3$) and 0D (fullerene), 1D small-walled carbon nanotubes & multi-walled carbon nanotubes (SWCNTs & MWCNTs)[80].

Figure 2.23 shows the timeline of selected events in the history of the preparation, isolation and characterization of graphene[95]. Although theory concerning graphene can be traced back to the year of 1840, the first renowned experimental discovery and investigation of graphene occurred in 2004 is a milestone for the graphene research[96-97]. Publication by Geim and Novoselov in 2004 announcing a remarkably simple method for preparing monolayer graphene and presenting ground breaking physical measurements on graphene[98]. This ground-breaking research was discovered by scotch tape method[92,99]. As shown in Figure 2.24, studied on

Graphene has shown rising trend and strong growth for the past decade, parallel with carbon nanotubes (CNTs) studied[91]. Graphene based polymer composites are one of the most promising and recent technology developments that combine unique features of graphene based materials and polymer materials in one nanohybrid material[100]. Graphene has applications in nanoelectronics, sensors, supercapacitors, composite materials, catalyst, and environmental[101,102]

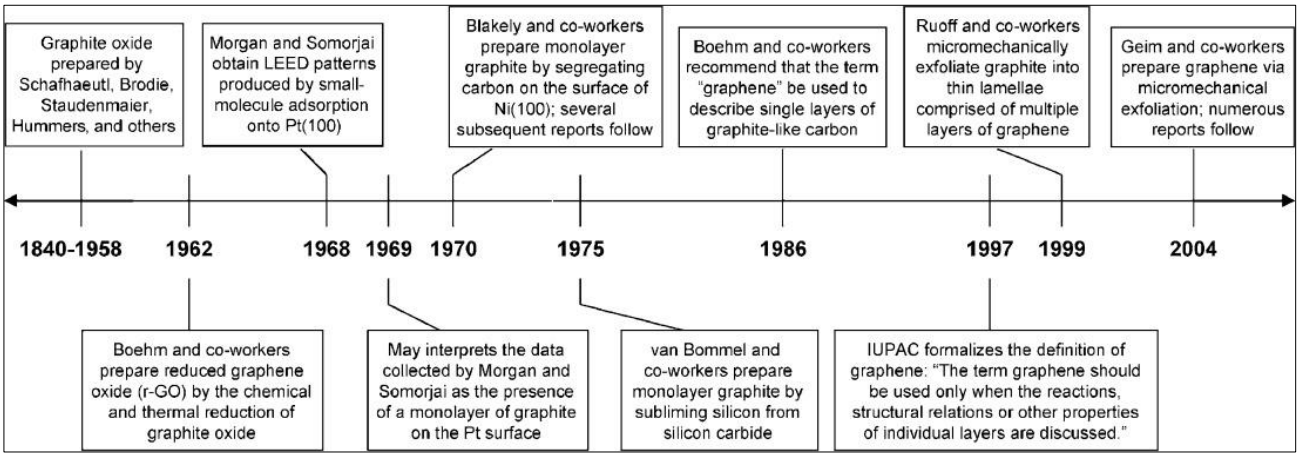

Figure 2.23: Timeline of selected events in the history of the preparation, isolation and characterisation of graphene[95].

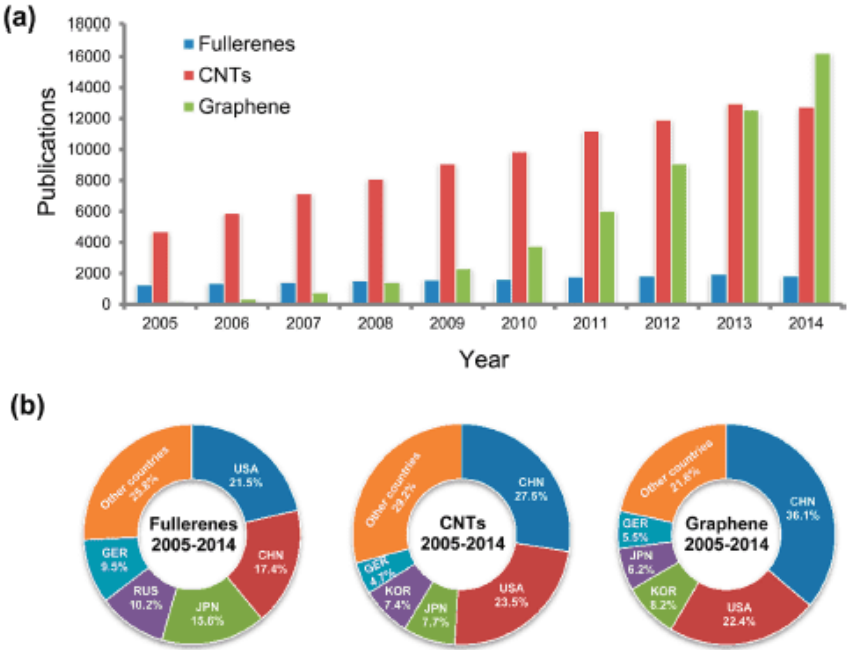

Figure 2.24: (a) Timeline of scientific publications relating to nanocarbons in the past decade (2005−2014); (b) Regional distribution of publications on each topic[91].

2.4.2 Graphene oxide

Even though graphene has remarkable mechanical properties, the lack of massive production of exfoliated graphene has limited practical applications. In particular, the drawback of graphene is an irreversible aggregate can be easily form through π-π stacking and van der Waals interactions[103]. This difficulty in the dispersion can generate bigger obstacles in the application as well. Solution exfoliation of graphite either by sonication or high-shear mixing is one procedure for large-scale production of graphene with high-quality[104]. Chemists developed an alternative using the heavily functionalised graphene derivative-GO, GO could be easily obtained through a chemical oxidation and exfoliation route from natural graphite via the Hummers method. GO is rich in oxidative groups epoxide (-COC), hydroxyl (-OH), carbonyl (-CO), and carboxyl (-COOH) groups can be obtained[105-106](Figure 2.25)[107]. Chemists and materials scientists have made great efforts in utilising GO because of low costs of mass production, abundant oxygen-containing groups for functionality and good dispersibility in water[108]. Besides, GO has the ability to be blended with polymers and incorporated in gels[109,86,110] and extends its application in many fields[111].

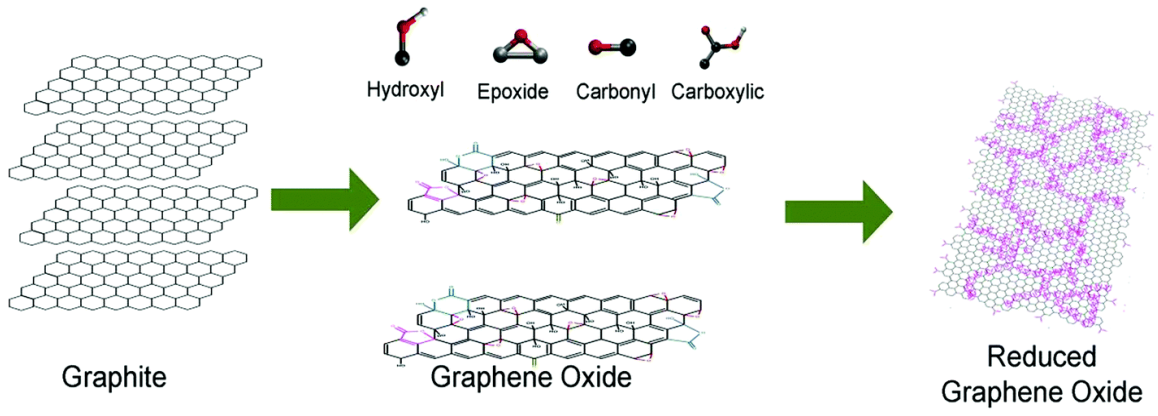

Figure 2.25: Synthesis and reduction process of GO. Graphite can be oxidised with different procedures in the presence of strong acids[107].

The most popular method to produce GO was invented by Hummers and Offeman which known as Hummers method[99]. In this method, potassium permanganate ($KMnO_4$) and H_2SO_4 were used. There were several models proposed for the structure of GO as shown in Figure 2.26[112]. However, the most accepted model is that proposed by Lerf, Klinowski and their co-workers. The main features of this model comprise the basal plane structure of GO containing unoxidized benzene rings and aliphatic six-membered rings. The degree of oxidation is dependent on the size of these two distinct groups. This model also proposed that the location of hydroxyl and epoxy groups is adjacent to one another, and random distribution of functional groups. In GO structure, carboxyl groups are formed at the edges of carbon sheets[105].

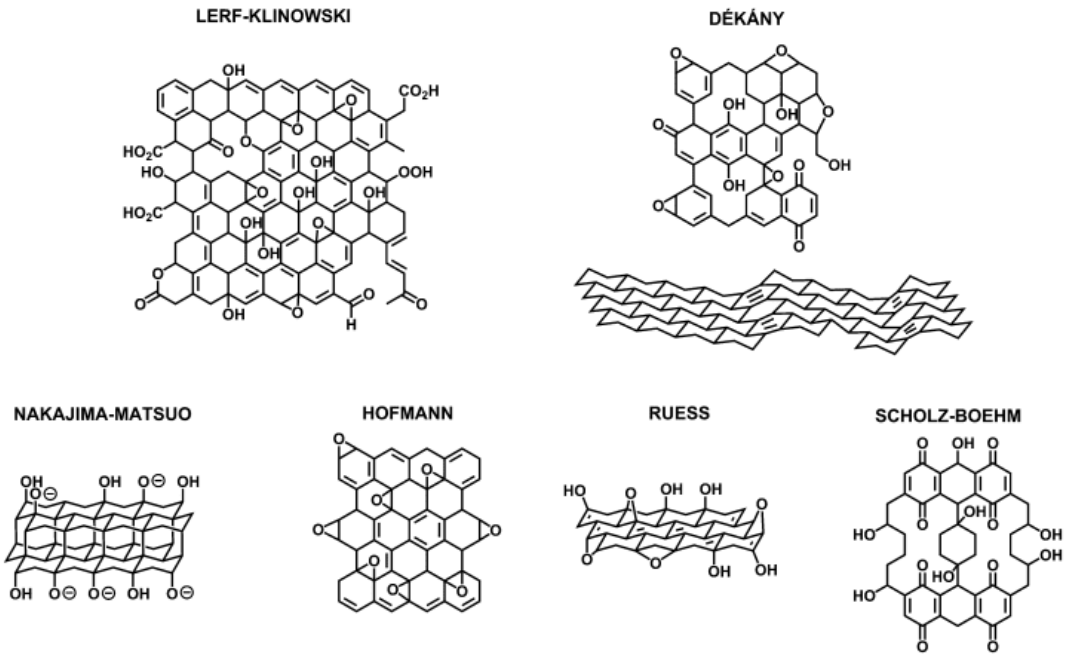

Figure 2.26: Summary of GO structural models that have been proposed[112].

The presence of abundant functional groups on the GO surface leads to the development of highly hydrophilic character, stable dispersion and provide active sites for metal ion complexation making it a potential sorbent[85,86,101]. Besides, an abundance of oxygen-containing functional groups on GO sheets also make it easily processable, which leads to the

growth of new type of graphene-based materials for instance GO acting as a physical crosslinker and widely used in preparing stimulus-responsive hydrogels[113]. The negative charges of GO are mainly contributed by the carboxyl group which prevent aggregation due to electrostatic repulsion forces. In the basic environment (pH > 7), ionisation occurred that resulted in stronger electrostatic repulsion whilst in acidic environment (pH <7), electrostatic repulsion is weakened due to the protonation of carboxyl group and hence resulted in the enhancement of hydrogen bonding[91, 104]. Nevertheless, graphene-like structure can be retrieved from GO by chemical reduction, thermal treatment or irradiation on GO and known as reduced GO (RGO)[114]. RGO is not further discussed as it is not explored in this work. High performance of smart materials be obtained by chemically modified graphene including GO, RGO and their derivative[104].

2.4.3 Graphene oxide as a filler to improve properties of the gels

One of the most promising applications of graphene is in polymer nanocomposites, wherein nanoscale fillers are incorporated into a polymer matrix. Pristine graphene as well as graphene derivatives such as graphene oxide and functionalized graphene oxide have been explored, all aiming at enhancing the final properties of the composite material in terms of conductivity, mechanical properties and other functional properties such as gas barrier properties[115]. The possibility of creating both structural and functional systems is even more feasible for graphene filled nanocomposites due to the larger specific area, improved interfacial adhesion, and outstanding properties. Besides, at extremely small loading, graphene as a filler manage to improve properties of the host polymer[93]. Rafiee et. al has reported on enhancement of mechanical properties of nanocomposite at low graphene content[116]. In that work, nanofiller weight fraction of ∼0.1% was used and amazingly managed to increase Young's modulus of the nanocomposite up to 31%; from 2.85 to ∼3.74 GPa. On the other hand, another previous

work reported by Wang et.al associated with GO as a physical crosslinker in hydrogel network. Recently, graphene and its derivatives have demonstrated their capability as effective adsorbents for contaminant removal from water[117]. The challenge that must be overcome is to exfoliate graphite in sufficiently large quantity to be used as an inexpensive and feasible substitute to CNTs and traditional filler materials. Figure 2.27 depicted the comparison of Young's modulus as a function of density for graphene with respect to other materials[107]. The reported binders or cross-linkers include polymers[118-119], organic or inorganic compounds[114, 120-121], metal ions[121-122] and biomolecules[123-124].

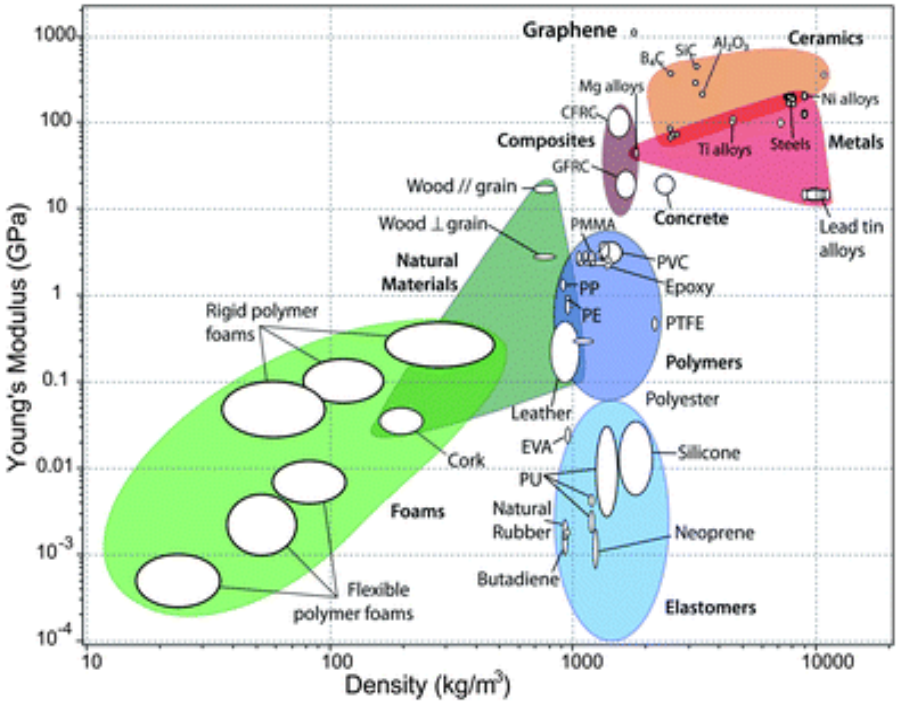

Figure 2.27: Chart of Young's modulus as a function of density to compare graphene properties with respect to other traditional materials[107].

Functionalisation is an important key tool to deliver graphene as an engineering material for various industries. As such, GO is a great representative for functionalised graphene. The organic functionalities are capable of enhancing the compatibility between graphene and polymeric matrices via hydrogen bonding. In addition, the wrinkled surface of graphene can mechanically intertwine with polymer chains to improve the interface. In the previous work

conducted by Ramathan et.al, the elastic modulus and ultimate strength of the PMMA were improved by nearly 80% and 20%, respectively, just by incorporation of 1 wt.% functionalised graphene (FG)[125]. In that work, it was found that PMMA chains were confined the polymeric regions on the surfaces of graphene exfoliated sheet. Owing to this reason, unprecedented increase in the glass transition temperature (T_g) of PMMA was obtained.

The significant reinforcing effect of GO was also found in a PVA system due to strong hydrogen bonding interaction between PVA and GO[126-128]. The addition of 0.3 wt.% GO resulted in 76% enhancement in tensile strength and 62% improvement of Young's modulus values. This fairly low concentration of GO resulted in an efficient load transfer between graphene filler and PVA matrix via strong hydrogen bonding. Additionally, the achievement of significant mechanical enhancement with such low loading indicates that matrix properties could be maintained for multifunctional graphene nanocomposite materials. Previous work related to PVA and GO was reported that Young's modulus and tensile yield strength obtained were 4.8 GPa and 110 ± 7 MPa, respectively with addition of 3 wt.% GO in the composite film. The reason for an improvement in mechanical properties mainly due to the homogenous dispersion of GO sheets in the polymer matrix and strong interfacial interactions between them. Rafiee et al reported that incorporation of 0.125 wt.% of FG resulted in ≈ 65% enhancement in the fracture toughness value. On the other hand, Zhang and Fan have found that only a small content of GO (lower than 2.0 wt.%) could significantly improve the hybrid polymers (cross-linked sodium acrylate and acrylamide copolymer graphene oxide) adsorption performances and mechanical strength[22]. Therefore, GO seems to be as an ideal filler to be incorporated with hydrogel and polymeric materials to obtain remarkable properties.

2.5 Effect on cation on the gel properties and structure.

Hydrogels with high toughness have received great attention owing to their application in many fields. Dynamic non-covalent bonds could be incorporated as crosslinks to develop tough physical gels. In toughening mechanism, the strong association served as permanent crosslinks and the weak association as sacrificial bonds to dissipate energy[129]. Introduction of materials containing metal−polymer complexes possess intriguing mechanical properties and potential applications in various industries such as ion-conducting solid membranes used in batteries, semiconducting material, pharmacological applications, membranes for artificial organs, polymer catalysts, materials with tuneable mechanical strength and wastewater management[130-131,132-133].

There are various cations can be incorporated into polymeric network such as divalent or trivalent cations (Ca^{2+}, Zn^{2+}, Cu^{2+}, Al^{3+}, and Fe^{3+}) to improve mechanical properties of the gels. The metal-ligand coordination bond resulted in tuneable properties with improved toughness and stiffness[132, 134]. Cations valence have profound effect on the stiffness of the gel[135-136]. Previous work by Maestri et. al in 2017 focused on negatively charged nanocrystal from cellulose with addition of cations such as Na^{2+} and Ca^{2+}. The cations in that work increase the interactions between the chains that form the gel and modify the gel properties drastically[136].

Research work done by Kaygusuz et al in 2016 concerned on addition of various dopants to alginate formulations that increased chemical and mechanical stability of the gels[137]. One of the candidates for dopants is type of surfactants. Previously, the effect of cationic surfactant cetyltrimethylammonium bromide (CTAB) on viscosity and the effect of SDS on aggregation of alginate solution were studied by Yang et al[138]. Previous work reported on alginate beads containing non-ionic Brij35 or anionic sodium dodecyl sulphate (SDS) surfactants that were

prepared with two different types of cations (Ca^{2+}, Ba^{2+}) as crosslinkers[137]. Most importantly, Young's modulus can be altered by changing the alginate concentration or the type concentration of the surfactants or crosslinking divalent cation. For DN hybrid gel, it was reported when Ca^{2+} was replaced by other multivalent ions (e.g., Ba^{2+}, Al^{3+}, and Fe^{3+}), the hybrid DN hydrogels showed improved mechanical properties. The dimensional stability and gel strength increased for alginate gels when exchanging the traditional Ca^{2+} ions with Ba^{2+}. The use of Ba^{2+} decreased the size of alginate beads and reduced permeability of alginate beads[139].

Another studied conducted in 2017 showed that storage moduli obtained for star block copolymer hydrogels crosslinked using Fe^{3+} were 26−1400 Pa and they were stable in PBS (pH 7.4) for up to 1 month[140]. The reason for good mechanical performances is due to sacrificial bonds such as metal coordination that act as non-covalent bond[132]**.** New materials with advanced properties such as photochemical, electrochemical and catalytic have been developed by reversible metal-ligand complexes by Chen et al in 2004[141]. This class of material has self-healing capability and the distribution of metal-ligand complexes are analysed. To select appropriate metal-ligand pair, it must be related with enthalpy (small and large depending on the first and second metal-ligand bond). Linear coordination polymers were obtained for different metal ions, such as Fe^{2+}, Zn^{2+}, Ni^{2+}, Cu^{2+}, and Co^{2+}[141]. Zhang and co-workers reported PAA hydrogels with Fe^{3+} ions to obtain new kind of hydrogel. PAA hydrogel itself has high stretch ability and toughness but is low in fracture strength. It was found that Fe^{3+} ions played a key role in the improvement of mechanical properties for two kinds of gels[142]. Ionic crosslinking between Fe^{3+} ions with carboxylic acid group were responsible for the increase in strength (the fracture stress obtained was quite impressive 308 kPa)[142]. By increasing the Fe^{3+} ion content, crosslinking density enhanced and resulted in de-swelling

behaviour. Meanwhile, at high swelling ratio, dissociation of hydrophobic interactions was responsible for the gels physically increased in size.

2.6 Pb toxicity and removal from water

Toxic heavy metals cause a range of ailments and threats to eco-system and public health. Heavy metals are of special because of their persistence and tend to accumulate in living organisms[143] and occur due to industrial processes and natural ones. There are several important heavy metals in the treatment of wastewater that requiring removal such as Cu, Zn, Pb, Cd, Hg, Ni and Cr[143-145]. These metallic elements are considered systemic toxicants that are known to induce multiple organ damage, even at low levels of exposure[22, 146]. Heavy metal ions are also classified as human carcinogens (known or probable) according to the U.S. Environmental Protection Agency and the International Agency for Research on Cancer[1]. However, primary concern is given to Pb due to its high level of toxicity and harmfulness to human, animals and plants. In fact, Pb is ranked as one of the five elements among the priority metals that are of great public significance because even at low level exposure it will induce multiple organ damage (systemic toxicant)[6,147]. Pb is very prominent in source area such as batteries, plastic construction, mining, combustion, and electronic devices[145,148-149]. Pb is one of the common heavy metals found in water bodies coming from industrial effluents, agriculture wastewaters, chemical manufacture and landfill leachates[150]. In addition, this element can be found as a component of insecticides, batteries and water pipes[8,151]. Pb also is widely used in car batteries, electronic items and ammunitions. In fact, Pb pollution may result from perovskite solar power as ongoing research focusing on solar cell in the presence of Pb for the metal form[152]. The improper disposal from these industries contributes to the rise level of Pb in the water. In children, blood Pb concentration is associated with learning impairments, as well as hyperactive and violent behaviour[8].

Adsorption is considered an eco-effective purification and separation technique used in wastewater treatment over the last few decades. This has led to the development of low-cost adsorbents with excellent adsorption efficiency, good mechanical stability, and simple operating performance[153-155]. Adsorption of heavy-metal ions with various adsorbents, such as clays, nanosized metal oxides, polymer and polymer-based hybrids has been a great deal of interest for water treatment[8, 156-157]. In recent years, various adsorbents have been used for the removal of Pb^{2+} from aqueous solution, and the efficiency of adsorption depends on many factors, such as the surface area, pore size distribution, polarity, and functional groups of the adsorbent[158]. Polymeric adsorbents can be effective for toxic heavy metal ions in wastewater treatment due to their ability to interact with these heavy metal ions[154, 159]. Pan et.al found there were many polymeric chelating adsorbents found for selective heavy metals removal from aqueous media such as poly(methacrylate-oylamidoglutamic) acid groups poly(MMA-MAGA) and poly(GMA-co-EGDMA) with the target pollutants Hg^{2+}, Cd^{2+}, Pb^{2+}, Pt^{4+} and Cu^{2+} [154]. Table 2. shows various of adsorbent specifically for Pb^{2+} and maximum adsorption capacity achieved. The table shows the comparison of existing adsorbents that were studied by various researchers from all over the world. These findings show the capability of the different types of composite hydrogel and graphene in removing Pb^{2+} ions at different adsorption capacity.

Table 2.1: Summary for maximum adsorption capacity (q_m) of Pb^{2+} uptake by various adsorbents.

Adsorbents	**q_m for Pb^{2+}**	**References**
Cottonseed protein PAA hydrogel composite	3.47 mmol/g	[160]
Chitosan-g-poly(acrylic acid)/ attapulgite/sodium humate (CTA-g-PAA/APT/SH)	900 mg/g	[157]
Magnetic attapulgite/ash/poly(acrylic acid) nanocomposites	91.8 mg/g	[161]
Nanofibrous membrane	137.7mg/g	[162]
Graphene aerogel	80 mg/g	[163]
Graphene oxide-chitosan hydrogel	90 mg/g	[164]
Chitosan-poly(acrylic acid) graphene oxide	138.9 mg/g	[165]
2-imino-4-thiobiuret-partially reduced graphene oxide (GO)	101.5 mg/g	[108]
Bentonite/sodium lignosulfonate graft-polymerized with acrylamide and maleic anhydride (BLPAMA).	314 mg/g	[149]
PVA matrix	123 mg/g	[166]
Activated carbon	21.8 mg/g	[167]
P(NIPAM-co-BCAm) hydrogels	143.1 mg/g	[168]
Crosslinked chitosan granules (CTS) with poly(acrylic acid)	294.1 mg/g	[153]
Chitosan PVA hydrogel	0.6 mg/g	[169]
Tetrathylenepentamine graphene foam (TEPA-GF)	304.9 mg/g	[170]
Carboxylic-functional carbon coated PAN nanofiber	153.4 mg	[171]

2.7 Summary of literature review

Despite extensive research involving MGs with co-monomer such as MAA, AA and MAA, none of the previous studies is reported on the formation of MGs with CEA as co-monomer by emulsion polymerisation. Therefore, further research related to this work is a breakthrough to develop greater understanding in the formation of MGs with CEA at different CEA content and further investigations on physical and mechanical properties are required. From the literature reviews that highlighted in this chapter, it has been reported the role of GO as filler in the polymer network even at low loadings which resulted in an enhancement of mechanical properties such toughness Young's modulus. Even though research on hydrogel with GO has been growing recently, limited studies have been published regarding GO and DX NGs (specifically for NGs), thus, comprehensive studies on the effect of low loading GO in this DX networks are required. Besides, the knowledge regarding the mechanical and physical properties of this DX network can provide further understanding in the network structure to suit the application for water purification. GO is an excellent candidate in coordinating with other materials or molecules due the surface functional groups of hydroxyls, epoxy and carboxy. Owing to the expanded structural diversity and improved overall properties, GO and its composites hold great promise for versatile applications of water purification. A comprehensive study on the Pb^{2+} removal by DX NG and DX NG/GO is required to investigate the potential of these gels in removing heavy metal ions. Besides, it is important to understand the connection between Pb^{2+} adsorption and its effects on the mechanical properties of the gels. Therefore, mechanism of Pb^{2+} removal by DX NG and DX NG/GO is required in understanding the effect of addition of GO into the gel network.

CHAPTER 3 : STUDY OF MICROGELS AND DOUBLE-CROSSLINKED MICROGELS CONTAINING 2-CARBOXYETHYL ACRYLATE

3.1 ABSTRACT

This chapter investigates a new pH responsive MGs containing 2-carboxyethyl acrylate (CEA) as co-monomer. In this work, MGs were synthesised by emulsion polymerisation and denoted as CEA*X* whereby *X* shows different CEA content in MGs. These MGs samples were denoted as CEA14, CEA21 and CEA28 and were compared with the previously reported system that containing methacrylic acid (MAA). The CEA MGs were vinyl functionalised and used to prepare three DX MGs gels denoted as DX CEA21, DX CEA28 and a blend system that contained both CEA21 and CEA28 in order to observe the effect of a binary system. The latter system is denoted as DX BL-CEA. The properties of MGs systems were investigated by dynamic light scattering (DLS), potentiometric titrations and zeta potential measurements. The MGs showed comparable swelling with the established MAA MGs. The performance of the gels was further studied by swelling ability, UV-visible spectroscopy, rheology and compression analysis. The morphologies of all systems were investigated by SEM and TEM analysis. The DX BL-CEA gel had much greater opacity than DX CEA21 and DX CEA28. The ductility of DX CEA gels was greater than the established DX MAA gels. The Young's modulus value of the binary system, DX BL-CEA was very close to DX CEA28 gel. Strong light scattering for DX BL-CEA gel was confirmed by UV-visible spectra and is further discussed. The data obtained in this chapter shows that the use of CEA in place of MAA resulted in tunable properties of the gels.

3.2 INTRODUCTION

In general, CEA molecule is structurally similar to 2-hydroxyethyl acrylate (HEA) but has -COOH groups[172]. CEA contains an ester group and is a vinyl acid monomer. In addition, CEA is water-soluble monomer, has low toxicity and is frequently used in co-polymerisation process[172-173,174]. The difference between CEA and MAA is their degree of ionisation which has significant effect on the swelling properties[175]. The rheological properties of such systems are strongly influenced by the degree of ionisation and the pH[176]. The distribution related to carboxylic acids monomers (CEA or MAA) between water and organic phase are different and CEA distributions are very much closer to AA than MAA[172].

A significant difference of CEA compared to other carboxylic acids is the flexibility as poly(CEA) has a low glass transition temperature (T_g)[177]. CEA is an ideal selection because it has higher molecular weight than MAA (144 g/mol and 86 g/mol for MAA) and it is commercially available. Furthermore, CEA can be more compatible with other co-monomers and may produce a uniform copolymer when prepared by free radical co-polymerisation[178]. The pK_a value of CEA is 4.99[178]. As reported in literature, pK_a value for MAA and AA are 4.45 and 4.23[172]. In this work, CEA-based MGs will be compared to MAA based MGs that reported in the previous work[179]. The behaviours of MGs containing different CEA content were analysed with respect to their particle size, swelling ability, morphology and mechanical properties. These systems are functionalised with glycidyl methacrylate (GMA) to enable subsequent formation of DX MGs, in example DX CEA.

The general concept of using a blend system is invoked to modulate the properties of DX gels. The blend DX MGs is denoted as DX BL-CEA which contains functionalised CEA21 and CEA28 MGs. It is hypothesised that the properties of the DX CEA gel such as swelling and light scattering can be tuned by blending between the two components. A depiction

of the preparation of DX CEA gels is shown in Figure 3.1 (see experimental section for the details). The chemical structures of AA and MAA were included for reference. In this work, DX CEA gels were denoted as DX CEA21 and DX CEA28. The aim of this work is to study the effect of CEA on MGs particle growth and how the blend CEA modifies the mechanical properties of the gels.

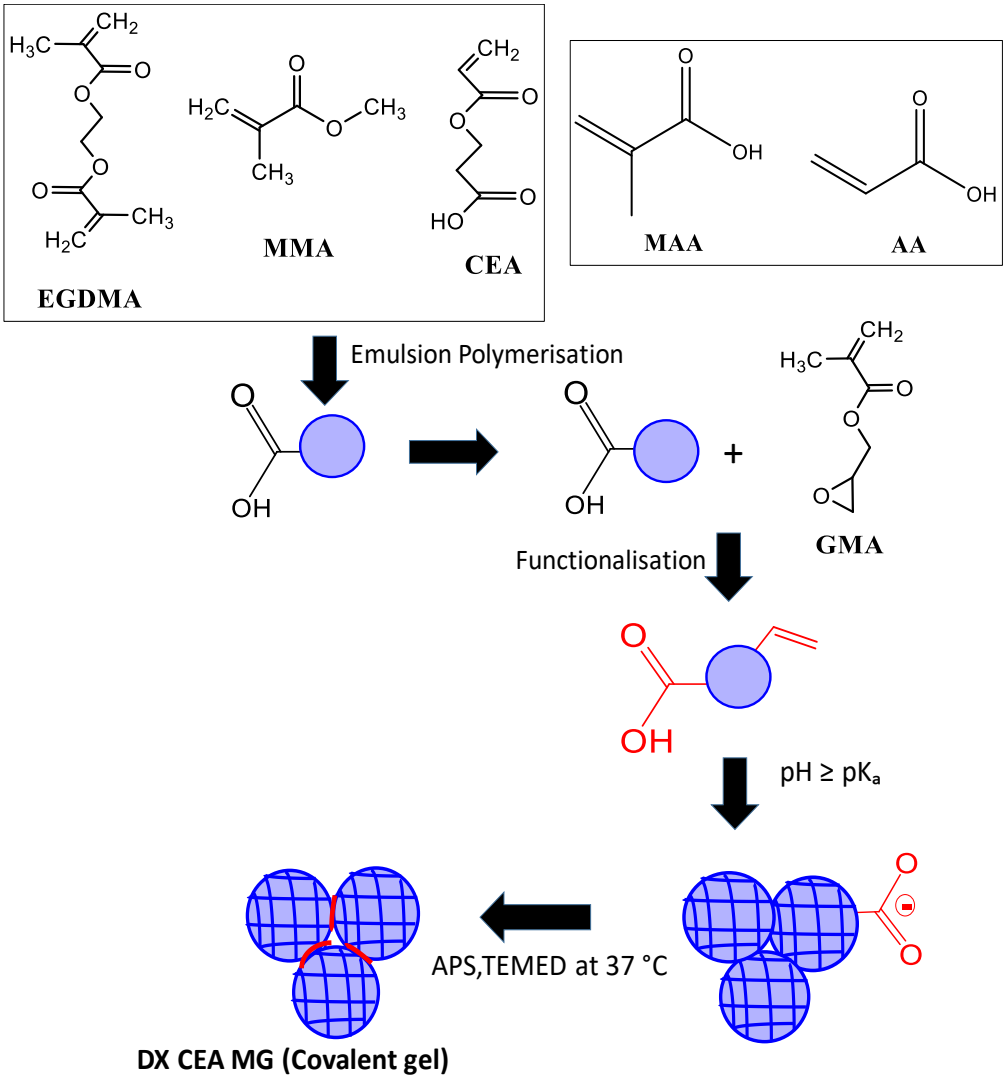

Figure 3.1: Schematic representation of the method used to prepare pH-responsive MGs and DX MGs. The particles were prepared by emulsion polymerisation. MGs were functionalised with GMA. The functionalised microgels was transformed to a physical gel (pH ≥ pK_a) and formed double-crosslinked gels in the presence of ammonium persulfate (APS) and *N*,*N*,*N*,*N*-tetramethylethylenediamine (TEMED) at 37°C. The structures of MAA and AA are shown for comparison.

3.3 EXPERIMENTAL

3.3.1 Materials

In this work methyl methacrylate (MMA, 99%), methacrylic acid (MAA, 99%), glycidyl methacrylate (GMA, 97%), 2-carboxyethyl acrylate (CEA), sodium dodecyl sulphate (SDS), ammonium persulfate (APS, xx%), $NaNO_3$ (> 99%), NaOH, ethylene glycol dimethacrylate (EGDMA,98%) and *N,N,N′,N′*-tetramethylethylenediamine (TEMED,99%) were obtained from Sigma-Aldrich and used as received. All aqueous solutions were prepared using high purity deionised water.

3.3.2 Synthesis of microgels

MGs were prepared by emulsion polymerisation at 80°C. A brief description of the procedures is given here for MGs containing MMA, CEA and EGDMA. Firstly, SDS (1.214 g) was dissolved in deionised water (240 g) and added to the glass reaction vessel. Before the monomer feed started, APS (0.158 g, 0.60 mmol) was dissolved in water (2.0 ml) and added to the vessel. The monomer feed contained a mixture of MMA (42.0 g, 0.419 mol.), CEA and EGDMA (1.06 g, 5.35 mmol) was prepared with mechanical stirring and fed into the reaction vessel at constant rate of 0.317 ml/min. The masses of CEA used to prepare CEA14, CEA21 and CEA28 were 9.94 g (0.069 mol), 16.27 g (0.113 mol) and 23.76 g (0.165 mol), respectively. After the comonomer solution feed was finished, the reaction was continued for 1 hour. The product was purified by extensive dialysis using water for 7 days. The deionised water that used for dialysis was changed twice a day to remove any excess of surfactant. The MGs obtained are denoted as CEA14 (14 mol%), CEA21 (21 mol%) and CEA28 (28 mol%). The mol% values are calculated with respect to the total monomers used. Data for a MG from related work[180] that contained methacrylic acid (MAA) in place of CEA is included for comparison in this study. That MG contained MMA, MAA and EGDMA with a MAA

concentration of 38 mol.%. Table 3.1 shows the composition of mixed co-monomer to prepare CEA MGs in this research work.

.

Table 3.1: Composition of mixed co-monomer solution used to prepare CEA MGs.

Abbreviations	**CEA**	**MMA**	**EGDMA**
CEA14	14 mol.%	85 mol%	1.0 mol%
CEA21	21.4 mol.%	77.68 mol%	0.92 mol%
CEA28	28 mol.%	71.14 mol%	0.86 mol%

3.3.3 Functionalisation of microgels

GMA was used to vinyl functionalise the MGs. GMA (3.0 g, 0.021 mol.) was added to a MG dispersion (120 g, 5.0 wt.%) and the pH of the mixture adjusted to 5.1 by addition of aqueous NaOH solution (0.05 M). The mixture was heated to 40°C for 8 hours with vigorous stirring. After the reaction was completed, hexane was used to wash the product twice by using separatory funnel. The product obtained was further concentrated by rotary evaporation at 25°C to remove residual hexane. GMA functionalised CEA MGs are denoted as GM-CEA*X* for the rest of the chapter where *X* is the mol.% of CEA that originally incorporated. The control GMA-functionalised MG is referred to as GM-MAA and was selected based on the GMA content.

3.3.4 Preparation of double-crosslinked microgels

DX MGs were prepared using similar method as has been reported here[64,181]. The method used here is a scalable synthesis method for NGs and MGs. To prepare DX gel, GM-CEA*X* (2.0 g of 14 wt.% dispersion) was vortexed with mixture solution of 0.2 ml of NaOH (4.0 M), APS (0.10 M) and an accelerator, TEMED (1.0 M). The addition of NaOH, APS and TEMED caused the viscosity to increase and physical gel was formed at pH 7.5. This physical gel was shaped into a 20 mm circular disc using a rubber O-ring placed between two glass sides. Two bulldog clips were used to clamp the glass slides together to prevent evaporation. The mould was heated at 37°C for 24 hours to allow crosslinking to occur and these DX gels were labelled as DX CEA21, DX CEA28 and DX BL-CEA.

3.3.5 Physical measurements

3.3.5.1 Potentiometric titration

Potentiometric titration measurements were carried out using a Mettler Toledo DL15 Titrator to determine carboxylic acid content of the MGs sample. For a typical preparation, 1.0 wt.% of dispersion was mixed in 40 ml of aqueous 0.05 M NaCl solution. The diluted dispersions were stirred mechanically for 20 seconds at room temperature. The diluted dispersion was titrated against a standardised NaOH (1.0 M) solution. The average apparent pK_a values were calculated using the pH at % neutralisation of 50%.

3.3.5.2 Dynamic Light Scattering

The hydrodynamic diameter measurements of the MGs were carried out using dynamic light scattering (DLS) with a Malvern Nano Zetasizer ZS90 instrument fitted with a 20 mW He-Ne and the 90° scattering angle was used. Typically, the sample had final concentration of 0.01 wt. % to remain the photon count rate between 100 and 200 kcps. Whilst, to change the pH of

the samples, different phosphate buffers of 0.1 M were used. The z-average diameter measured by DLS at low pH shows the collapsed particle size(d_{coll}) whereas high pH shows swollen particle size (d_{swoll}). These measurements were used in equation 3.1 shown below to calculate the particle swelling ratio:

$$Q = (d_{swoll} / d_{coll})^3 \quad (3.1)$$

3.3.5.3 Zeta Potential Measurements

Zeta potential measurements were calculated using a Malvern Zetasizer NanoZS90 instrument. The dispersion concentration of 0. 1 wt. % with presence of 0.001 M $NaNO_3$ were prepared. Then, the dilute mixture was transferred to the measurement cell using 1 ml plastic syringe. The average zeta potential was measured from three measurements at pH 4, 5, 6, 7, 7.5,8, 9 and 10. The temperature was set to 25°C.

3.3.5.4 Gel Swelling

Swelling measurements were conducted by placing the gels of each system in the beaker filled with phosphate buffer solutions to observe the swelling behaviour. The diameter of the gels was 20 mm. The gels were placed in the beaker for four days and were weighed once a day. Before weighing, the gel was gently wiped to remove excess water on the surface. The phosphate buffer solutions were replaced every day to maintain the consistency of the pH. The volume swelling ratio was calculated using the equation below[71-72]:

$$Q_{DX} = \rho_p \left(\frac{Q_{DX(m)}}{\rho_s} + \frac{1}{\rho_p} \right) - \frac{\rho_p}{\rho_s} \quad (3.2)$$

where $Q_{DX(m)}$ is the mass swelling ratio and ρ_p and ρ_s values are the densities of the polymer and solvent, respectively. The values for ρ_p and ρ_s values were taken as 1.2 and 1.0 g/ml, respectively.

3.3.5.5 Dynamic Rheology

Dynamic rheology measurements were conducted using a TA Instruments AR-G2 temperature-controlled rheometer equipped with an environmental chamber. A plate geometry of 20 mm diameter was used with a solvent trap to prevent the sample from evaporate. An oscillating stress was applied to the gels in a frequency sweep where a constant strain (1%) and increasing frequency (from 0.01 rad/s to 0.1 rad/s) was applied. Strain sweep was conducted with a constant frequency (0.628 rad/s). The gap was set at 2500 μm. Three samples were tested for each system.

3.3.5.6 Uniaxial Compression

Uniaxial compression measurements were conducted using an Instron series 5569 load frame equipped with a 100 N load cell. The compression rate was conducted at 2 mm/min and the average height and diameter of the gel cylinders were 12 mm and 11 mm (the appropriate dimension for compression analysis), respectively. Young's modulus values were calculated from the initial gradient of stress-strain curves at strains (ε) of less than 10%. Engineering stress and strain are used in this work.

3.3.5.7 Scanning Electron Microscopy

SEM images for the gels were recorded using a Philips XL30 FEG-SEM HKL EBSD instrument with accelerating voltage of 15 kV. For scanning electron microscope (SEM) morphology observation, the MGs were diluted into different concentrations using water. A droplet from each sample was pipetted onto glass slide that was placed on the stub and was left

to dry overnight at room temperature. All crosslinked gel samples were freeze-dried in the liquid nitrogen for 3 days. Then. the samples were cut into fine pieces and placed on the carbon tape on the stubs.

3.3.5.8 Transmission Electron Microscopy

TEM images were obtained using a Philips CM20 instrument. All samples were prepared on 400 mesh copper grids and analysis was operated at 200 keV. For sample preparation, 0.4 ml of 0.2 wt.% of dispersion was mixed with 1.6 ml of 2 wt.% of phosphotungstic acid (PTA) around 15-20 minutes at room temperature. The final mixture concentrations used were approximately 0.04 wt.%. A single drop (μL) of the mixture was pipetted onto a 400-mesh copper of holey carbon grid (Agar Scientific Ltd.) and left for 2 minutes before the excess liquid evaporated. The samples were left to dry overnight in the desiccator. At least 100 particles were used to calculate the number-average diameter (d_{TEM}) by using the following equation:

$$d_{TEM} = \frac{\sum n_i d_i}{\sum n_i} \tag{3.3}$$

where d_i is diameter of particles in group i and n_i is the number of particles in group i. The coefficient of variation (CV) was calculated from the standard deviation (SD) using equation 3.4:

$$CV = \frac{(100\ x\ SD)}{d_{TEM}} \tag{3.4}$$

3.3.5.9 UV-Visible Spectroscopy

UV-Visible spectrometer Perkin Elmer Lambda 25 UV/VIS was used to record the spectra and further investigate the potential of DX MGS for UV-blocking properties. The sample was prepared in gel form with diameter of 10 mm and placed on the quartz glass slide. The glass slide then was placed in the sample holder compartment. The measurements were conducted with the wavelength range between 290-900 nm. The equilibration time for each temperature measured was 1 min. The similar procedure was used for UV-vis analysis for DX NG and DX NG/GO in Chapter 4.

3.4 RESULTS AND DISCUSSION

This section provides the findings related to CEA based MGs prepared by emulsion polymerisation. The physical and mechanical properties of the MGs are studied. The results of MGs and DX MGs containing MAA as co-monomer reported by Milani et.al[179] will be compared to DX CEA gels.

3.4.1 Dispersion characterisation and properties

3.4.1.1 Dynamic light scattering and zeta potential of CEA microgels

Four different structural of monomers with various CEA content were prepared to understand the relationship of CEA with particle size and distribution. Table 3.2 shows the summary of MGs characterisation data for the MGs. The experimental values from potentiometric titration of three different MGs systems with difference CEA contents were obtained; 20.5, 29.4 and 60.4 mol.%. A possible explanation for the different values compared to theoretical values might be related to an interaction between another co-monomer such as MMA and EGDMA with CEA during polymerisation. This result may be explained by the fact that -COOH groups in CEA being more available than those in the conventional carboxylic acid and can be

incorporated into co-polymer at higher level[182]. Another important finding is the use of higher CEA contents (beyond 28 mol.%) caused aggregation possibly due to an excess water-soluble of CEA-rich polymer that occurred due to instability of the colloid dispersion[183]. The system contains beyond 28.mol% of CEA is not further investigated. From an implication stated above, three systems denoted as; CEA14, CEA21 and CEA28 were explored.

Table 3.2: Characterisation data for the MGs studied; CEA14, CEA21, CEA28 and MAA.

System	**CEA**[a]**/ mol %**	**pK_a**[b]	**d_{TEM}**[c] **/ nm**	**d_z**[d] **/ nm (pH 4)**	**d_z**[e]**/ nm (pH 10)**	**Q**[f]	**ζ**[g] **/ mV (pH 4)**
CEA14	20.5	7.2	28 ± 7	39	71	6	-38.0 ± 0.3
CEA21	29.4	7.1	59 ± 9	84	210	16	-43.4 ± 2.4
CEA28	60.4	5.9	204 ± 29	255	980	57	-55.6 ± 3.5
MAA[h]	38.0	-	-	89	184	-	-

[a] CEA content obtained from titration analysis with respect to total monomer.
[b] p*Ka* value obtained from titration analysis.
[c] Number-average diameter determined from TEM measurements.
[d] Particle size obtained from DLS measurements.
[e] Particle size obtained from DLS measurements.
[f] Swelling ratio determined using equation 3.1 at pH=4 and pH=10.
[g] Zeta potential value obtained below p*Ka* at pH 4.
[h] MAA mol.% from Ref.[179].

Figure 3.2 depicts SEM morphologies for CEA14, CEA21 and CEA28 systems. From the SEM images, higher CEA content resulted in larger particle size. The particle sizes for all systems are homo-dispersed and in spherical shape. Figure 3.3 shows the morphologies for CEA14, CEA21 and CEA28 obtained by TEM and the particle size obtained is consistent with SEM results. For validation, the MGs were further characterised by DLS and zeta potential. The z-average diameters (d_z) from DLS measurements for these three systems are 39 nm for CEA14, 84 nm for CEA21 and 255 nm for CEA28 at pH 4.0

(collapsed state). These values are larger than the number-average diameters from TEM (Figure 3.3) due to the presence of water in the dispersed particles and their polydispersity. The DLS size distribution of each system can be seen in Figure 3.4a. From this graph, it was observed that CEA14 and CEA21 have narrow size distribution compared to CEA28. Nevertheless, CEA28 still has low polydispersity index of 0.087 (as supported by SEM shown in Figure 3.2). From the data obtained in Table 3.2, the MGs size strongly increased when CEA content increased (Figure 3.4b). At higher CEA content, growing particles was stabilised more effectively than MMA which resulted in fewer particles would form and they would be larger[183]. In general, surfactant concentration, monomer concentration and initiator are important parameters in determining particle size[184].

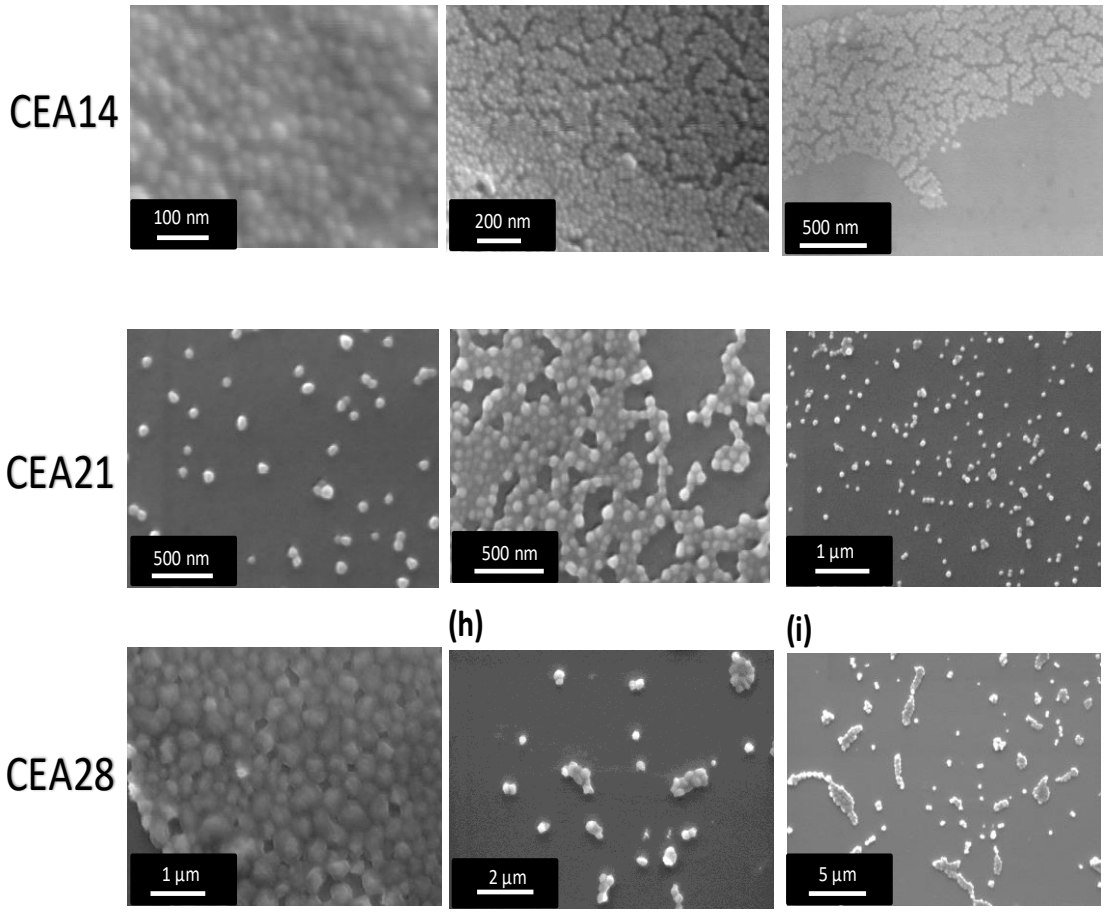

Figure 3.2: SEM images of CEA14, CEA21 and CEA28 at different magnification.

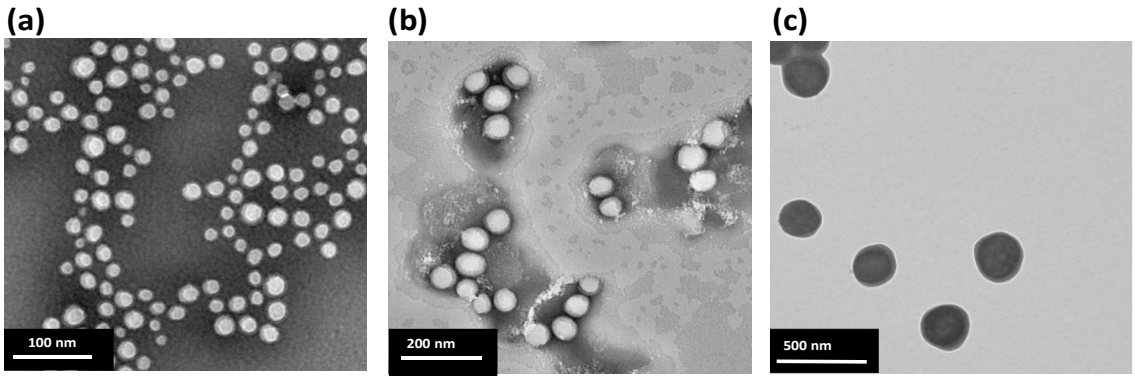

Figure 3.3: TEM images for (a) CEA14, (b) CEA21 and (c) CEA28 particles.

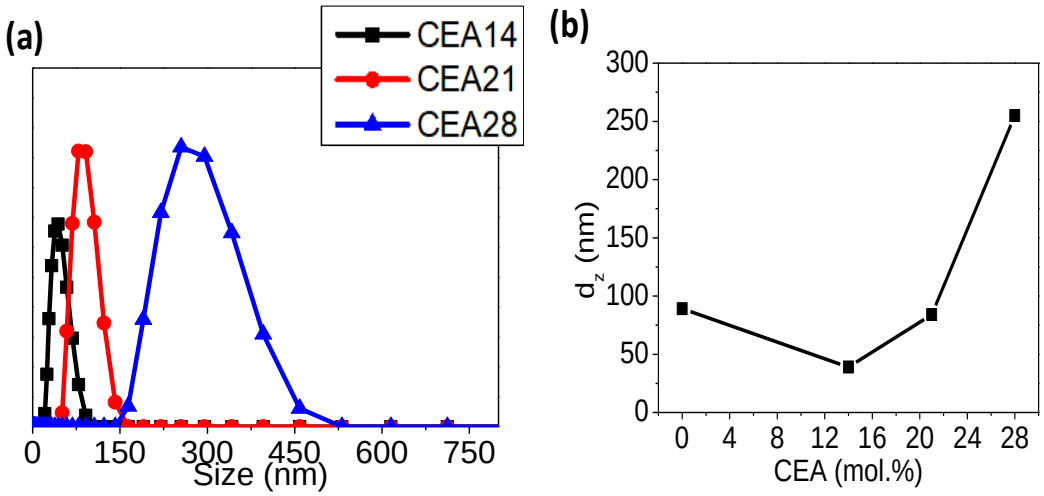

Figure 3.4: (a) Size distribution obtained from DLS for CEA14, CEA21 and CEA28; (b) Correlation between CEA content (mol.%) and MGs particle size.

The pH dependence of the z-average diameter (d_z) and zeta potentials (ζ) are compared for MGs containing CEA system (Figure 3.5). The results show a significant transition from collapsed state to expanded state when the pH approaches the pK_a of the MGs which is considered the same as the pK_a of ionisable groups. It is reasonable to associate the region of main particle swelling for the MGs with its effective pK_a. It was observed that the swelling extent gradually increases, and complete swelling occurred by pH of about 9. The MGs particle exhibited pH-dependent swelling with maximum diameter

at pH=9 for CEA14, CEA21 and a CEA28. The particles at that specific pH had d_z of 71 nm for CEA14, 213 nm for CEA21 and 980 nm for CEA28. The maximum particle swelling ratio (Q) was obtained by CEA28 (Table 3.2). As the CEA content for each system is different (CEA28 contains highest acid content), possibly more ionisable groups enabled higher swelling degree[185]. The MGs particle size for another two systems remain below 240 nm.

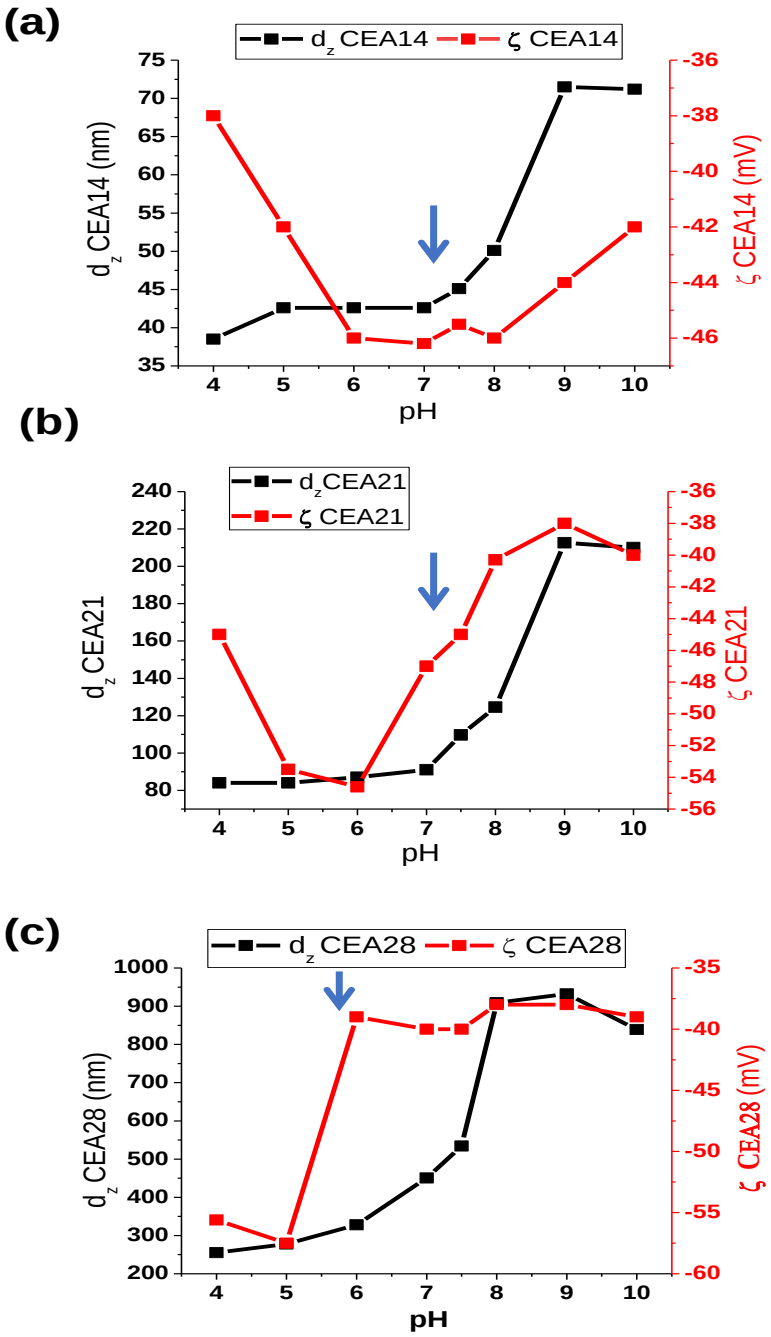

Figure 3.5: pH-dependent z-average diameter, d_z (nm) and zeta potential, ζ (mV) values for (a) CEA14; (b) CEA21; and (c) CEA28. The blue arrow shows the pK_a values.

In all cases, the ζ values initially increase in magnitude as the pH increases from 4.0 and a maximum value is reached. As the pH further increases, ζ decreases which corresponds to the pH being greater than the pK_a values. The ζ value for MGs is known to be most sensitive to the charge density at the particle periphery[186]. This behaviour demonstrates swelling of the shell of the MGs. The closer the onset of the d_z and ζ values are, the distribution of carboxylic acid group in the particle are becoming more homogeneous due to the changes in the whole particle and surface swelling. Accordingly, it is suggested that the CEA groups are well-distributed throughout the CEA14 particles. However, they are increasingly located at the shells for the CEA21 and CEA28 particles.

3.4.1.2 GMA functionalisation of microgels

GMA was used to functionalise the MGs to provide the vinyl groups for DX MG formation[72,85]. The acrylic/vinyl groups permit crosslinking with other vinyl monomers[187]. The mechanism of GMA attachment with carboxylic acid groups is believed to have involved a ring-opening reaction[64]. This functionalised MGs particle exhibited pH-dependent swelling with maximum diameter at pH=9 for all systems; 71 nm for GM-CEA14, 217 nm for GM-CEA21 and 1000 nm for GM-CEA28. Above pH=9, the size is constant because particle swells to most of its maximum volume.

Titration data for all systems are shown in Figure 3.6. Potentiometric titration analysis is widely applied to characterise the total acid group content as well as the behaviour of counterions within the MGs matrix. Titration results confirmed the decrease of acid content after functionalisation (see summary in Tables 3.2 and 3.3). The GMA contents were in the range of 5.3 to 17.9 mol.% and were calculated by the difference in CEA content before and after functionalisation. From the graphs obtained, we observed that the pK_a decreased as the

CEA content increased, and these values ranged from 7.2 for CEA14 to 5.9 for CEA28 (Table 3.3). The apparent pK_a values were determined from the pH that corresponding to 50% of carboxylic acid groups reacted as shown by the vertical dot line. It was proposed that addition of GMA contributed to the changes of pK_a. Comparison of MGs system before and after functionalisation was shown in Figure 3.6 and the pK_a values obtained were displayed in Table 3.2 and Table 3.3. By referring to Table 3.3, the pK_a values were decreased significantly because of GMA functionalisation for CEA21 and CEA28, which had the highest GMA contents. This behaviour is unexpected because an increased in hydrophobicity should increase the pK_a[188]. Nevertheless, the same reverse trend has been seen in amino(base) containing amphiphilic macrogels (pK_a decreased with increasing hydrophobic content)[189-190]. This finding was unexpected and suggests that it could be associated with a disruption of physical crosslinks which oppose swelling and provide greater chain flexibility[181]. The possible reason for the pK_a decreased upon functionalisation is due to distribution of functional groups that are "buried" within polymer networks and typically have higher effective pK_a values[191]. In addition, MGs system contained high GMA contents which is up to a third of CEA groups reacted.

Table 3.3: Characterisation data for GMA functionalised MGs at different CEA content.

Abbreviations	**CEA[a]/ mol %**	**pK_a[b]**	**GMA/ mol%**	**d_z[c] *TEM / nm***	**d_z[d] / nm (pH 4)**	**d_z[e]/ nm (pH 10)**	***Q*[f]**	**ζ[g] / mV (pH 4)**
GM-CEA14	15.2	6.8	5.3	35 [8]	41	74	6	-39 ± 0.7
GM-CEA21	21.2	6.3	8.2	62 [15]	92	217	13	-44.5 ± 1.8
GM-CEA28	39.1	5.4	21.3	219 [17]	278	1000	47	-52 ± 6.6
GMA-MAA[h]	20.1[h]	6.5	17.9	77 [15]	90	277	29	-

[a] CEA content obtained from titration analysis after considering GMA functionalisation.
[b] pK_a value obtained from titration analysis.

[c] Particle size obtained from TEM measurements and values in the "[]" are coefficient of variation.
[d,e] Particle size obtained from DLS measurements.
[f] Swelling ratio value obtained at pH=4 and pH=7.4
[g] Zeta potential value obtained at pH 4.
[h] MAA mol.% from Ref. [179] after taking into account GMA functionalisation.

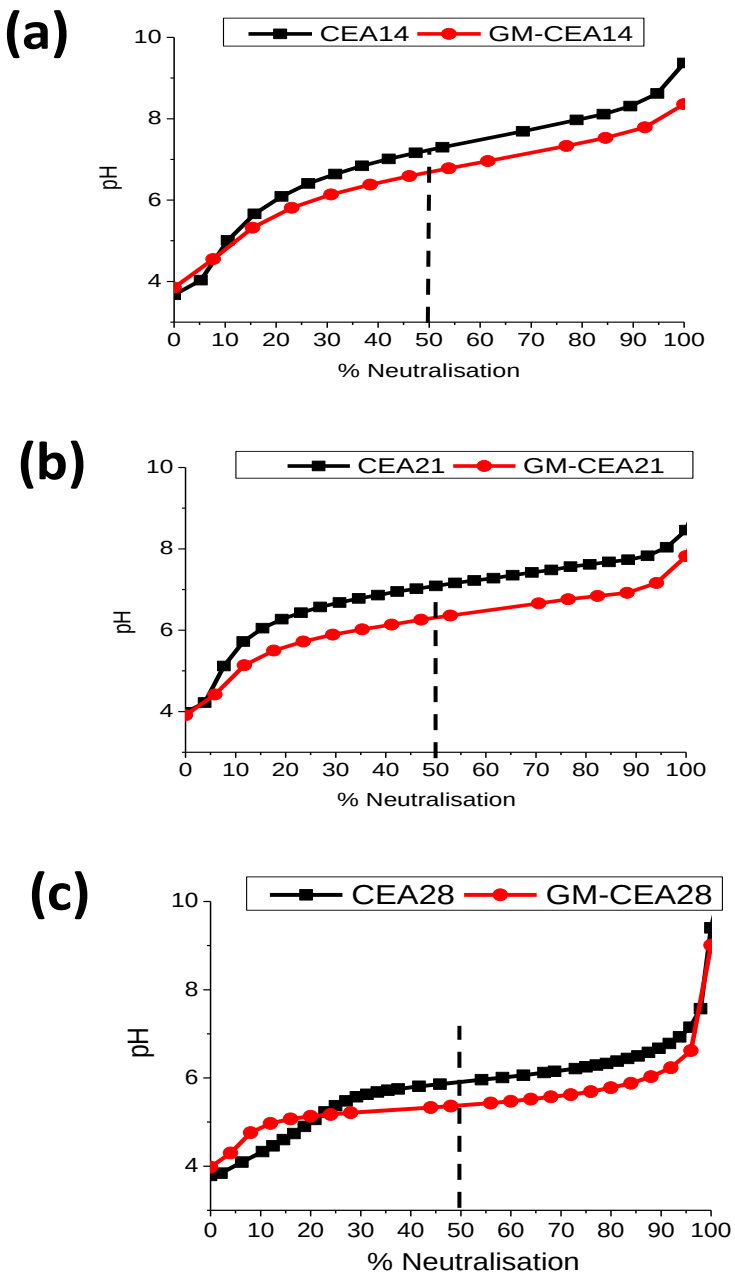

Figure 3.6: Titration analysis for CEA14, CEA21 and CEA28 and functionalised CEA dispersions. The vertical lines correspond to the apparent pK_a values.

The chemical reaction of COOH containing polymers with GMA as modifier is a potentially suitable method to produce vinyl functionalised macromolecules. GMA monomer was used for functionalisation as it offers flexibility due to its dual functionality[192]. It worth to mention that GMA contains epoxide group that highly reactive due to angular strain and therefore able to react with carboxylic acid even without the presence of catalyst[193-194].

In this study, the possible chemical reaction between CEA microgels with GMA is shown in Figure 3.7. As shown in Figure 3.7, epoxide group from GMA reacted with COOH group via ring-opening mechanism in aqueous medium. For this reaction, the carbocation is more stable in position 1 than position 2 and the main product is probably in position 1 as was discussed by Reis et.al. In that work, -COOH group in polymer were attached to position 1[195]. The GMA enabled covalent interparticle cross-linking to occur[196]. MGs containing GMA that obtained from this reaction which will be used to form free radical covalent crosslinking.

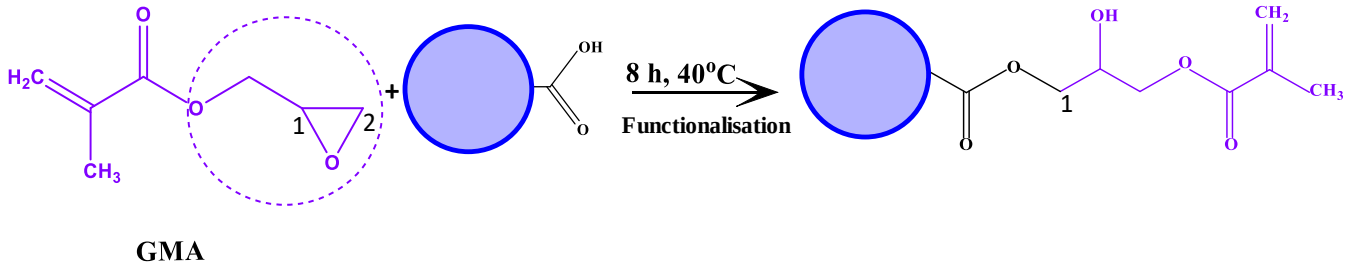

Figure 3.7: Chemical reaction of GMA with CEA microgels via epoxy ring-opening mechanisms[188].

3.4.1.3 Particle morphology

Figure 3.8 shows TEM images morphology of functionalised systems; GM-CEA14, GM-CEA21 and GM-CEA28. The particles were spherical and appeared like the non-functionalised particles. In addition, there is a ring effect noticeable in all the TEMs for all particles. This could be due to staining used during sample preparation. There is a possibility that these regions were CEA-rich. However, this suggestion cannot be certain. The GMA functionalisation did not change the morphologies.

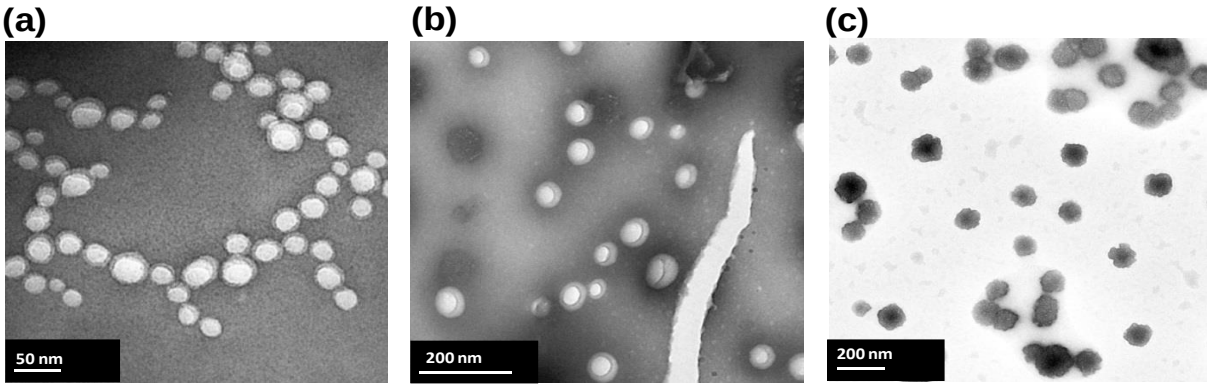

Figure 3.8: TEM images for (a) GM-CEA14, (b) GM-CEA21 and (c) GM-CEA28 particles.

Subsequently, the properties of MGs before and after functionalisation with GMA is shown in Figure 3.9 that obtained from DLS analysis. The MGs after functionalisation show only a slight increase in particle size (see also Table 3.3). Modification with GMA should result in higher hydrophobicity of MG and hence the increased swelling is counter-intuitive (Figure 3.9). GMA-functionalisation involves solvent washing (and subsequent removal) and this may disrupt physical bonds (reducing entanglements and intra-particle crosslinks) between the MMA units which oppose swelling and provide physical crosslinks as suggested in the earlier study[64]. Hence, for MMA-based MG, there are two types of crosslinking; permanent links due to EDGMA and reversible links due to MMA that cause by reduced cross-link efficiency/density and by the copolymerisation effect[197]. This finding is remarkable as the

pH-triggered swelling is not influenced by GMA functionalisation given large proportion of CEA units were reacted. This could be associated CEA with GMA, which enable more GMA to infiltrate into the MG interiors. It is proposed that the slight increase in d_z values is because of the dominance of physical bond disruption.

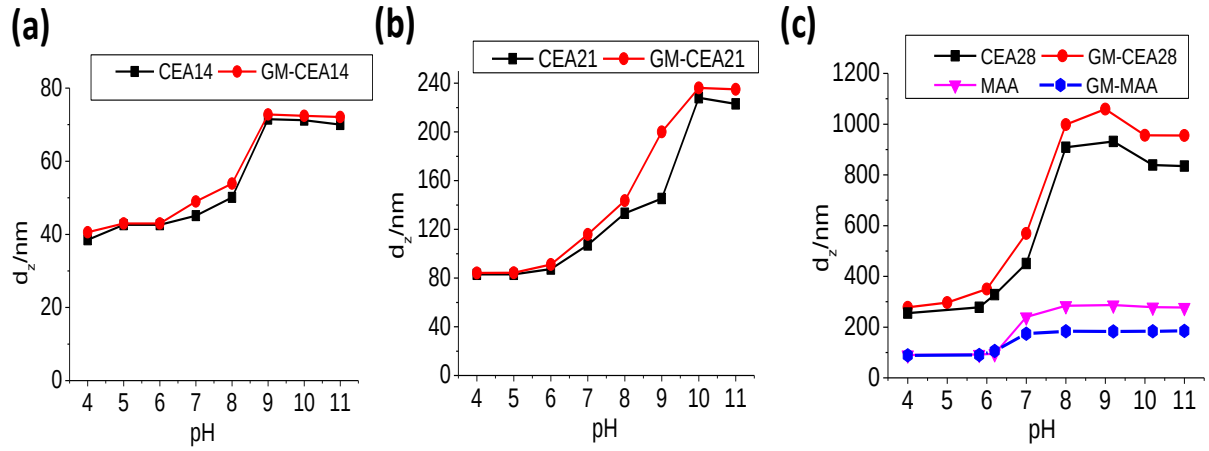

Figure 3.9: Variation of d_z with pH before and after functionalisation with GMA for all systems.

3.4.1.4 DX MGs gel morphology and properties

The GM-CEA MGs were used to prepare DX MGs. MG swelling is essential to form DX MG and GM-CEA14 was not considered further because it was not fulfill this principle. An investigation was conducted on a gel that prepared using a blend of CEA21 and CEA28 by mixing these two systems equally and it was denoted as DX BL-CEA (in the later section). Figure 3.10 shows the SEM morphology of freeze-dried DX CEA21 and the morphology of freeze-dried DX CEA28 is shown in Figure 3.11. The surfaces show undulating morphology with evidence of coalesced MGs (arrows) can be seen in SEM images in Figure 3.10. This morphology is similar to that reported earlier for DX MGs based on poly (MMA-MAA-EGDMA)[64, 71]. In Figure 3.11, the particles can be seen on the surface of this freeze-dried gel.

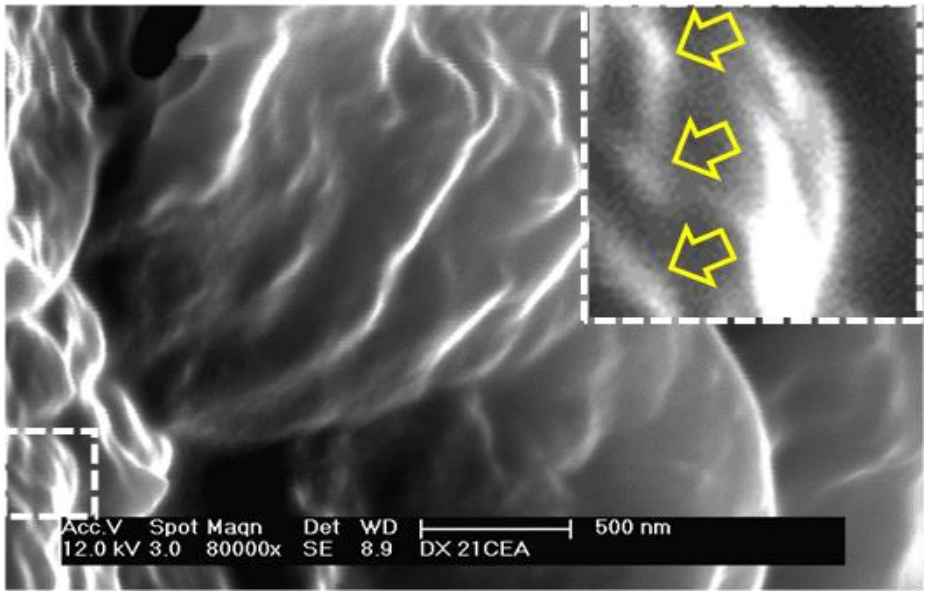

Figure 3.10: Representative SEM image for the surface of a freeze-dried DX CEA21 gel. The arrows highlight partially coalesced MGs.

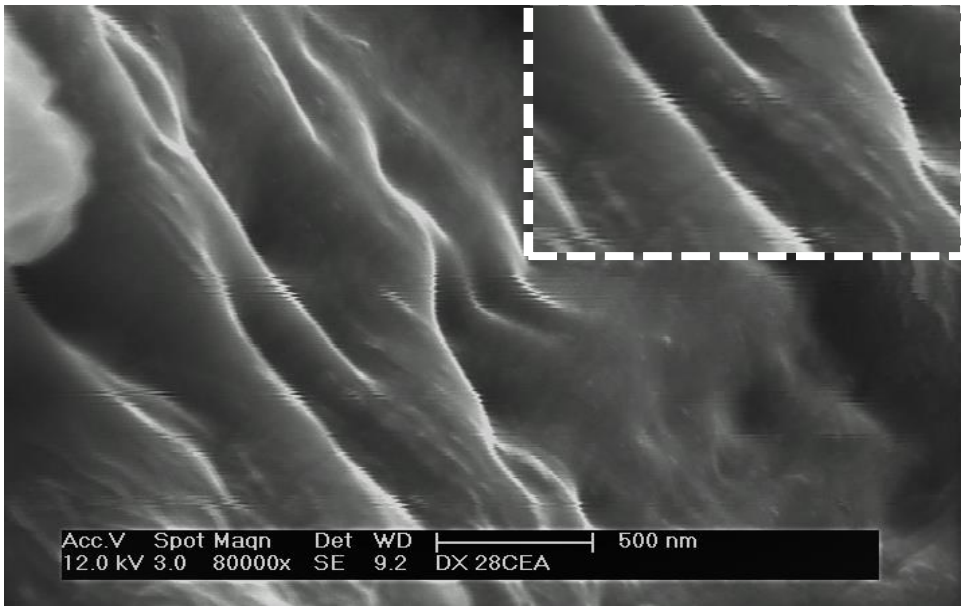

Figure 3.11: Representative SEM image for the surface of a freeze-dried DX CEA28 gel.

3.4.1.5. Rheological properties of gels

The mechanical properties for the new DX MGs was analysed by rheology technique.

Frequency sweep data are shown in Figure 3.12. Frequency sweep data (Figure 3.12a)

show the storage modulus (*G'*) and loss modulus (*G''*) values are not dependent on the frequency which is indicative of solid-like behaviour[71-72]. Figure 3.12c shows the graph of G' vs composition of CEA/MAA in the MGs. The values for G' for each system were obtained at angular frequency, ω= 1 rad/s. From the data obtained, the *G'* values at 10 rad/s decrease in the order: DX MAA > DX BL-CEA > DX CEA28 > DX CEA21. This indicates that the crosslinking was strongest in the DX MAA gels and least in the DX CEA21 gels. Further analysis for the gel transition was obtained from the values of tan δ (= *G''* / *G'*) that are shown in Figure 3.12b. Figure 3.12d shows the values of tan δ for each system at ω=1 rad/s. It demonstrates low frequency dependency in which indicates the gels were low viscous and mostly elastic[198]. For DX CEA28 gel, the tan δ values was increased as ω increased which give indication of energy dissipation by intermolecular friction. In DX CEA28, more ionic groups were present compared to DX CEA21 gel.

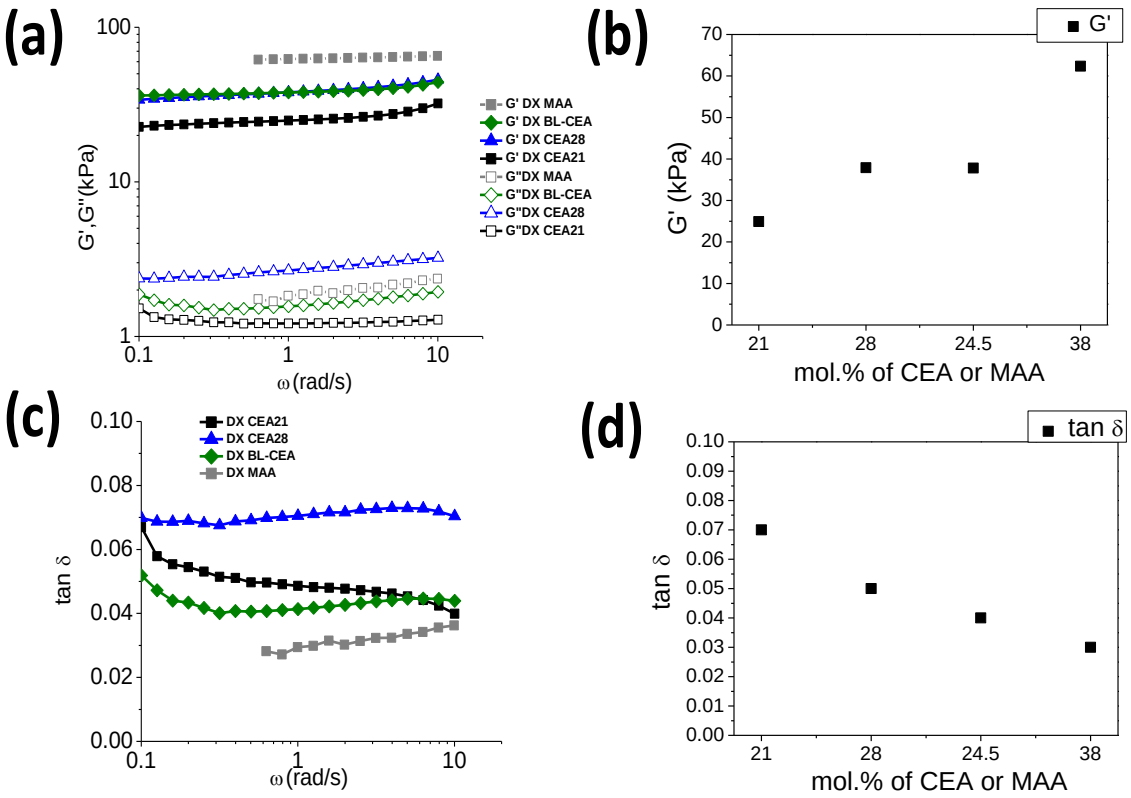

Figure 3.12: Frequency-sweep studies for various gels, (a) G'(closed symbols) and G" (open symbols) data; (b) G' as a function of mol.% of CEA/MAA at ω=1; (c) tan δ data for DX CEA21, DX CEA28, DX BL-CEA and DX MAA gels; (d) tan δ as a function of mol.% of CEA/MAA at ω=1 rad/s.

3.4.2 Swelling and stress-strain properties of the gels

The volume swelling ratios (Q_{DX}) for each gel was measured at three different pH and are shown in Figure 3.13. The values obtained are summarised in Table 3.4. Gel swelling was measured gravimetrically with equation 3.2. The Q_{DX} values reached constant values on day 4 for all systems. The equilibrium Q_{DX} values as a function of pH are shown in Figure 3.13d. It can be seen in all cases that the swelling increased with pH. This trend is broadly similar to that observed for the constituent MGs (Figure 3.5). Swelling of the gels is related to the charge group concentration[199]. Inter-segment electrostatic repulsion can be controlled by the pH. The lower CEA content (21 mol.% in DX CEA21) reduced the swelling ratio due to the greater separation between the CEA groups. The DX CEA28 contained 39 mol.% CEA and swelled more because of the higher CEA content. The increased GMA content for this system (Table 3.3) did not dominate the swelling. The swelling behaviour for the DX BL-CEA gel was in between that of DX CEA21 and DX CEA28 (Figure 3.13d). This behaviour shows that the swelling of the DX CEA gels can be tuned by blending between the extremes of the two components. A comparison of swelling ratio at high and low pH swelling data show that DX MAA gel is similar to DX CEA21.

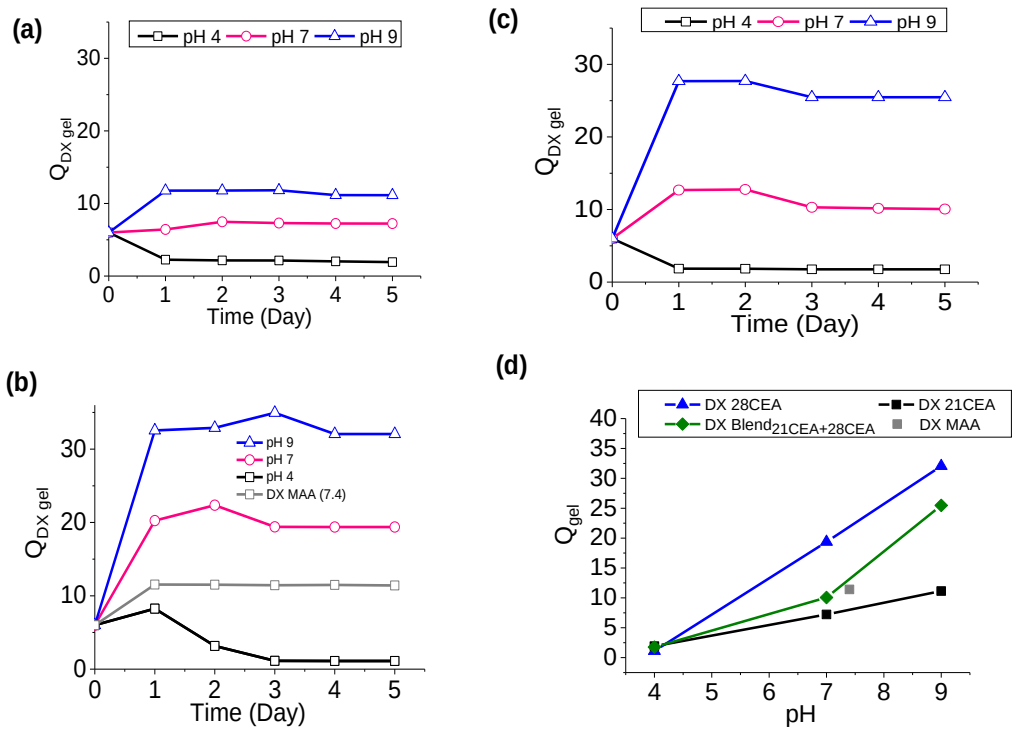

Figure 3.13: Volume swelling ratio (Q_{DX}) vs. pH data for the gels; (a) DX CEA21, (b) DX CEA28 (c) DX BL-CEA gels and (d) Q_{DX} vs pH for all gels. Data for DX MAA gel obtained from Milani et.al are included for comparison.

Table 3.4: Data obtained from volume swelling ratio (Q_{DX}) of DX CEA21, DX CEA28, DX BL-CEA and DX MAA.

Abbreviations	ϕ [a]	ϕ_p [b]	Q_{DX} [c]	Q_{DX} [d]
DX CEA21	0.14	0.090	1.9	11.1
DX CEA28	0.14	0.030	1.1	32.1
DX BL-CEA	0.14	0.039	1.8	25.5
DX MAA	0.12	0.063	1.8	15.9

[a] Volume fraction of polymer in gel.
[b] Polymer volume fraction calculated from Q_{DX} at equilibrium swelling pH 9.
[c] Volume swelling ratio obtained at pH 4.
[d] Volume swelling ratio obtained at pH 9.

To further investigate the mechanical properties of the new systems, uniaxial compression analysis was conducted (see Figure 3.14). The gels were prepared in cylindrical shape (10 mm x 12 mm). A summary of the data is shown in Table 3.5. DX CEA21 is a relatively soft gel with a Young's modulus (E) of 3.57 ± 0.07 kPa and a breaking strain (ε_B) of 58.4%. As the amount of CEA increased, the DX CEA28 gels became stiffer and the value of E increased to 34.5 ± 12.5 kPa (ε_B = 62%). Meanwhile, for DX BL-CEA the E value is 39.2 ± 10.5 kPa (ε_B = 62.3%). Hence, the GMA content or blend gel did not influence the ε_B values as well as the ductility of the gels. However, the E values were affected. It is interesting that the E value for the blend system is very close to that for the DX CEA28 gel. This indicates that the CEA28 MGs distributed most of the stress within these blend gels. The DX MAA gel has highest modulus (100 kPa) but lowest breaking strain, 49.5% compared with other CEA gels. This indicates that use of CEA in place of MAA increased the ductility of the DX MGs and is a new observation.

The number of elastically effective chains per unit volume (v_e) can be calculated using rubber elasticity theory[200]:

$$E = 3v_e\, kT \tag{3.5}$$

where k and T are Boltzmann's constant and absolute temperature. The v_e value for the blend system is the highest value for v_e (Table 3.5) followed by DX CEA28 and then DX CEA21. It appears the larger MGs (CEA28) contributed most to the stress distribution in the mixed system.

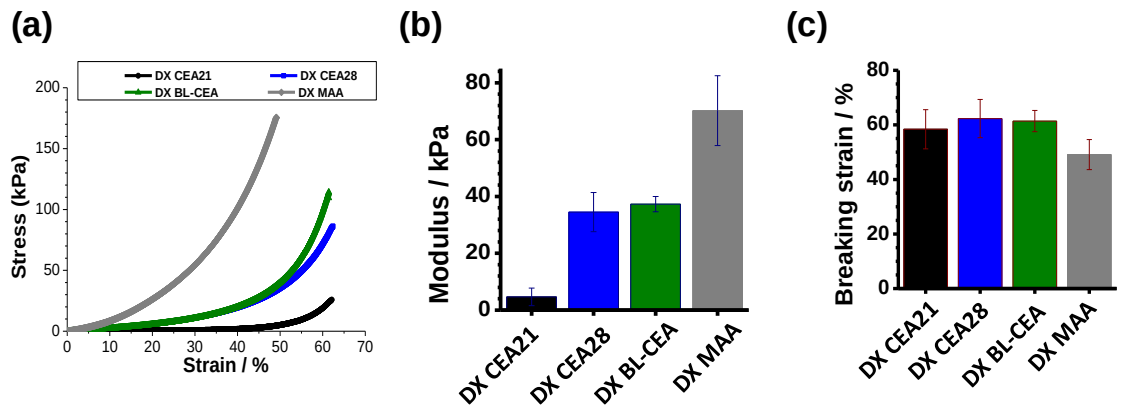

Figure 3.14: (a) Stress-strain graph for DX CEA21, DX CEA28, DX BL-CEA and DX MAA gels; (b) Modulus values and (c) Breaking stress values for the gels.

Table 3.5 : Characterisation data obtained from uniaxial compression analysis.

	E[a] / kPa	**ε_B[b] / %**	**σ[c]/ kPa**	**v_e[d] /m^{-3}**
DX CEA21	4.68 ± 3.1	58.4±7.18	14.9±12.9	1.05 x 10^{-27}
DX CEA28	34.5 ± 6.9	62.3±7.01	86.1±1.84	7.65 x 10^{-27}
DX BL-CEA	37.3 ±2.7	61.4±3.86	113.6± 13.4	8.31 x 10^{-27}
DX MAA[e]	70.2	49.5	176	-

[a] Calculated from the initial gradient of stress vs. strain curves
[b] Strain-at-break values.
[c] Stress-at-break values
[d] Obtained from equation 3.5.
[e] The values obtained from here[179]

3.4.3 Optical properties of CEA gels

UV-visible spectra were obtained for all samples as shown in Figure 3.15. From the spectra obtained, the MGs do not absorb light over the wavelength range studied. It was found that the gels scattered light and therefore the optical density (OD) graph was plotted. The OD has the same numerical value as the absorbance. From Figure 3.15a it can be seen that DX CEA21 has lower OD values than DX CEA28. Presumably, this is due to the differences in MGs size, DX

CEA28 has a larger size (Table 3.2). The OD volumes for the DX BL-CEA gel was surprisingly high (Figure 3.15a). This gel ratio for DX BL-CEA is 50:50. Therefore, two other blends DX gels system were prepared contained CEA21 and CEA28 in the weight ratios of 25:75 (DX BL-CEA(25:75)) and 75:25 (DX BL-CEA(75:25)). Those spectra also showed strong scattering (see Figure 3.15a). To probe the origin of the scattering spectra, data from Figure 3.15a are plotted on a log-log scale in Figure 3.15b. Tyndal scattering has a power law relationship between turbidity (and hence OD) and wavelength[201-202]. The fact that a linear relationship is present for the DX CEA-blend gels in Figure 3.14a shows that the behaviour is dominated by light scattering. Figure 3.15c shows the variation of the OD measured at 550 nm (OD550) with weight fraction (wt.%) of CEA28. In the blend system, a maximum is an evident for the DX blend containing 50 wt.% of CEA28 MGs.

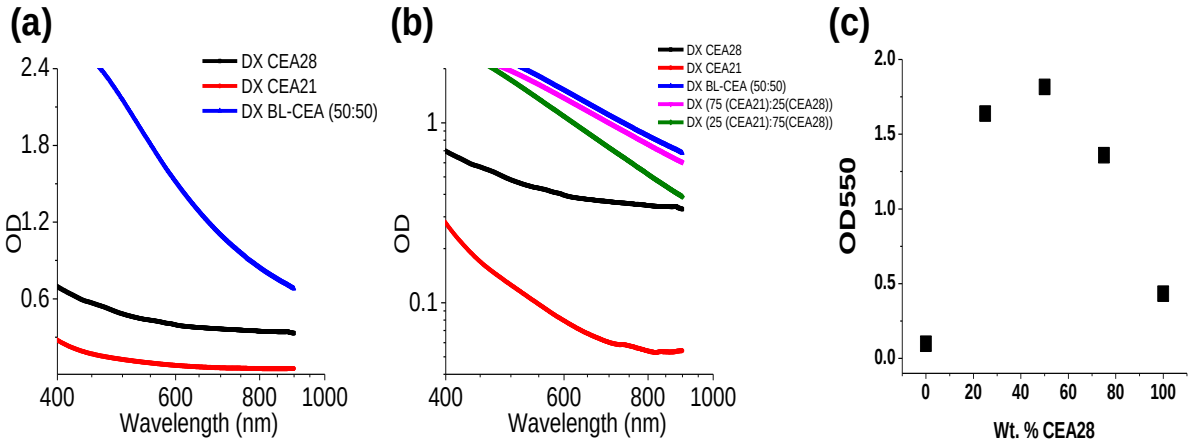

Figure 3.15: (a) Optical density (OD) vs. wavelength for DX CEA28, DX CEA21 and DX BL-CEA; (b) Optical density (OD) vs wavelength for five systems as shown in the graph; (c) Variation of OD at 550 nm with wt% of CEA28 in the DX MGs.

Figure 3.16a, 3.16b and 3.16c show photographs of the gels physically and the opacity of blend gel, DX CEA-BL (50:50). The causes for the opacity of the gels are the different particle size and the differences of the swelling of the two particle types (large and small) which give rise to different refractive indexes for the large and small particles. So, there are two sources of scattering; particle size and refractive index differences[204-205]. As shown in Figure 3.16b, DX

BL-CEA was opaque gel. In contrast, DX CEA21 and DX CEA28 were transparent gels. Figure 3.16d shows TEM image of blend gel of GM-CEA21 and GM-CEA28 at 50:50 weight ratio. As can be seen from the TEM morphology, the difference in MG sizes is pronounced. It is proposed that the strong scattering from the blend originates from differences in particle sizes of the CEA21 and CEA28 particles in the DX BL-CEA gels. The DX gels were prepared at pH 7.5 and from Figure 3.17 the extent of swelling was different for CEA21 and CEA28 such that CEA28 was more swollen than CEA21 at the preparation pH. The strong scattering occurred due to the difference of density combined with the size differences[206]. Highly scattering gel might have advantage to be tuned for UV-blocking properties[207]. To the best of my knowledge, this is the first example of strong scattering that can be modified within a gel using colloidal blending.

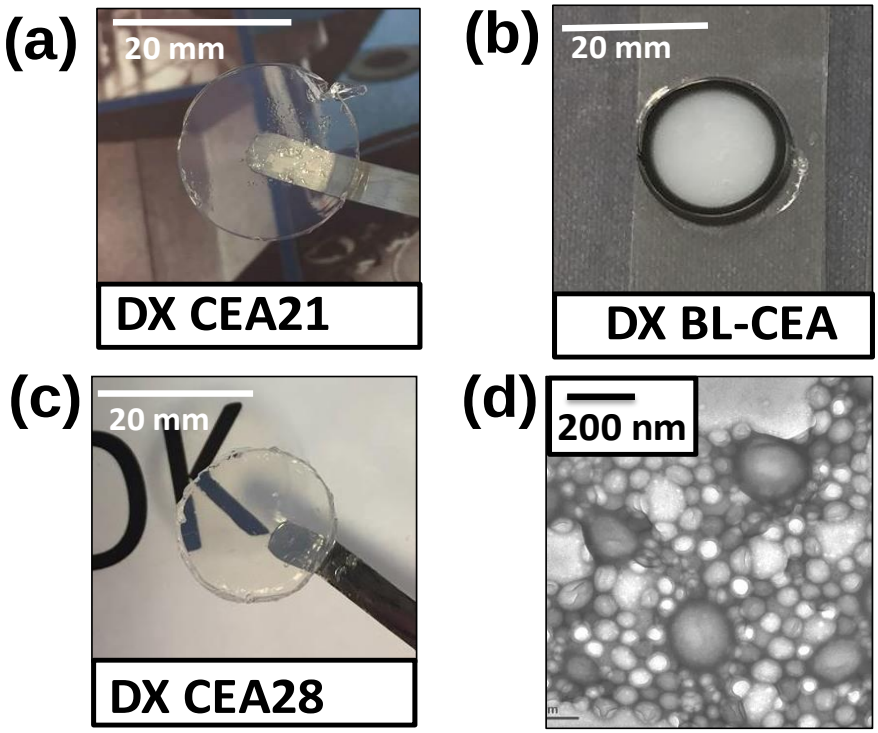

Figure 3.16: Gel images of (a) DX CEA21, (b) DX BL-CEA (50:50), (c) DX CEA28. TEM image of a blend CEA of GM-CEA21 and GM-CEA28 particles is shown in (d).

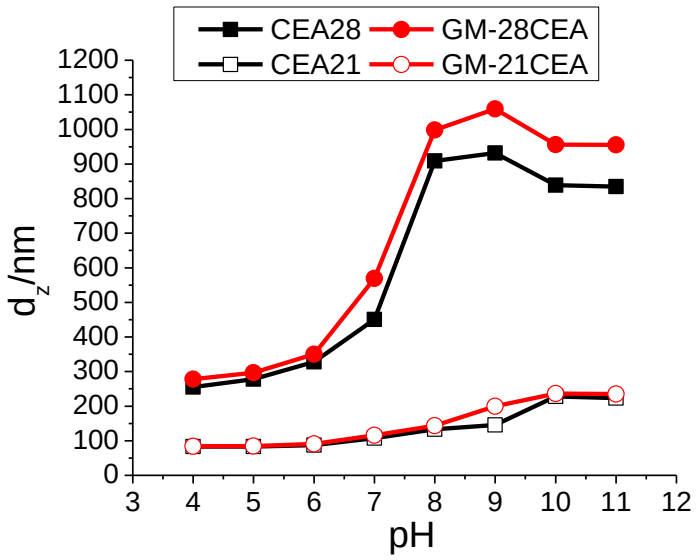

Figure 3.17: Variation of d_z for pH-responsive microgels corresponding to the pH prior to functionalisation and after functionalisation with GMA for CEA28, GM-CEA28, CEA21 and GM-CEA21.

Unfortunately, the MGs system containing CEA was not considered to be well suited as for matrix for next two chapters due to low modulus compared to the reference system; 4.68 kPa for DX CEA21, 34.5 kPa for DX CEA28, 37.3 kPa for DX BL-CEA and 100 kPa for DX MAA(see Figure 3.14b). Therefore, a different MGs system was explored for Pb capture in the next chapter.

3.5 CONCLUSIONS

The MGs size increased strongly with increased CEA content used to prepare the MGs. The d_z data showed the MGs increased in size when the pH approaches the pK_a values which was due to ionisation of the carboxylic acid groups. The MGs showed comparable swelling to the established MAA MGs. An improvement in the ductility was evident when compared to the established DX MAA gels, which may favour biomaterial applications. It was observed that at higher CEA content, growing particles was stabilised more effectively than MMA which resulted in fewer particles to form and hence larger size was obtained. The increased of GMA content for the functionalised system (Table 3.4) did not dominate the swelling properties. Interestingly, the swelling behaviour of DX BL-CEA gel was in between of DX CEA21 and DX CEA28. The effect of blends of MGs on the properties of the DX CEA gels resulted in tunable swelling properties and strong light scattering. The Young's modulus value of the blend system was very close to the DX CEA28 gel indicated that CEA28 distributed more stress within these blend gel. It was proposed that the strong scattering for the blend system originated from the differences in densities and particle sizes of CEA21 and CEA28 particles in the blend gel**.** The data obtained in this study are the first example of DX MGs prepared using a carboxylic acid monomer other than MAA.

CHAPTER 4 : STIMULI RESPONSIVE NANOGEL COMPOSITE; NEW DX NG AND DX NG/GO GELS

4.1 ABSTRACT

NGs are crosslinked polymer colloids with diameter less than 100 nm when measured in swollen state. NGs can have a high-water content, tuneable chemical structures and biocompatibility. An advantage of their nanoscale size is their large surface area for adsorption and release applications. In this chapter the properties of NGs and double crosslinked (DX) gel are investigated. In this work, composite gel is denoted as DX NG/GO and GO-free gel as DX NG. Functionalised NGs were mixed with low concentration of GO dispersion to form mixture of composite NGs. Then, covalently interlinked gels were constructed by free radical reaction with pendant vinyl groups. It was found that inclusion of low amount of GO remarkably enhanced the storage modulus (G') value from 10.3 kPa (DX NG) to 60.3 kPa (DX NG/GO). Taken together, this result suggests that GO changed the dissipation because covalent interlinking of the NG particles more effectively trapped the GO sheets within the gels. The gels in this work will be used for Pb^{2+} removal in the subsequent chapter.

4.2 INTRODUCTION

The past decade has seen that gels have been the focus of intensive studies due to their attractive properties such as high hydrophilicity, permeability and biocompatibility and have been explored for applications such as sensing, drug delivery and tissue engineering[169, 208] and water treatment[209-211]. In recent years, hybrid NGs with multifunctionality and novel properties have been developed to accommodate the demand for new materials in many research fields from materials science to medicine[212-215]. A hybrid refers to NGs that combined with different polymers or with nanoparticles such as plasmonic[216-217] and carbonaceous materials [113, 218-219]. Meanwhile, NGs are crosslinked polymer particles that have characteristics of hydrogels and nanomaterials[181, 220]. Just like hydrogels, NGs have features desirable chemical and mechanical properties, tuneable size from nanometres (NGs) to micrometres (MGs)[29], and its primary advantages are larger surface area and permit an attachment of various ligands due to its multi-valent interaction[27] of an interior network. Besides, NGs has excellent sensitivity to pH that is provided by the hydrophilic network[221-223]**.** Although numerous studies have reported on pH-responsive NGs, publications that report measured swollen diameters between 1 and 100 nm are infrequent[224-225].

Major problems of most hydrogels are lacking in mechanical strength[169, 181, 209-211], heterogeneity of the network structure[226] and have limited stiffness[227]. In fact, polymer hydrogels are usually soft and fragile in the swollen state[228]. Due to the problems mentioned above, nanocomposite hydrogels are attracting much attention because of their improved mechanical properties and introduced additional functionalities[229]. Composite gels can be formed by the inclusion of inorganic or organic components (can be called additive or filler) in the network[214,230]. The additives which enhance the breaking strength of hydrogel with a range of different fillers include GO, clay or carbon[227,231-232]. GO has attracted wide-spread

interest due to its high water permeation and molecular sieving properties as well as good prospects for industrial scale production[233-235]. The good dispersion ability of GO is attributed to the abundant hydrophilic functional groups on the GO sheets[91, 236]. The GO sheet surface contains different functional groups including epoxide and hydroxide, whereas, the edge of the sheets contain a "hedge" of carboxylic groups[237] (Figure 4.1)[238]. In addition, GO is a carbonaceous material that has groups that function as ligands for heavy metal ions such as -COOH groups. Due to this dual-functionality, GO offers potential to be implemented in wastewater treatment [209-210]. Moreover, GO also offers great opportunities for gel applications because just by inclusion of low amount of GO (1 wt.% or lower), the mechanical properties of the gels are greatly improved[91]

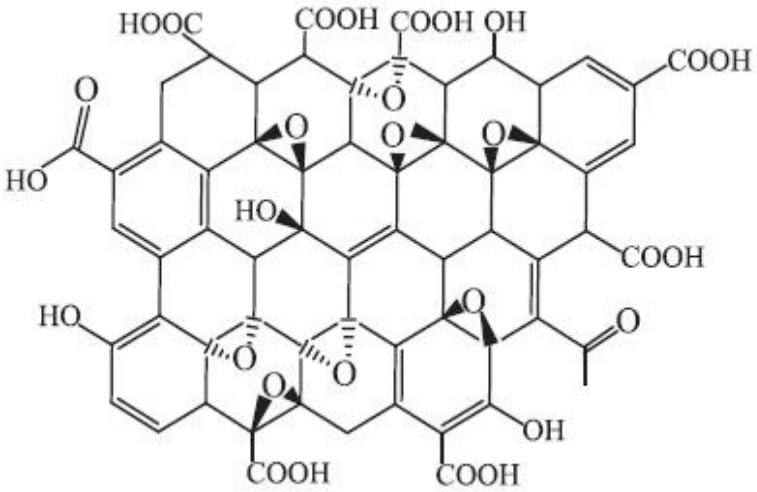

Figure 4.1: Chemical structure of GO[221].

Recently, Milani et.al demonstrated that pH-responsive DX NG gels can be prepared by covalently interlinking NGs[181]. It was reported that DX NG gels prepared using covalently interlinked NGs had improved ductility compared to DX MG gels[181]. DX NG gels differ substantially from conventional hydrogels because they are assembled using pre-formed NGs particle. This scalable method uses only free-radical coupling at the gel formation stage and is

well suited to inject or moulding into different shapes. In this study, the primary aim is to investigate on new DX NG/GO composite gel to observe the effects of low loading GO on the properties. The approach to construct DX NG and DX NG/GO composites is depicted in Figure 4.2. The NGs were prepared by emulsion polymerisation of MMA, MAA and EGDMA. Then, the NGs were vinyl functionalised with GMA at pH 5.1. To prepare the physical gel, a concentrated NGs dispersion was mixed with GO and the pH was raised above pK_a. Subsequently, covalent coupling via free-radical reaction was linked to the pendant vinyl groups to form DX gel. It is expected that DX NG/GO gels exhibit an enhancement in Young's modulus and ductility compared to the previous studies related to NGs[181]. It will be concluded that they are potentially well suited for Pb^{2+} removal. The adsorption ability of DX NG and DX NG/GO for Pb^{2+} removal is investigated in chapter 5. Whilst the NGs and DX NG studied here are not new[181], the DX NG/GO composites *are new materials*.

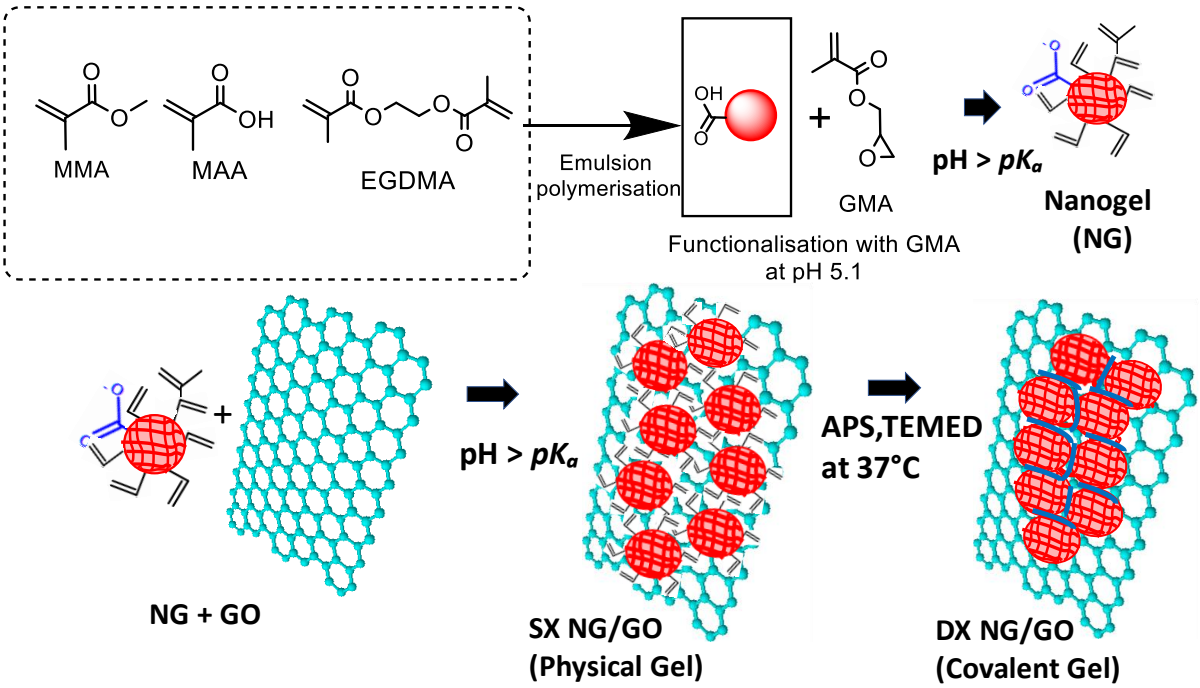

Figure 4.2: DX NG/GO composites were prepared using concentrated dispersions of vinyl-functionalised NG particles mixed with GO. The NGs underwent pH-triggered swelling at pH values greater than their pK_a to form a physical gel. The latter was transformed into covalent gel by free-radical coupling between surface vinyl groups of neighbouring NGs with ammonium persulfate (APS) and *N,N,N′,N′*-tetramethylethylenediamine (TEMED). The covalent linkages at the periphery of the NG particles are indicated in blue.

4.3 EXPERIMENTAL

4.3.1 Materials

Graphite (Grade 2369) was purchased from Graphexel Ltd.UK. Other chemicals such as methyl methacrylate (MMA, 99%), methacrylic acid (MAA, 99%), glycidyl methacrylate (GMA, 97%), sodium dodecyl sulphate (SDS), ammonium persulfate (APS), $NaNO_3$ (> 99%), NaOH, $KMnO_4$, H_2O_2 (>35%), EGDMA (98%) and *N,N,N′,N′*-tetramethylethylenediamine (TEMED, 99 %) were obtained from Sigma-Aldrich. H_2SO_4 was purchased from Fisher Scientific. All chemical reagents were used without further purification. All aqueous solutions were prepared using high purity deionised water. GO was prepared according to a modified Hummers method which has been described earlier[85].

4.3.2 Synthesis of nanogels

The NGs were produced by starved-feed emulsion polymerization at 80°C as has been reported in the previously[72]. A brief description is given here. The method described here is for the preparation of NGs containing MMA, MAA and EGDMA (79.1 wt.% MMA, 18.9 wt.% MAA and 2.0% EGDMA). This nanogel (NG) is the precursor as shown in Figure 4.2. SDS (1.214 g) was dissolved in water (240 g) and added to a four-necked round bottom, within a water bath set at 80°C. The four-necked round bottom was equipped with a stirrer; a monomer feed inlet tube, a nitrogen gas inlet tube/sampling hole and a condenser. The solution was de-gased using nitrogen. APS (0.158 g, 6 x 10^{-4} mol) was dissolved in water (2.0 g) and added to the vessel. A monomer solution was prepared that contained MMA (42.0 g, 0.419 mol), MAA (10.0 g, 0.116 mol) and EGDMA (1.06 g, 0.00535 mol). Then, the monomer solution was transferred into 60 ml plastic syringe (20 mm diameter) with an injection needle attached. The syringe was secured with parafilm to a length of thin plastic tubing that was inserted into the glass reactor. The syringe was secured into a syringe pump set at constant feed rate of 0.317

ml/min. Once the monomers feed had finished, the reaction was left for 1 h. After that, the glass reactor was placed in the ice bath to terminate the reaction and the solution was filtered. The product was transferred into membrane tubing and purified by extensive dialysis using water for 7 days. The deionised water that used for dialysis was changed twice a day to remove any excess of surfactant. The dialysed product was placed in the fridge (~ 4°C) for further characterisation and analysis.

4.3.3 Gelation test

To test and ensure the polymer dispersion produced a gel when subjected to an increase in pH; drops of aqueous 4M NaOH were added to ~1-2 ml NGs dispersion. If a gel was formed, then the particles within the NGs had swelled substantially. The formation of physical gel is essential prior to the formation of DX NG by heating process. This gelation test is shown in Figure 4.3.

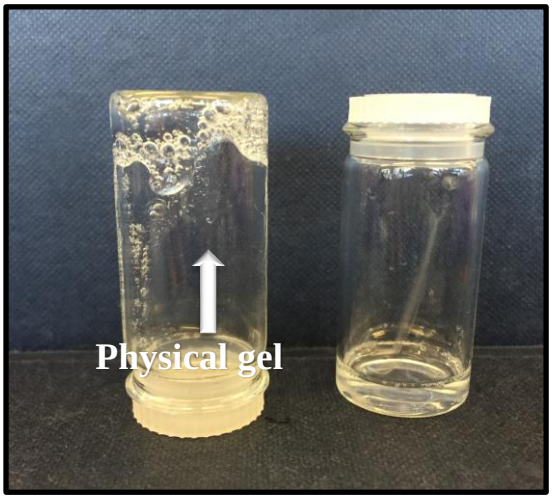

Figure 4.3: Formation of physical gel at pH > pK_a. The NGs concentration is 10 wt.%.

4.3.4 Functionalisation of nanogels

The purified NGs were functionalised with vinyl groups from GMA. NGs dispersion (120 g, 5 wt.%) was mixed with GMA (3.0 g, 0.021 mol.) and the pH was adjusted to 5.1 by addition of aqueous NaOH solution (0.05 M) in a stopped round bottom conical flask (250 ml). The conical flask was secured onto a clamp stand and immersed in an oil bath. The mixture was heated to 40°C for 8 h with vigorous magnetic stirring. After the reaction was finished, hexane was used sequentially to wash the product to remove excess of GMA using a separatory funnel. The separating funnel was shaken to ensure the hexane mixed well with the NGs. The washing step was repeated twice. The product was concentrated by rotary evaporation at 25°C to remove residual hexane. The GMA-functionalised NGs were abbreviated as NG.

4.3.5 Graphene oxide synthesis by Hummers method

Preparation of GO was conducted using a modified Hummers method. Graphite powder (5.0 g) was added into concentrated H_2SO_4 (95-98%,170 ml) while stirring. An ice bath was prepared in a beaker and used to cool down the mixture. Then, $NaNO_3$ (3.75 g, 0.04 mol) was added into the mixture and stirring continued for 5 h. $KMnO_4$ (25 g, 0.16 mol) was gradually added at a rate that prevented the temperature of the mixture exceeding 20°C. After all the additives were dissolved, the ice bath was removed. The temperature was increased to 35°C and continuously stirred for 2 h. After that, the dispersion was further stirred at room temperature for 7 days. To produce exfoliated GO, the obtained product was slowly dispersed into 550 ml of 5 wt.% H_2SO_4 solution and stirred for another 3 h. Next aqueous solution of H_2O_2 (15 g, 30 vol.%) was carefully added over a period of 5 min. The mixture turned into gold colour dispersion and stirring was continued for 2 h. The suspension was diluted with 500 ml of 3 wt.% H_2SO_4 solution containing 0.5 wt.% H_2O_2 and was left overnight. The final product was centrifuged at 4500 rpm for 30 min and the clear supernatant liquid obtained on

the top was removed. Again, the remaining viscous liquid was further diluted with 500 ml of 3 wt.% H_2SO_4 / 0.5 wt.% H_2O_2 solutions. The washing process was repeated nine times and eventually the mixture was purified by dialysis for 7 days. The final pH obtained for the purified and exfoliated GO dispersion was 7.2.

4.3.6 Double crosslinked nanogels/graphene oxide

The NG was double crosslinked using aqueous solution contains APS (0.1M), NaOH (2.0 M) and TEMED (1M), respectively. A 10 wt.% NG dispersion was added with mixture of APS/NaOH/TEMED (200 µL) solution using micropipette. After mixing and shaking for about 3 min a gel was formed which was moulded into a sphere rubber ring using metal spatula. The physical gel was formed at pH 7.8 in a circular disc shape using a rubber round ring was placed between two glass sides. Two bulldog clips were used to clamp the glass slides together to prevent evaporation. The mould was placed in an oven at 37°C for 24 h.

DX NG/GO gels were prepared using similar method. DX NG/GO was prepared by mixing NG dispersion (2.80 g, 12 wt.%) with GO dispersion (0.722 g, 1.0 wt.%). DX NG/GO contained 0.2 wt% of GO and the NG content was 10 wt.%. The composite gels were double crosslinked using a solution mixture containing APS (0.10 M, 150 µL), NaOH (4.0 M, 50µL) and accelerator, TEMED (1 M, 100 µL). The similar procedure mentioned above was used to form the composite gels.

4.3.7 Physical measurements

Potentiometric titration measurements were carried out using Mettler Toledo Titration unit. The measurements were conducted using aqueous NaOH solution (1.0 M). Dynamic light scattering (DLS) were conducted using a Malvern Nano Zetasizer ZS90 instrument. SEM images for freeze-dried DX NG, DX NG/GO and GO were performed using a Philips XL30

FEG-SEM HKL EBSD instrument with an accelerating voltage of 15 kV. Dynamic rheology measurements were conducted using a TA Instruments AR-G2 temperature-controlled rheometer equipped with an environmental chamber. A plate geometry (20 mm diameter) was used. The strain-sweep measurements were conducted using a frequency of 1 Hz. The uniaxial compression tests were conducted using an Instron series 5569 load frame equipped with a 100 N load cell. The average height and diameter of the gel cylinders were 12 mm and 11 mm, respectively. The compression rate was 2 mm/min. Modulus values were calculated from the initial gradient of stress-strain curves at strains (ε) of less than 10%. For AFM analysis, GO samples were prepared with mica. The tape was removed from the mica surface and 200 µL of poly-lysine was dropped on the mica surface for two minutes. Then, the surface was cleaned with copious of deionised water. The diluted GO dispersion (1:1000) was deposited on the cleaned mica surface and dried for 1 hour. For NGs, the sample was deposited on the glass substrate and rinsed with deionised water to clean the surface. The glass substrate was dried overnight. The AFM measurements were performed with a tip oscillation frequency 273-397 kHz with scan speed of 5 lps (line per second). The data was collected in height mode, which means constant force was applied on the film by the cantilever (silicon nitride) during scanning. The swelling behaviours of DX NG and DX NG/GO in different electrolytes were studied. Gel samples were left in different beakers that were filled different buffer solutions (pH 4, pH 7 and pH 9) for 7 days. Samples were weighed once a day and the buffer were replaced every day to maintain the consistency of the pH. For sol fraction (SF) measurements, the gels were dried in the oven at 80°C to a constant weight. The SF was calculated with the initial mass of the dry gel (M_i) and the final mass of dry gel (M_f) according to equation 4.2 and GF is obtained using equation 4.1 and 4.2:

$$SF = \left(\frac{M_i - M_f}{M_i}\right) \quad (4.1)$$

$$GF = 1.00 - SF \quad (4.2)$$

Fourier transform infrared spectroscopy (FTIR) is a technique, which is used to obtain an infrared spectrum of transmission of the gel samples. In this work, FTIR was used to identify the presence of carboxylic functional group. All samples were freezing dried before FTIR analysis. Raman scattering signals were detected by using Raman spectroscopy (Raman, Renishaw InVia 4.0). The excitation wavelength was 785 nm with scanning range 1000–3500 cm^{-1}.

4.4 RESULTS AND DISCUSSION

The discussion in this chapter is focused on the characterisation of NG, GO, DX NG, DX NG/GO and their properties. In the end of this chapter, preliminary studies on infiltration in four different solvents is reported to observe the stability and appearance of DX NG and DX NG/GO gels.

4.4.1 Characterisation of non-functionalised and vinyl-functionalised nanogels and GO

In this work, the precursor is referring to non-GMA NGs while NG is representing vinyl (GMA) functionalised NGs. The precursor and NG were characterised by potentiometric titration to determine MAA content and the extent of GMA functionalisation as well as the pK_a of each system (Figure 4.4). The apparent pK_a is equal to the pH at 50% neutralisation. From this analysis, the pK_a of precursor and NG were found to be 7.1 and 6.7, respectively. The reason for the lower value of pK_a after functionalisation is not clear at this stage. At pH > pK_a, the concentrated NG dispersion will form a gel. The NG had MAA and GMA contents of 21.7 mol. % and 2.0 mol. %, respectively (Table 4.1). The mol.% of GMA is shown in Table 4.1

and it was calculated from the difference between the measured mol.% of MAA content before and after functionalisation. The decrease in MAA (RCOOH) content resulted from reaction between GMA vinyl groups with the acid groups via the epoxide ends (Table 4.1).

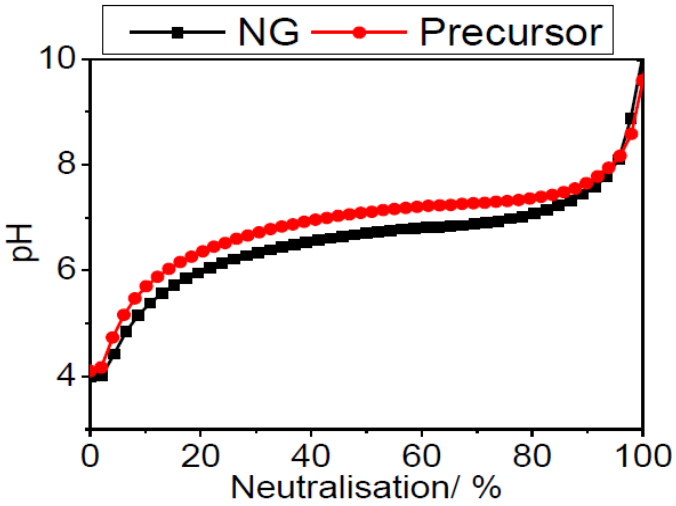

Figure 4.4: Potentiometric titration for NG and precursor. The apparent pK_a is obtained at 50% neutralisation.

Table 4.1: Potentiometric titration analysis for DX NG and DX NG/GO.

	pK$_a$	***MAA/ mol.%***	***GMA/ mol.%***
Precursor	7.1	23.7	-
NG	6.7	21.7	2.0

The number-average size of the NG particles determined from TEM was 26 ± 4.5 nm (Figure 4.5). At pH 4.0, the z-average particle diameter (d_z) measured by DLS was 33 ± 1.5 nm. There is only a slight difference compared to the particles measured by TEM which is due to the well-known sensitivity of DLS to scattering from larger particles. The reason for the larger diameter measured by DLS is due to the size of hydrodynamic layer around the hydrated particles, whereas the diameter obtained from TEM is for dehydrated particles. It was reported that to

achieve more uniformly crosslinked particles, the reactivity ratio of structural monomer and crosslinker need to be matched[239-240]. This can be seen in precursor system (Figure 4.2) as the structural monomer (MMA) and crosslinker (EGDMA) have the same end groups. Using monomers with similar structure contribute to higher possibility of homogenous distribution of co-monomers within the MG particles[56]. Homogenous and heterogenous distributions resulted in different size, structure and properties of the MGs[241]. In addition, the size of MGs are influenced by the solubility of monomers[241]. The NGs was functionalised with GMA. It is known that carboxylic acid groups from MAA can react with epoxide group of GMA via ring opening mechanism in aqueous medium[72, 195]. In the previous literature, MG particles were GMA-functionalised and these groups were sufficiently close in the swollen state to enable formation of a permanent gel[76]. The initial method was taken from Liu et.al[64]. This method involved temperature of 50ºC with fast mechanical stirring to avoid aggregation during this process. Besides, GMA amount that added into NGs solution must be controlled to avoid precipitation. In addition, GMA reaction is irreversible due to an epoxide group that reacts with carboxylic acids. Epoxy groups also react with a range of nucleophiles[242]. The high reactivity of epoxide is due to angular strain which causes the ring to open easily and consequently makes the reaction condition more favourable[243] (see Figure 4.4) **.** Studies on GMA functionalisation reported by Muzammil et.al confirmed the reaction of epoxy group yielded functionalised polymer chains[67].

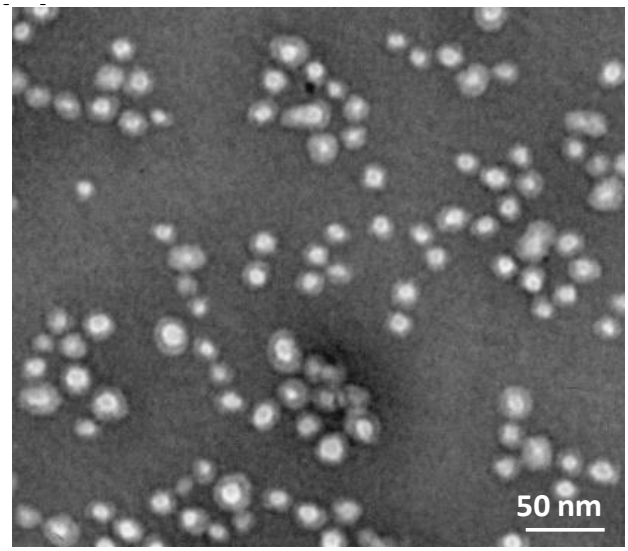

Figure 4.5: NGs morphology obtained by TEM.

The difference of precursor and NG of pH responsive particles with respect to various pH are shown in Figure 4.6. It can be observed that a major increase of d_z occurs at pH values greater than 7, which is above the pK_a. This is because of the particles swell due to -COOH deprotonation and inter-segment repulsion. These changes are consistent with the zeta potential data in Figure 4.7 which show an increase in magnitude at pH greater than 5.0.

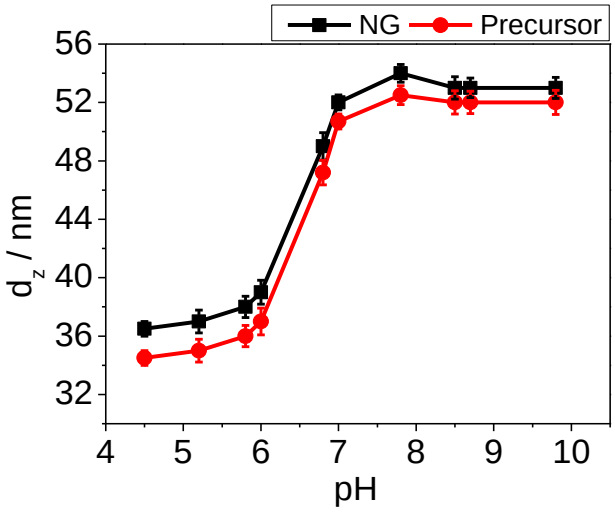

Figure 4.6: Shows the variation of d_z of particles corresponding to the pH of precursor and NG.

Zeta potential (ζ) is an important factor for characterising the stability of colloidal dispersions and provides an indirect measure of the magnitude and sign of the electrical potential of colloid particle. The zeta potential data (Figure 4.7) shows that GO was highly negatively charged which indicates a high amount of $–COO^-$ groups[244]. GO can readily form stable aqueous dispersion through electrostatic stabilization over a restricted range of pH 4-11.5 values.

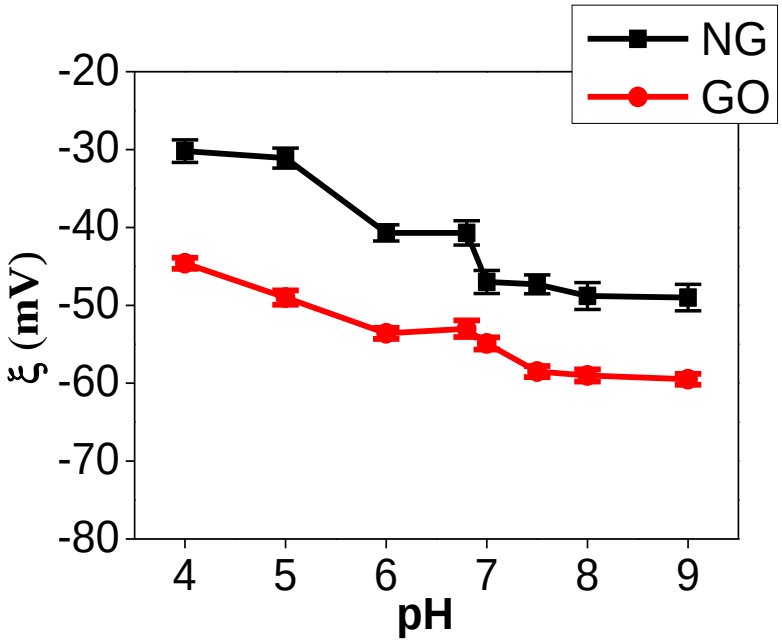

Figure 4.7: Zeta potential (ζ) values of NG and GO corresponding to pH.

An AFM topographic image of GO deposited onto glass substrate is shown in Figure 4.8. The GO sheets size is in the range of 800 nm in length and between 1.5 nm to 2.0 nm in height. The thickness of the GO sheet is approximate 1.3 nm obtained from high profile graph. The similar result was obtained by Ramesha et al for GO film thickness with size varies between 1.2~2 nm[245] and similar to GO thickness that was reported earlier[246]. GO can further exfoliate by various technique to get smaller size of GO sheets such as nanoplatelet[247]. The thickness obtained for GO by previous studied was 106 nm and depends on the exfoliation process[248].

The morphology of GO sheets is shown in Figure 4.9, as obtained by TEM. Folded sheets of GO were observed from TEM.

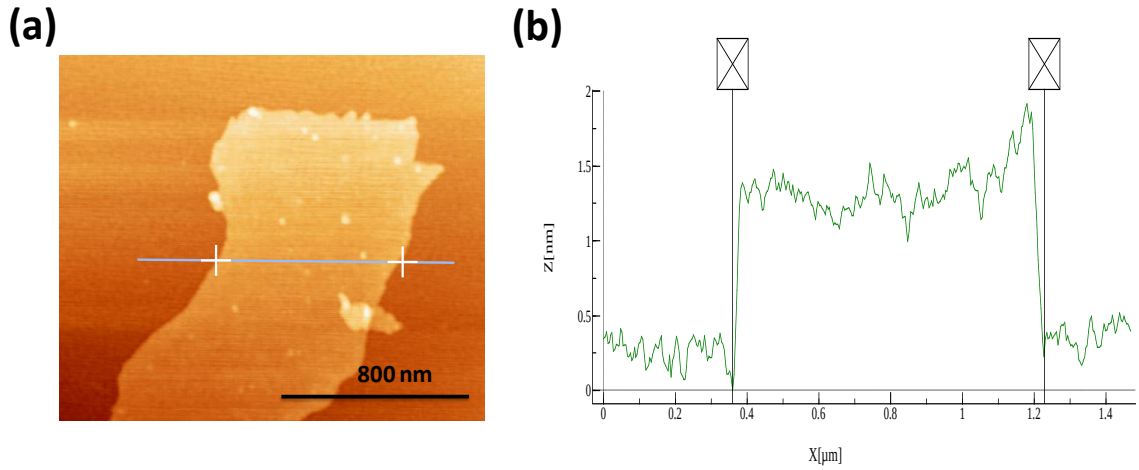

Figure 4.8: AFM topographic image and magnification of GO deposited on a glass slide. (b) The height profile of the GO sheet

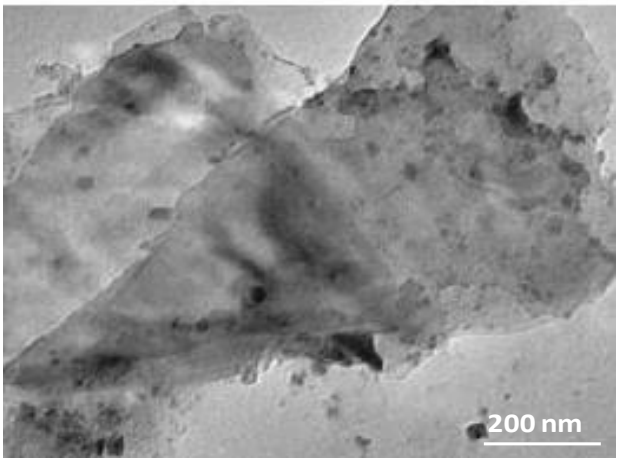

Figure 4.9: TEM morphology for GO sheets.

4.4.1.1 Raman spectroscopy analysis of GO sheets

Raman Spectroscopy is a well-established technique to investigate GO[249-250]. Raman spectroscopy analysis was conducted to measure the D and G bands of GO (Figure 4.10). A conjugated carbon material, if not defect-free, usually has three common peaks in its Raman spectrum, i.e., a D peak at 1350 cm^{-1}, a G peak at 1582 cm^{-1}, and a 2D peak at 2700 cm^{-1} [245, 251]. Figure 4.10 shows two prominent peaks of GO. The G band is referring to the sp^2 (graphite-like) structure and D peaks is correlated with structural defects of sp^3 (diamond-like) carbon [106, 252-253]. The value of D and G bands are apparent at 1347 cm^{-1} and 1612 cm^{-1}, respectively**.** The value obtained for these D and G band are similar to the theoretical value[126]. However, the G band value is slightly different due to the existence of defects in the GO structure. As compared to pristine graphite, higher G band was obtained for GO structure due to several reasons; 1) overlap between G band with D band that becomes active due to defects; 2) Blue shifted due to reduced number of sheets; 3) Isolated double bond separated by functional group on the carbon network of GO[245]. For perfect graphene lattice, the D band peak is relatively low and nearly invisible due to the symmetry breaking at the edge[106]. However, when oxidation and graphene oxide is present, the D band will be visible. A measure of extend disorder is obtained by the intensity ratio of D and G bands expresses the sp^2/sp^3 carbon ratio[106]. In this work, the value obtained for the D/G ratio is 0.85 ± 0.05.

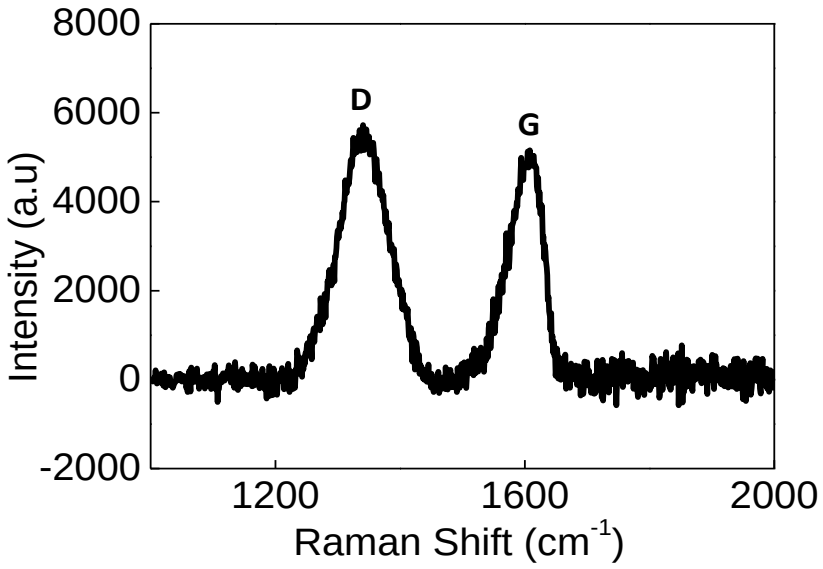

Figure 4.10: The Raman spectrum for GO sheets.

4.4.2 Double-crosslinked nanogel/graphene oxide gels

In this work, two types of gel were prepared and denoted as DX NG and DX NG/GO. Both gels contained 10 wt.% of NG particles. The DX NG/GO gel contained 0.20 wt.% of GO. These gels will be used will as adsorbents in the next chapter. Figure 4.11 shows images of DX NG and DX NG/GO gels. For both gels, APS and TEMED were used during NG inter-crosslinking because TEMED is an accelerator that promotes radical formation, which allow this process to occur at moderate temperature. DX NG is a transparent gel whereas the DX NG/GO is a black gel due to the presence of GO. Figure 4.11c and d show free-standing gels of DX NG and DX NG/GO.

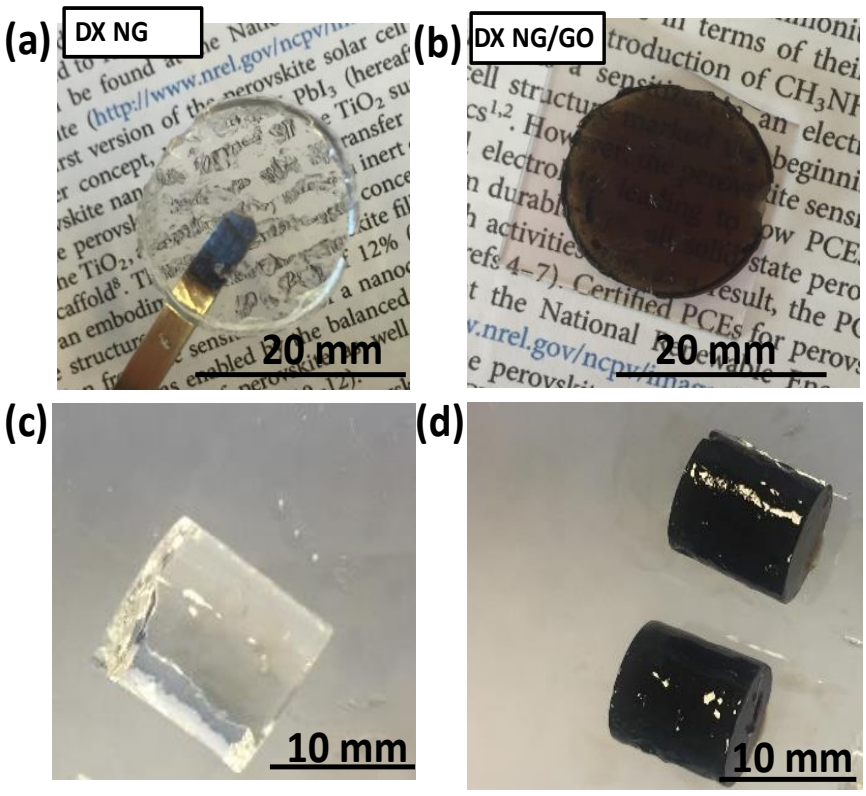

Figure 4.11: Images of DX NG and DX NG/GO in different dimension. Gels in (a) and (b) are in circular shape; Gels in (c) and (d) are in cylindrical shape.

In order to investigate the swelling behaviour of the gels, we define the mass and volume swelling ratios as $Q_{DX\,(m)}$ and Q_{DX}, respectively. Equation 4.3 shows how Q_{DX} can be calculated by finding $Q_{DX\,(m)}$ and densities of polymer ($\rho_\rho = 1.2$ g/cm^3) and solvent ($\rho_s = 1.0$ g/cm^3), respectively[72]. The equation is shown below:

$$Q_{DX} = \rho_\rho \left(\frac{(Q_{DX(m)}}{m} + \frac{1}{\rho_\rho} \right) - \frac{\rho_\rho}{\rho_s} \tag{4.3}$$

Figure 4.12 shows volume-swelling ratio (Q_{DX}) for DX NG and DX NG/GO gels in three phosphate buffers at different pH values; 4.0, 7.0 and 9.0 (The gels images are in Figure 4.13). At pH 4.0, it is evident that Q_{DX} for both samples were similar and relatively low. In contrast, at higher pH (7.0 and 9.0), the gel swelled. For DX NG, Q_{DX} was 19.3 (at pH 7.0) which is

higher in comparison to the values for DX NG/GO; 11.7. GO sheets in DX/NG GO inhibited the swelling of the gel because they acted as crosslinking points[85]. Theoretically, more crosslinking leads to lower swelling ratio as it inhibits network expansion[132, 254].

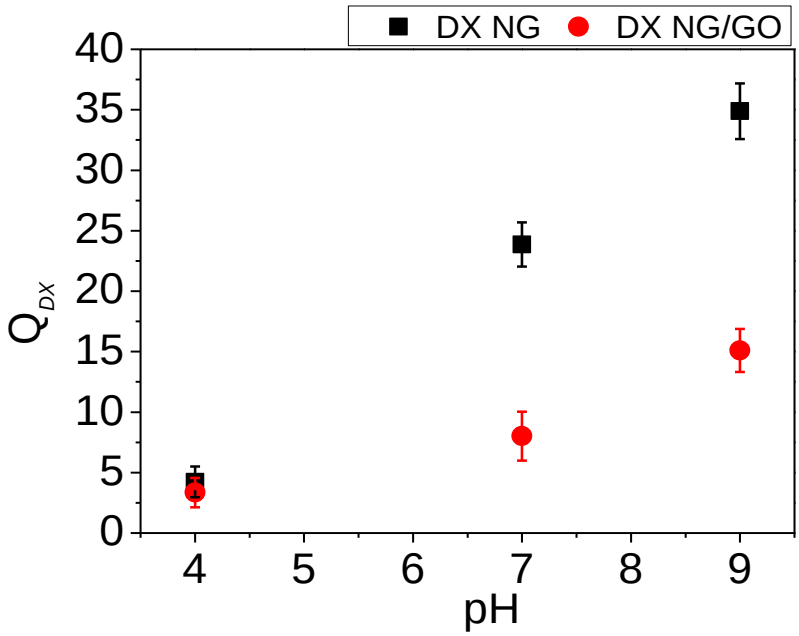

Figure 4.12: Volume swelling ratio (Q_{DX}) of DX NG/GO and DX NG gels corresponding to pH.

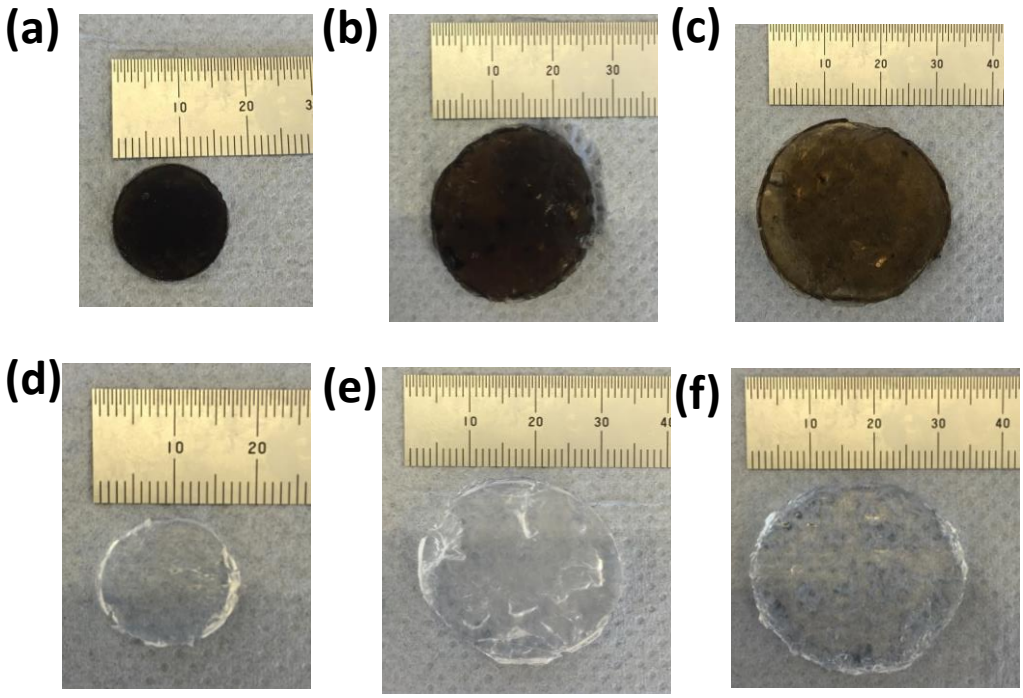

Figure 4.13: Gel images after swelling in different buffer solutions for 7 days; DX NG/GO gels in (a) pH 4; (b) pH 7; (c) pH 9. DX NG gels in (d) pH 4; (e) pH 7; (f) pH 9.

In addition, sol fraction (SF) and gel fraction (GF) were measured for the gels. The SF values for DX NG and DX NG/GO are 0.43 % and 1.5%. These data confirm that significant dissolution did not occur and confirm efficient network formation. A complete network is formed by the gels[64]. The swelling properties of DX NG/GO and DX NG are important for potential application in water purification specifically for Pb^{2+} removal because of good stability (as discussed in Chapter 5).

4.4.2.1 FTIR analysis of GO, DX NG and DX NG/GO

The chemical structure of the GO contains epoxide, hydroxyl, carbonyl, carboxyl, and ether functional groups[255-256]. The concentration and dispersion of these groups is dependent on a variety of factors, primarily the graphite starting material and the oxidation route, and as a result GO is a non-stoichiometric material. In FTIR spectrum of GO (Figure 4.14), the presence of carboxylic functional group is confirmed by those bands below. A band at 3385 cm^{-1} is attributed to the hydroxyl stretching vibrations of the C–OH groups and a weak band at 1718 cm^{-1} and a strong band at 1618 cm^{-1} are assigned to the C=O stretching vibrations of the –COOH groups[257]. A strong band at 1403 cm^{-1} is due to the O–H deformations of the C–OH groups, and a strong band at 1059 cm^{-1} is attributed to C–O stretching vibrations.

For DX NG and DX NG/GO, 1720 cm^{-1} and 1724 cm^{-1} below are present corresponding to C=O stretching vibration of carboxylic group and 2900 cm^{-1} due to CH_2 stretching. A stretching band for O-H represented at 3317 cm^{-1} for DX NG is present but disappeared in DX NG/GO. This may be due to the difference in drying. Due to the low concentrations of GO in DX NG/GO, a difference of functional groups could not be determined by FTIR.

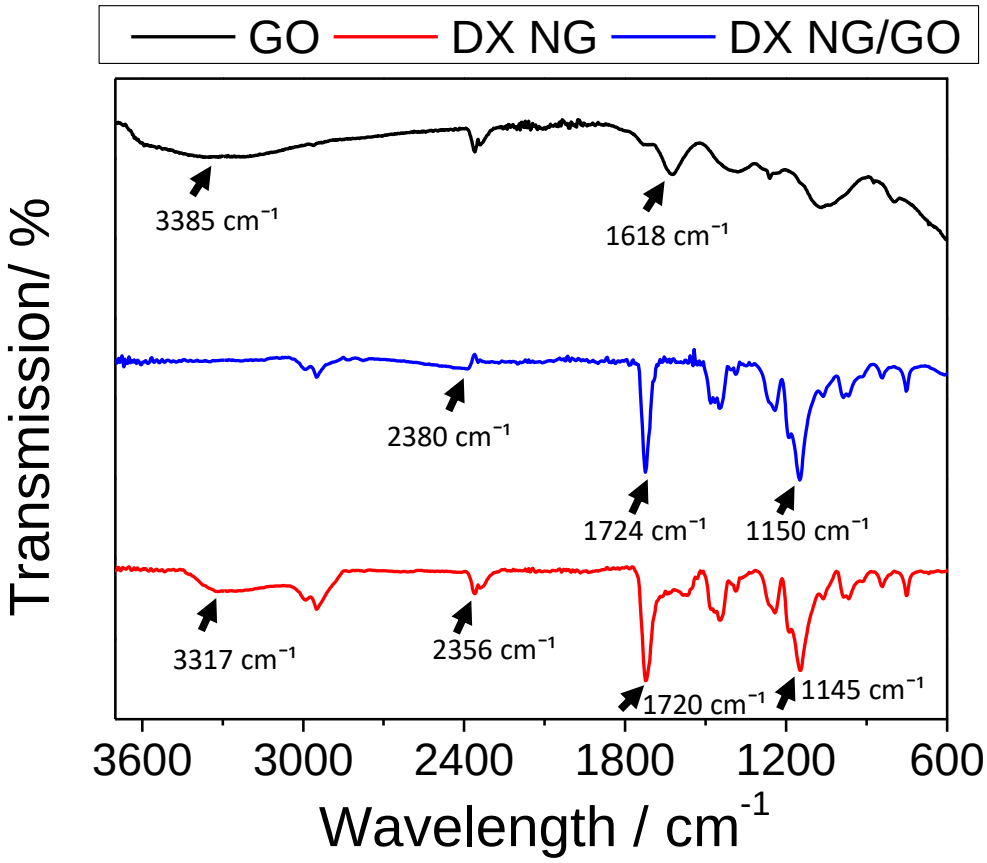

Figure 4.14: FTIR Spectrum of dried DX NG, DX NG/GO and GO.

4.4.2.2 Morphology of DX NG and DX NG/GO

The morphologies of the gels were investigated using SEM. Figure 4.15 show SEM images for freeze-dried DX NG and DX NG/GO gels. For the DX NG gel the NGs had mostly coalesced which meant that few NGs were evident (Figure 4.15a). In the case of the DX NG/GO gel the NGs can be seen covering the GO sheets (Figure 4.15b and c). Figure 4.15c shows the zoomed-in image of Figure 4.15b. This image supports the view that there was an interaction between the GO sheets and the NG particles. GO has a higher thermal stability than the NG particles and we therefore used heating at 800° C to remove the NG particles. Upon

heating the NGs had disappeared as can be seen in Figure 4.15d. These data confirmed the morphology of DX NG/GO and DX NG are related.

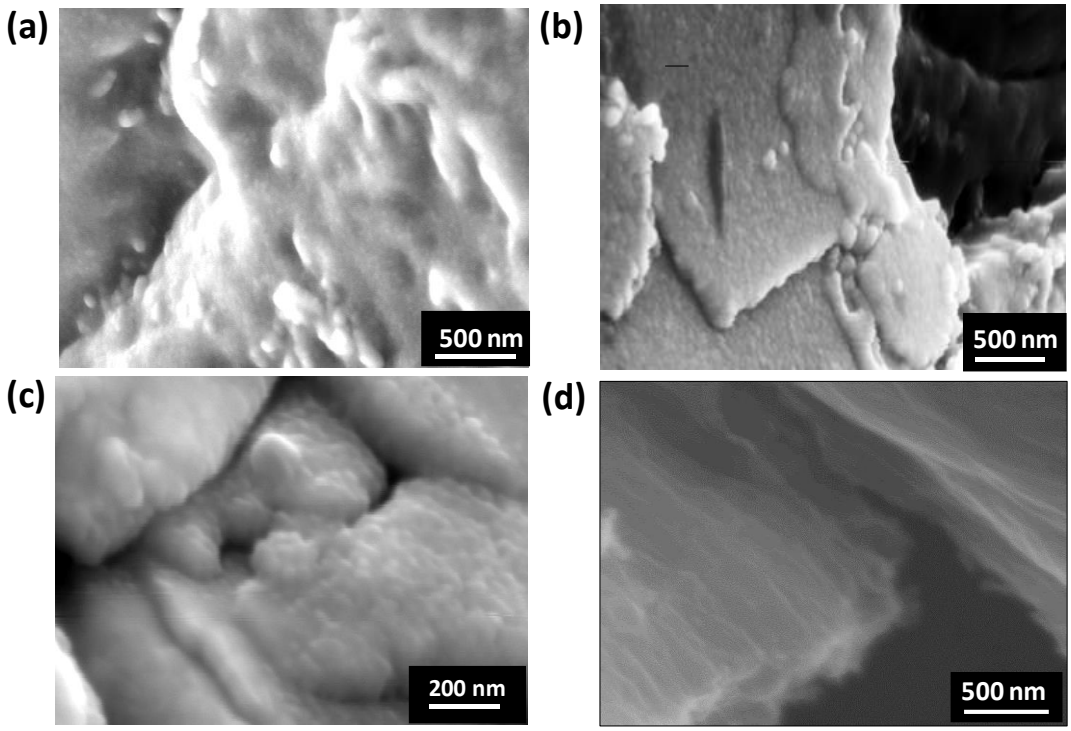

Figure 4.15: SEM images for (a) DX NG; (b) and (c) for DX NG/GO at different magnification; (d) SEM image for DX NG/GO after heating at 800°C to remove NGs.

4.4.2.3 Mechanical properties of DX NG and DX NG/GO gels

The mechanical properties of the gels were investigated using dynamic rheology as well as uniaxial compression measurements. Frequency and strain-sweep rheology data were obtained and shown in Figure 4.16. In Figure 4.16b, it also showed strain independent storage modulus values (*G'*) until the strain exceeded 10%. Inclusion of GO increased *G'* from 10.2 kPa to 60.3 kPa (obtained at 1 Hz frequency), which is a remarkable enhancement given that only 0.2 wt.% of GO was present. The relative modulus enhancement is far greater than observed previously for DX MG/GO gels[85]. This is because of NGs much smaller than MGs. Increase in the GO loading is known to increase gels stresses and dissipated more energy [134]. We propose that an

interlaced non-covalent association between the DX NG phase and GO is present for the present system and that GO acted as a crosslinker. The functional groups of GO nanosheets offer hydrogen bonding with polymer chains[258]. As a result, the GO nanosheets can act as reinforcing nanofillers for further enhancing the mechanical performance of the gels. GO provides additional crosslinking in the polymer chains which restricted the movement of the GO sheets that resulted in less swelling ability compared to GO free gel (DX NG) (Figure 4.13). It is confirmed that the gels are covalently crosslinked they did not re-disperse in water. At higher strain values, *G'* began to decrease and the loss modulus (*G"*) increased. The latter behaviour is attributed to the onset of cage breaking[85]. The intersection of *G'* with the *G"* maxima correspond to the critical strain (γ^*) which is a measure of ductility. This decreased from 170 % for the DX NG to 34 % for DX NG/GO. This decrease in gel ductility is because of the low ductility of GO and additional crosslinking[259]. The low ductility of GO is possibly caused by a lack of epoxide groups (due to inclusion of a low amount of GO). Dissipation of strain energy could not excess effectively and accelerated crack propagation[259].

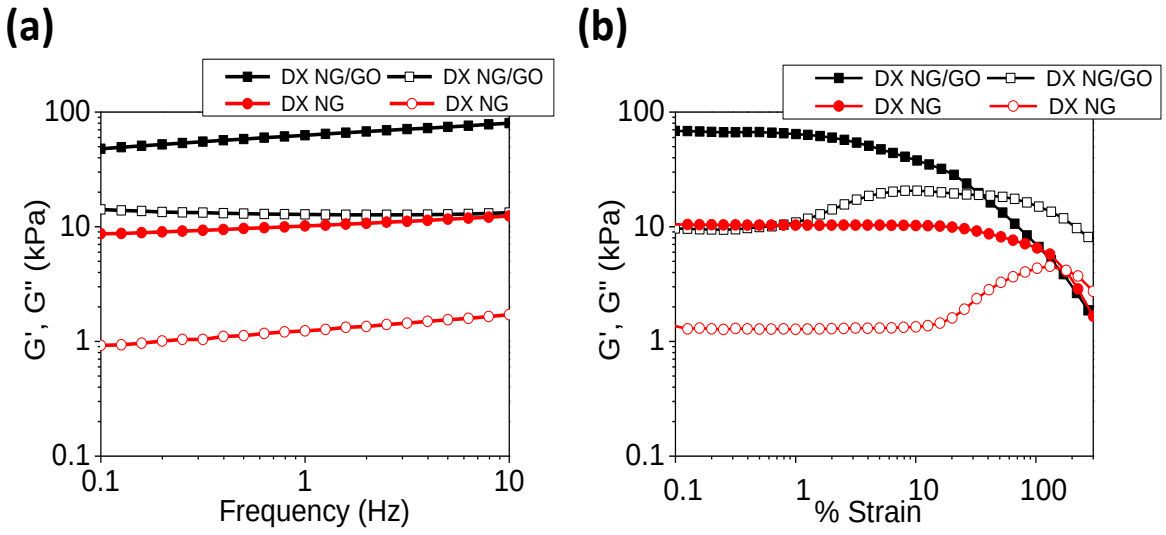

Figure 4.16: Frequency-sweep data for (a) DX NG and DX NG/GO and strain-sweep data for (b) DX NG and DX NG/GO. G' is denoted by closed symbol and G" is denoted by open symbol.

Uniaxial compression data for DX NG/GO and DX NG are shown in Figure 4.17. The values from data analysis for DX NG and DX NG/GO are shown in Table 4.2. The values for the modulus (E) obtained were 82.4 kPa and 19.6 kPa for DX NG/GO and DX NG, respectively. (Figure 4.17b). These data confirm the trend noted for the rheology data with a major increase in modulus for the composite. The strain-at-break (ε) for DX NG/GO and DX NG were 42.3% ± 4.4 and 63.7% ± 7.4, respectively. These values confirm the trend reported earlier for DX MG/GO composites that inclusion of GO decreases the ductility and stretch ability but leads to the increase in stiffness[85]. Importantly, the ε value for the DX NG/GO gel (Figure 4.17c) is much higher than the value of 25% reported for the DX MG/GO gels[85]. This confirms that the use of NGs enabled more ductile GO composites to be prepared. It is expected that the presence of more inter-particle linking as the size decreases (smaller size) and resulted in fewer critical paths to break the gels.

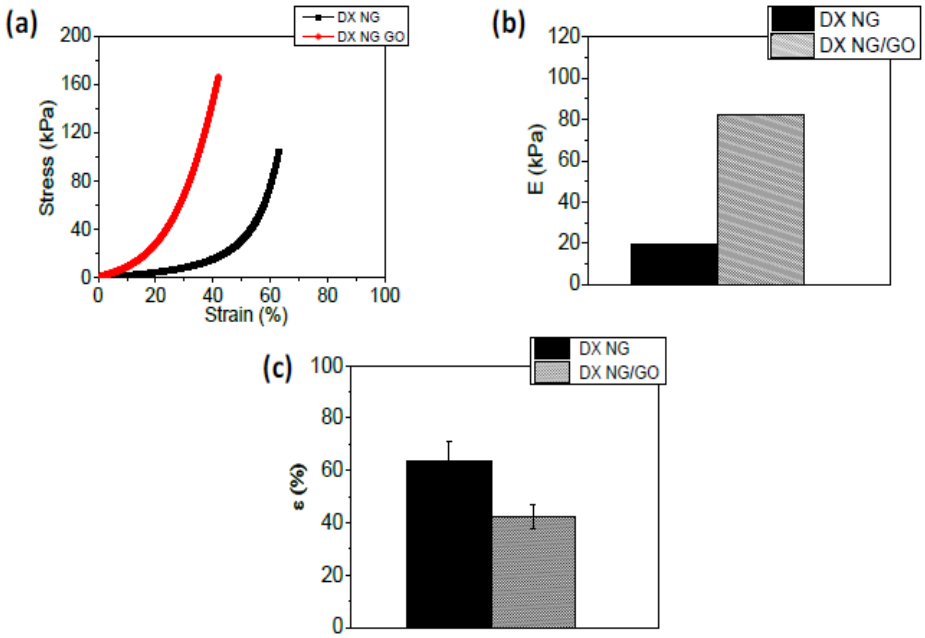

Figure 4.17: (a) Stress-strain data for DX NG and DX NG/GO; (b)Young's modulus values (E) of DX NG and DX NGO; (c) Breaking strain (ε) of DX NG and DX NG/GO.

Table 4.2: Characterisation data for DX NG and DX NG/GO from frequency-sweep and uniaxial compression analysis.

Abbreviations	***Q_{DX}*** [a]	***G'/kPa*** [b]	***Breaking ε/%*** [c]	***Breaking σ/kPa*** [d]	***Young's Modulus/ kPa*** [e]
DX NG	19.3	10.2	63.7 ± 7.4	110 ± 4.6	19.6 ± 0.04
DX NG/GO	11.7	60.3	42.3 ± 4.4	170 ± 10.6	82.4 ± 0.25

[a] Volume swelling ratio.
[b] Obtained from frequency sweep at 1% strain.
[c, d, e] Obtained from uniaxial compression using 100 N load.

4.4.2.4 Optical properties of DX NG and DX NG/GO

To investigate the optical properties of both gels, UV-visible spectroscopy analysis was conducted by preparing DX NG and DX NG/GO gels. The thickness for the gels was 3 mm. The UV-VIS spectra in Figure 4.18 corresponding to DX NG and DX NG/GO samples. The signal monotonically decreased from UV to the visible region which occurred for both samples[260]. The maximum absorption peaks obtained for DX NG/GO and DX NG were at 303 and 295 nm. From the spectra, there is almost no absorbance of DX NG in the UV region from 300 to 800 nm. Meanwhile, a sharp increased absorbance was observed when GO nanosheets are introduced, even the content as low as 0.2 wt.%. The high absorbance of DX NG/GO because of the presence of GO in the system that enhanced UV light adsorption[261]. In addition, the optical properties of the gels can be tailored by adjusting the transparency of the gels. DX NG is a transparent gel while DX NG/GO is a black gel.

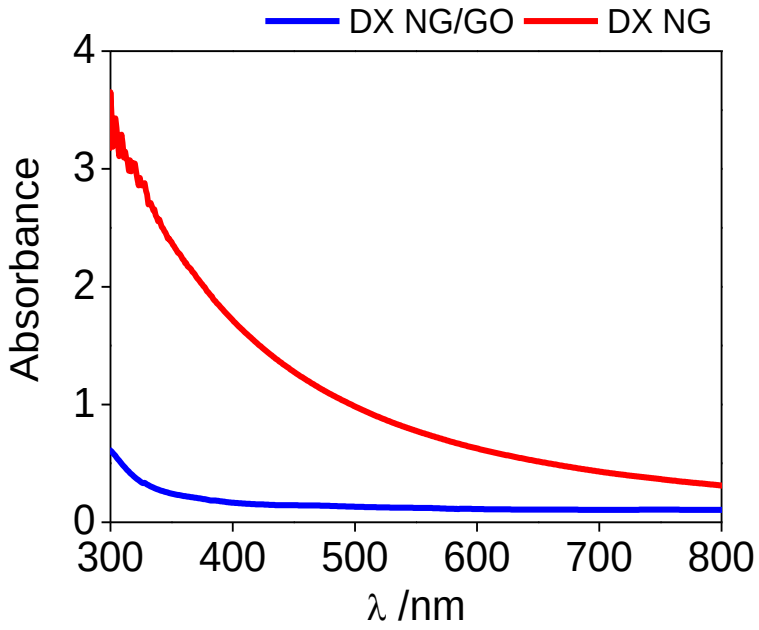

Figure 4.18: UV-vis spectra for DX NG and DX NG/GO gels. The thickness of the samples was 3.0 mm.

4.4.3 Preliminary studies to investigate the stability of DX NG and DX NG/GO in different solvents.

Preliminary studies on DX NG and DX NG/GO were conducted by immersing them in four different solvents; DMSO, DMF, ɣ-butyrolactone (GBL) and acetone for five days. The purpose of the studies is to observe the stability of the gels in other solvents apart from water. All these solvents are polar solvents[262-263]. The structures of each solvents used are shown in Figure 4.19. The type of penetrating solvent (polar solvents in this work) can also have a profound effect on polymer dissolution. The appearance of DX NG and DX NG/GO after being immersed in each solvent is shown in Figures 4.20 and 4.21. This experimental observation will be used as a guidance to conduct further future investigations related to perovskite solar cell[264-265]. After five days, it was observed that both DX NG and DX NG/GO remained intact and maintained their initial shape (see Figure 4.20b and Figure 4.21b). GBL, DMSO and DMF have been used to prepare perovskite solar cells which contain Pb[266]. Poly(methyl

methacrylate) (PMMA) was used for solar cell encapsulation. PMMA was introduced in perovskite solar cell as a coating layer and eventually resulted in better stability of perovskite solar cell[266]. The utilisation of polymer in perovskite solar cell has been reported previously and mostly as the capping layer on top of perovskite[265, 267-268]. This present experiment shows that hydrogel based networks may be designed that remain intact on swelling in solution used for perovskite solar cells. However, DMF is carcinogenic and it is recommended to replace it with DMSO instead. In addition, GBL is a low solubility solvent and a good candidate to produce high quality perovskite[269]. On the other hand, acetone is a thermodynamically bad solvent for the gel as shown in Figure 4.20. Besides, the gels have good stability in these four solvents and may have potential to be used for perovskite solar cell or hybrid solar cell. More study is required on this aspect.

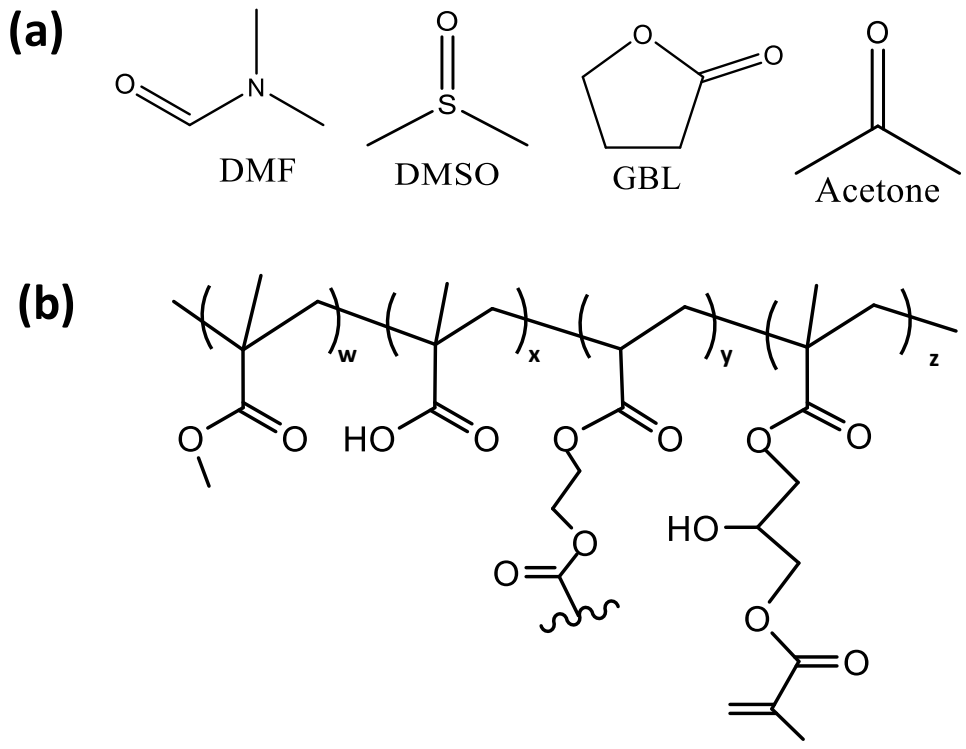

Figure 4.19: (a) Chemical structure of different solvents; DMSO, DMF, GBL and acetone; (b) Structure of crosslinked NGs.

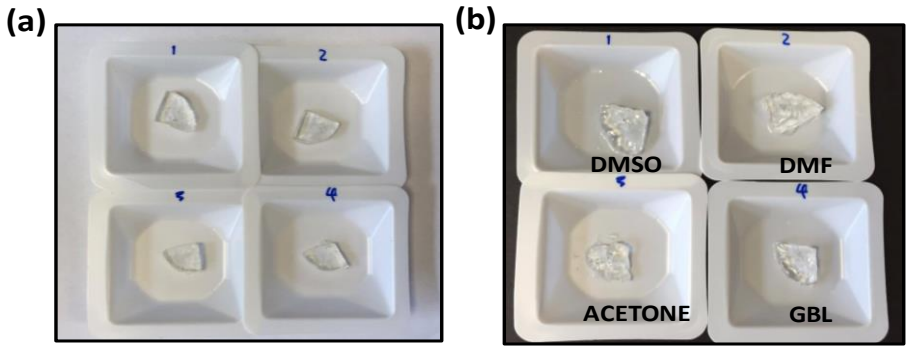

Figure 4.20: (a) As-made DX NG gels; (b) After immersed in four different solvents for 1h.

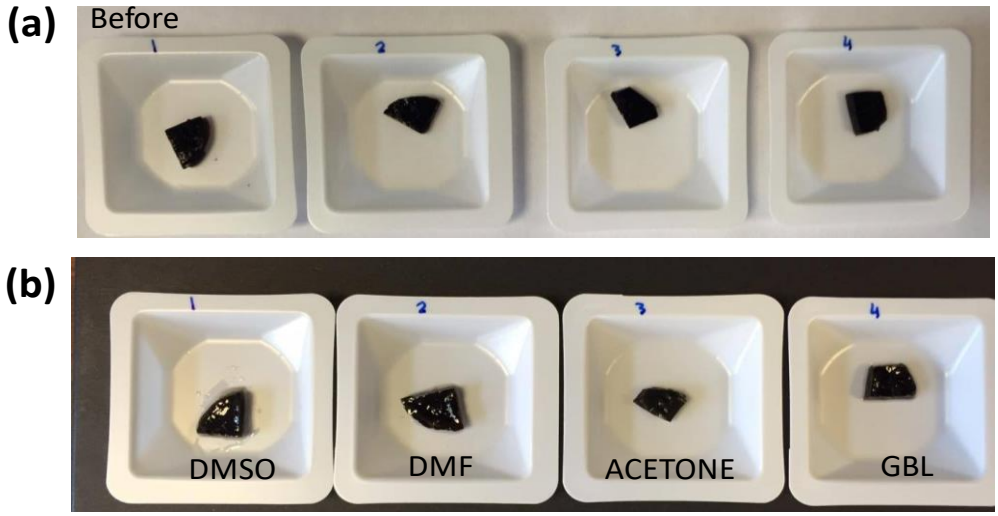

Figure 4.21: (a) As-made DX NG/GO gels; (b) After immersed in four different solvents for 1 h.

4.5 CONCLUSIONS

In this chapter, GO (0.2 wt.%) was successfully included in the DX NG structure for the first time to observe the effect of low amount of GO on the mechanical properties of the gels. There are four main systems that were thoroughly studied to build the understanding; non-functionalised NGs (precursor), functionalised NGs (NG), DX NG and DX NG/GO. The incorporation of GO in polymer network structure had major effects and improved the physical and mechanical properties of the gels. From results obtained by rheology and compression, it was found that G' considerably increased for DX NG/GO (60.3 kPa) compared with as-made gel, DX NG (10.2 kPa). From compression analysis, the E values for DX NG/GO and DX NG were 82.4 kPa and 19.6 kPa, respectively. Whilst, the strain-at-break for DX NG/GO and DX NG were 42.3% and 63.7%, respectively. From strain sweep data however, for DX NG/GO, it was found that covalent interlinking of NG particles decreased γ^* values and ductility. This research demonstrates that DX NG/GO and DX NG may have potential to be an effective way to capture more Pb^{2+} ions due to the presence of GO and improved mechanical properties (>10 kPa). This will be further investigated in the next chapter. The DX NG and DX NG/GO gels have good stability in polar organic solvents (DMSO, DMF, GBL and acetone) that commonly used in perovskite solar cell/hybrid solar cells.

CHAPTER 5 : LEAD ADSOPRTION BY DX NG AND DX NG/GO

5.1 ABSTRACT

In this chapter DX NG and DX NG/GO will be further investigated for their potential for green environmental application which is to capture toxic Pb^{2+} ions. This work will be focused on the mechanism and interactions that occur between the gels and Pb^{2+} ions. GO is covalently bound with abundant of oxygen functionalities such as carboxyl groups and phenolic hydroxyl group that are suitable for heavy metal cation removal, hence favour removal of Pb^{2+} ions. In addition, carboxylic acid groups from DX NG system that containing methacrylic acid (MAA) have a role in the removal of Pb^{2+} ions as well. It was observed that incorporation of GO in DX NG has elevated the removal percentage of Pb^{2+} ions despite only 0.2 wt.% of GO present in the composite gel. The Pb^{2+} adsorption capacity of DX NG and DX NG/GO were 204 mg/g and 254 mg/g, respectively. In this work, FTIR analysis was conducted to investigate the mechanism and interaction between Pb^{2+} ions and functional groups in both systems. The modulus values for DX NG and DX NG/GO after Pb^{2+} uptake showed major improvement due to the formation of ionic crosslinks involving Pb^{2+} and $-COO^{-}$. From XPS analysis, the data obtained supported the presence of linkages established between carboxyl groups and Pb^{2+}. The gels studied here have potential application for water purification.

5.2 INTRODUCTION

Heavy metal contamination is a major environmental threat and has become an important worldwide problem[145,270-271]. Unlike organic wastes, heavy metals ions are accumulated in the environment and living tissue. For instance, Pb transfers into the food chain causing various diseases and disorders of living organisms even at a trace level[146, 272]. Pb emerges as a second among the harmful heavy metal pollutants[11]. The USA environmental protection agency (EPA) and World Health Organization (WHO) established the maximum acceptable level for Pb value in drinking water as 0.015 and 0.01 ppm[8]. Pb is widely used in various industrial processes, such as production of batteries, metal plating, painting and smelting[145]. There are many techniques being explored to remove heavy metal ions from water such as chemical precipitation, ion exchange, chemical oxidation/reduction, reverse osmosis, electrodialysis, and ultrafiltration[11,146,272]. Nevertheless, all these techniques have shortcomings such as low efficiency, high costs and generation of toxic sludge and other waste products[273].

Adsorption is a conventional and important separation process and has been used widely in environmental applications[274]. Adsorption is one of the most popular methods for heavy metal ion removal and has attracted considerable attention because of its simplicity, convenience, cost and efficiency[8]. In general, effective adsorbents should have good physicochemical stability, low cost , easily separated and regenerated for reusability[78]. Besides, a good adsorbent material should possess a permeable (porous) structure to provide large contact area between adsorbent (adsorbing material) and adsorbate (substance being adsorbed) to facilitate the adsorption process[275]. The porous surface should also contains functional groups to enable solute adsorption[22, 159].

In recent years, hydrogels have spurred great interest in the adsorption of heavy metal ions due to their hydrophilicity, low toxicity, biocompatible, crosslinked nature, and the existence of functional groups such as -COOH and -OH that have a strong chelating ability for heavy metal ions[159,274,276]. Furthermore, the functional groups in the network of hydrogel can be consolidated with the target molecule to attain large adsorption capacity. One of the first work regarding Pb adsorption by MGs was reported by Morris et.al[277]. In that work, the ability to remove Pb^{2+} ions from water using –COOH groups was demonstrated. Other studies involved with hydrogels in removing heavy metal ions from aqueous solution including acrylamide (AAm)-2-acrylamido-2-methylpropane sulfonic acid (AMPS) sodium salt clay hydrogel, xylan-rich hemicelluloses-based hydrogel, polymers based on methacrylic acid and poly(ethylene glycol) and other polymeric adsorbents[146, 278-281]. Besides, chemically cross-linked hydrogels with carboxylic or amine groups have been used for heavy metal ion sequestration[84].

However, a major problem with conventional hydrogels for heavy metal ions adsorption is their poor mechanical properties and low selectivity that constraints their practical application in wastewater remediation. Introducing sacrificial bonds in hydrogel network has good potential to develop a new class hydrogel with enhanced mechanical properties. Based on the built-in energy dissipation, a series of a physically chemically hybrid crosslinked DN were prepared composed of two complementary network structures. The first network was always constructed by physically crosslinked gels, while the second network is chemically linked[61-62]. Those reports demonstrated that the covalent bonds serve as permanent crosslinks to construct the primary structure and maintaining the integrity of the DN gels; whereas the noncovalent bonds (such as hydrogen bonds, metal coordination bonds, and hydrophobic interaction) acted as sacrificial bonds that can be reversibly disrupted and spontaneously reform, resulting in enhanced mechanical performance[282].

Recently, considerable progress in developing tough hydrogels occurred which lead to the broad application prospects in biomaterials, soft robotics, smart actuators, sensors and water treatment[283-284]. The use of hybrid hydrogels has potential impact for Pb^{2+} removal from water. In this work, the performance of a pH-responsive hybrid polymer gel comprised of NG with GO for Pb^{2+} removal was explored. The inclusion of GO has improved the mechanical properties of the composite gels and due to the presence of carboxylic acid groups on the edges of the GO sheets which can act as scavengers for metal ions. It is also shown that the mechanical properties of both gels were far improved and robust after Pb^{2+}adsorption. Herein the adsorption ability of DX NG and DX NG/GO gels in removing Pb^{2+} ions are investigated. The adsorption isotherm and mechanical properties of the gels after adsorption of Pb^{2+} are studied. This study aims to address the structure-property relationships governing the physical and mechanical properties of the gels after Pb uptake. It is hypothesised that when DX NG/GO gels are exposed to metal cations, they will form reversible ionic complexes due to $RCOO^-$ to metal chelation.

5.3 EXPERIMENTAL

5.3.1 Materials

The methods used to prepare DX NG and DX NG/GO were fully described in Chapter 4. $Pb(NO_3)_2$ (>99%) was purchased from Alfa Aesar to prepare Pb aqueous solution. All chemical reagents were used without further purification. All aqueous solutions were prepared using high purity deionised water.

5.3.2 DX NG and DX NG/GO

In this section, DX NG and DX NG/GO will be further studied for Pb^{2+} uptake. For Pb^{2+} adsorption studies, 10 gels were prepared for each system. The adsorption experimental works were conducted for seven replicate data under identical condition to ensure the reproducibility of the data.

5.3.3 Swelling measurements.

Swelling measurements were conducted for the gels in different concentrations of Pb^{2+} aqueous solution. Swelling measurements are important to observe the relationship between swelling ability of the gels with Pb^{2+} adsorption for 24 h. The initial mass of each gel was 1.0 ± 0.2 g and was accurately measured. The gels were placed in different concentration of Pb^{2+} aqueous solution; 100 ppm, 200 ppm, 500 ppm, 750 ppm and 1000 ppm. The volume of Pb^{2+} aqueous solution was 40 ml. After specific time interval similar to adsorption experimental work, excess Pb^{2+} solution on the gels was carefully removed by paper towel prior to weighing. The pH of Pb^{2+} aqueous solution was maintained at 6.8.

5.3.4 Pb stock solution preparation

Different concentrations of Pb^{2+} were prepared using $Pb(NO_3)_2$ for adsorption experimental work. There were five different concentrations of Pb^{2+} prepared to monitor the adsorption behaviour of Pb^{2+} ions at low and high concentrations; 1000 ppm, 750 ppm, 500 ppm, 200 ppm and 100 ppm. To prepare 1000 ppm, 1.598 g of $Pb(NO_3)_2$ salt was dissolved in 100 ml of deionised water until it was fully dissolved and diluted to 1000 ml in a flat bottom volumetric flask. From 1000 ppm of Pb aqueous solution, it was diluted to 750 ppm, 500 ppm, 200 ppm and 100 ppm. The initial pH of the solution was increased to pH 6.8 by addition of aqueous NaOH (0.5M).

5.3.5 Pb uptake experiments.

All gel samples (DX NG and DX NG/GO) were stated above and added to 40 ml solution containing aqueous $Pb(NO_3)_2$ solution. The pH of solution was maintained at pH 6.8 ± 0.1 using aqueous NaOH (0.5M) and the samples (in 200 ml container) were placed in a thermostatic shaker **(**Julabo SW23**)** bath at 37ºC for 24 hours. The samples were protected to avoid interference of light which may affect the accuracy of the results. The speed of the shaker bath was fixed at 100 rpm to ensure mixing of Pb solution and to avoid the gel from fragmentation due to fast shaking. For each measurement, 1.0 ml aliquot of Pb^{2+} solution was taken at specific time interval, and the volume removed was replaced with fresh Pb^{2+} solution. The Pb^{2+} concentration in the sample was analysed using inductively coupled plasma mass spectrometry (ICP-MS). The amount of Pb^{2+} adsorbed by the composite gels was determined by calculating the difference of initial and equilibrium concentration of Pb^{2+} solution. The adsorption capacity (q in mg/g) was obtained from the equation 5.1:

$$q = \frac{(C_i - C_f)V}{m} \tag{5.1}$$

Where C_i and C_f are the initial and final concentration (mg/L) of Pb^{2+}, respectively. V is the volume (L) of Pb^{2+} aqueous solution used, and m is the dry gel mass (g).

5.3.6 Desorption experiments

To examine the desorption behaviour of Pb^{2+} ions, DX NG and DX NG/GO gels containing adsorbed with Pb^{2+} ions were separated from the solution and added into 0.1 M of HCI at pH 3.5 in a beaker to elute the adsorbed Pb^{2+} ions. The contents of the beaker were stirred at 100 rpm in the water bath shaker for 24 h at room temperature to determine how much Pb^{2+} can be desorbed from the gels. This experiment was performed for one cycle only due to time constraint (four samples). The DX NG and DX NG/GO gels remained intact.

5.3.7 Physical measurements.

SEM images for freeze-dried DX NG, DX NG/GO and GO were performed by Philips XL30 FEG-SEM HKL EBSD instrument with an accelerating voltage of 15 kV. Dynamic rheology measurements were conducted using a TA Instruments AR-G2 temperature-controlled rheometer equipped with an environmental chamber. A plate geometry (20 mm diameter) was used. The strain-sweep measurements were conducted using a frequency of 1 Hz. The uniaxial compression tests were conducted using an Instron series 5569 load frame equipped with a 100 N load cell. For this testing, more than three sets of the gels were prepared for each system. The average height and diameter of the gel cylinders were 12 mm and 11 mm, respectively. The compression rate was 2 mm/min. Modulus values were calculated from the initial gradient of stress-strain curves at strains (ε) of less than 10%. The surface chemistry of the gels after Pb uptake was investigated using X-ray photoelectron spectroscopy (XPS, Kratos Axis Ultra Hybrid X-ray photoelectron spectrometer) equipped with an Al Kα monochromated X-ray source (1486.6 eV). The X-ray beam was 300 x 700 μm. Prior to each measurement, the gel samples were dried in a vacuum chamber at 40°C for 2 days. The amount of the adsorbed Pb^{2+} ions by the gels was quantified by inductively coupled plasma-atomic emission spectrometer (ICP-AES). For ICP analysis, Pb^{2+} aqueous solution was diluted to 10 wt.%, filtrated by 0.22 μm filter and transferred to 10 ml centrifuge tubes.

5.4 RESULTS AND DISCUSSION

This chapter will discuss the research findings related to Pb^{2+} removal by DX NG and DX NG/GO. The discussion is focused on the effect of initial Pb concentration, swelling behaviour of the gels after adsorption, adsorption isotherm, physical and mechanical properties of the gels after Pb uptake.

5.4.1 Effect of initial Pb concentration on adsorption

Figure 5.1 shows the effect of initial concentration on the adsorption of Pb^{2+} by DX NG and DX NG/GO. Within the first few hours, it can be seen that the adsorption increased rapidly in the beginning, slowed down afterward and started to reach a constant value after 5 hours of contact time for DX NG and slightly longer for DX NG/GO gels. For the latter, the adsorption process reached a plateau after 10 hours. At higher initial Pb^{2+} concentration from 500 ppm to 1000 ppm, the maximum adsorption capacities obtained for DX NG and DX NG/GO are 122 mg/g and 142 mg/g (for 500 ppm), 174 mg/g and 190 mg/g (for 750 ppm) and 193 mg/g and 210 mg/g (for 1000 ppm), respectively. By increasing the initial Pb^{2+} concentrations, the adsorbed amount also increased. Higher initial concentrations resulted in a higher driving for ingress into the gels for Pb^{2+} ions and hence increased contact between Pb^{2+} ions with available sites for adsorption. Consequently, the diffusion of Pb^{2+} ions into the gels was accelerated[285]. The results obtained showed that a higher adsorption capacity of Pb^{2+} was achieved by DX NG/GO in comparison to DX NG. Better adsorption capacity of Pb^{2+} ions for DX NG/GO can be attributed to the high affinity of Pb^{2+} ions to the hydroxide (−OH), epoxide (−O−) and carboxylic (−COOH) groups on the GO nanosheets[286]. The incorporation of GO into the polymer matrix even at low concentration enhanced the adsorption due to –COOH (from MAA) which were converted into $–COO^-$ providing chelation for the positively-charged Pb ions[165].

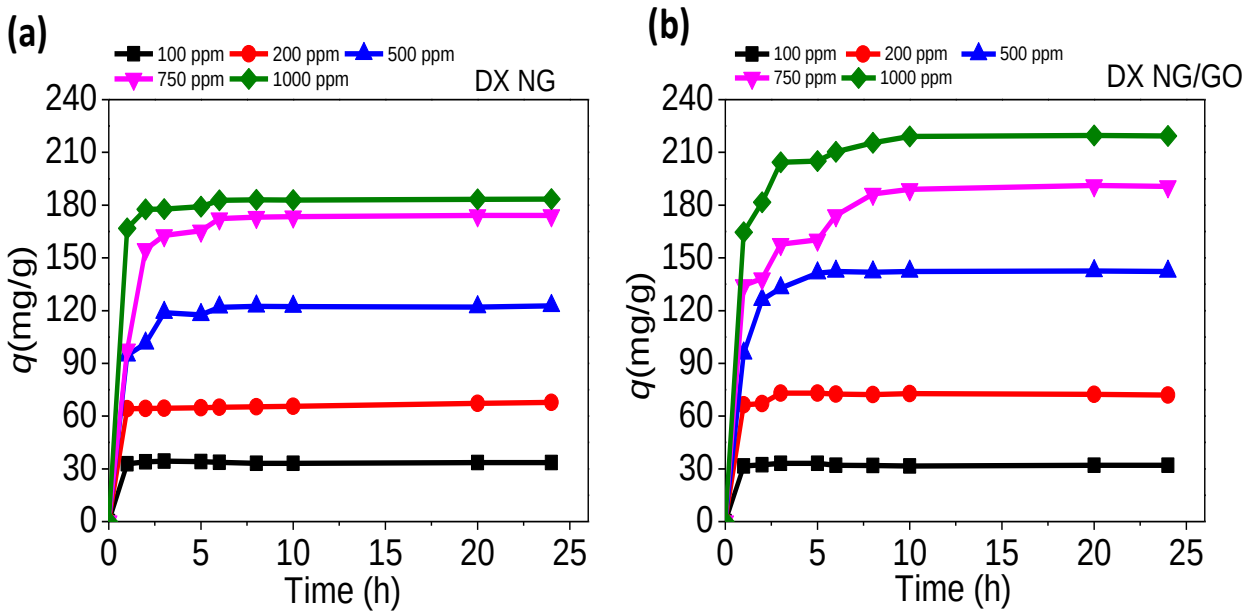

Figure 5.1: Adsorption capacity (*q*) as a function of time for (a) DX NG and (b) DX NG/GO gels.

Adsorption of Pb^{2+} at various initial concentration (C_o) vs equilibrium concentration (C_e) are shown in Figure 5.2 for DX NG and DX NG/GO. The data show that the maximum values for the equilibrium adsorption capacity (q_e) attained by DX NG and DX NG/GO are 183 mg/g and 215 mg/g. Hence Pb^{2+} uptake is more pronounced for DX NG/GO as described above. The maximum *q* in this work is higher than that obtained in previous work reported involving activated carbon (43.85 mg/g)[165, 287-288]. In fact, the *q* values are comparable to the maximum adsorption capacity reported for magnetic nanocomposite (148 mg/g)[271] and chitosan–poly(acrylic acid) (CS–PAA) beads (109-138 mg/g)[289]. This is the first time that DX NG and DX NG/GO have been used to capture Pb^{2+} ions.

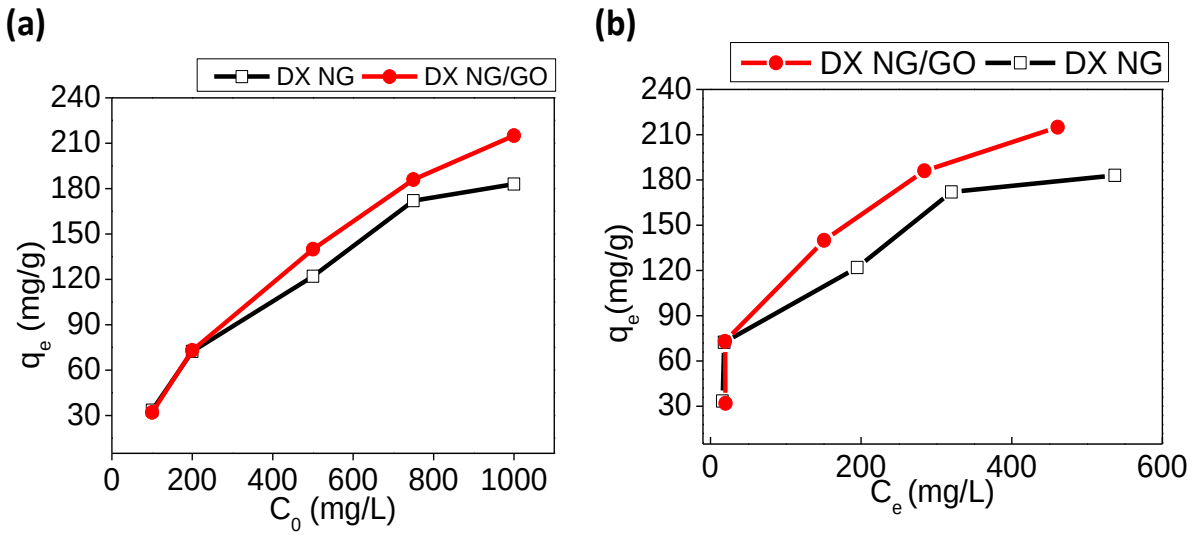

Figure 5.2: Data of equilibrium adsorption capacity (q_e) of Pb^{2+} as a function of C_0 in (a) and data of q_e as a function of equilibrium concentration (C_e) of Pb^{2+} in (b).

The images of DX NG and DX NG/GO after Pb^{2+} adsorption is shown in Figure 5.3. When placed in low concentration of Pb^{2+} aqueous solutions (100 ppm and 200 ppm), both gels swelled. However, the gels highly de-swelled at higher Pb^{2+} concentration aqueous solution (500 ppm, 750 ppm and 1000 ppm). Images for all samples confirmed that they remained intact after Pb^{2+} adsorption.

.

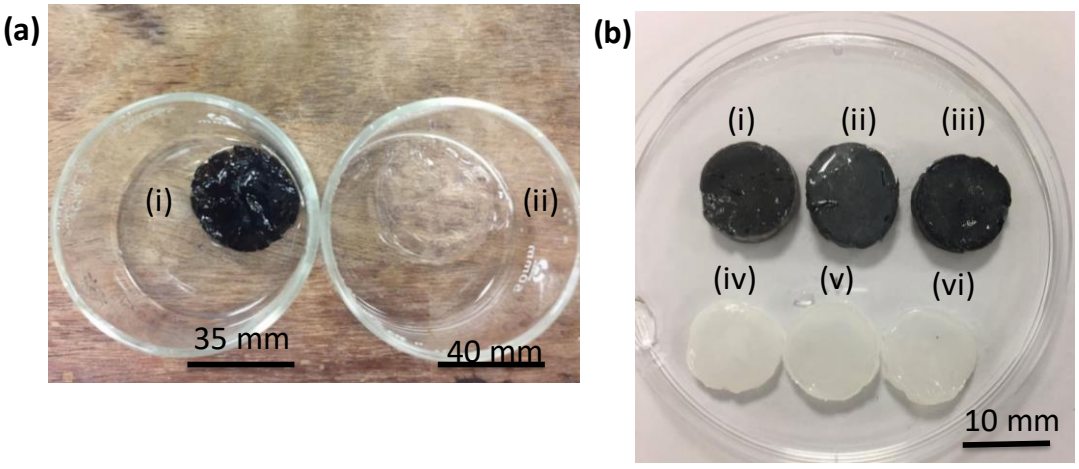

Figure 5.3: Images of (a) (i) DX NG and (ii) DX NG/GO after Pb uptake in 100 ppm of Pb^{2+} solution; (b) DX NG and DX NG/GO after Pb uptake in 1000 ppm of Pb^{2+} solution (i) and (iv); in 500 ppm of Pb^{2+} solution (ii) and (v); in 750 ppm Pb^{2+} solution (iii) and (iv). The samples had been exposed to Pb^{2+} solution for 24 h. The black gels contained GO.

5.4.2 Swelling of the gels and adsorption capacity

The volume swelling ratio (Q_{DX}) with time for DX NG and DX NG/GO after Pb adsorption was measured at pH 6.8 and is plotted in Figure 5.4a and 5.4b. The equation for Q_{DX} is given in section 3.3.5.4. The control samples of DX NG and DX NG/GO in Figure 5.4c and 5.4d were measured at pH 6.8 in phosphate buffer solutions. The values of Q_{DX} for the control samples were 19.1 (DX NG) and 11.3 (DX NG/GO). In the buffer solutions (at pH 7), the gels swelled due to the ionisation of carboxyl groups (-COOH). Electrostatic repulsion forces between the polymer chains are generated by $-COO^-$ and resulted in the enhancement of swelling. In the addition of salt, the decay in water uptake reduced the swelling of the gels.

As depicted in Figure 5.4a and 5.4b, the Q_{DX} reached equilibrium in a few hours as indicated by the constant values obtained. It was observed that the value of Q_{DX} changes dramatically as adsorption occurs. A possible explanation for this result is that most of adsorption occurs within the "breathing in" region. Breathing in regions refers to the adsorption of Pb^{2+} by the gels at 100 ppm and 200 ppm whereby the gels in swollen state and tend to absorb more water. In this region, Q_{DX} values are largest for the gels. At low concentration of Pb^{2+}, the amount of Pb^{2+} ions bound to carboxyl group is small and greater swelling is produced by the difference between ionic pressure inside and outside of the gels (osmotic pressure). The higher value of osmotic pressure enhance the water uptake in the gels and resulted in higher swelling[290]. The results coincided well with previous study by Katime et.al regarding absorption of metal ions and swelling properties of poly(acrylic acid-icoitaconic acid) hydrogels[292].

When the initial concentration of Pb^{2+} increased, the formation of complexes between Pb^{2+} and carboxylic groups is more probable. Furthermore, at higher concentration of Pb^{2+} (from 500 ppm to 1000 ppm) only a small amount of additional adsorption occurs, and the gels had de-swelled considerably. The findings obtained at high Pb^{2+} concentration (500-1000 ppm)

suggest that more Pb^{2+} ions were present that decreased the repulsive forces and formed ionic crosslinking. Hence the gels contracted[293] and decreased in swelling capacity[294]. The Q_{DX} values of the gels with respect to initial concentration of Pb^{2+} (C_0) and equilibrium concentration of Pb^{2+} (C_e) are shown in Figure 5.4c and d. The graph that shown in these figures is to validate the data obtained for Q_{DX} values. The diffusion of Pb^{2+} ions into the gel network structure is confirmed by the data obtained in Figure 5.4d. It was found that at higher equilibrium concentration of Pb^{2+}, formation of ionic crosslinking resulted in lower Q_{DX} values. In contrast, diffusion of water is more pronounced at lower equilibrium concentration of Pb^{2+} (100 ppm to 200 ppm) and resulted in higher swelling.

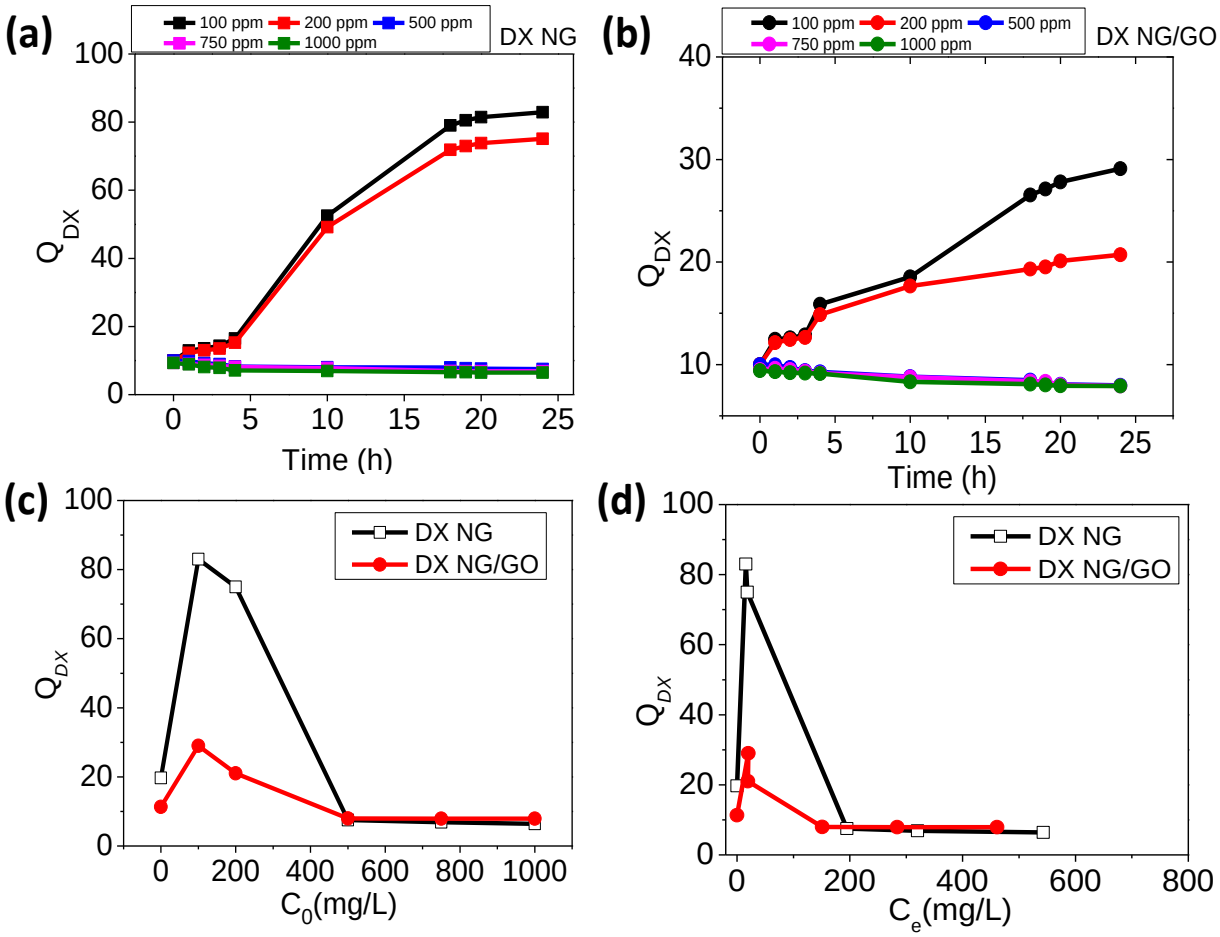

Figure 5.4: (a) Volume swelling ratios (Q_{DX}) vs time after Pb adsorption for DX NG in; (b) Q_{DX} of DX NG/GO after Pb adsorption. The data is measured under the same conditions as in Figure 5.1; (c) Data of Q_{DX} vs initial concentration of Pb^{2+} (C_0); (d) Equilibrium concentration of Pb^{2+} (C_e) for DX NG/GO and DX NG. The Q_{DX} for control samples is denoted at 0 ppm for both DX NG and DX NG/GO.

5.4.3 Adsorption isotherm studies

The adsorption data is further analysed using Langmuir and Freundlich isotherm models. The Langmuir isotherm is based on three assumptions; i) adsorption is limited to monolayer coverage, ii) surface sites are alike and can accommodate the adsorbed ion, iii) the ability of a molecule to be adsorbed on a given site is independent on its neighbouring occupancy[155]. The Freundlich model on the other hand is applicable to heterogeneous surfaces. The Langmuir and Freundlich adsorption isotherm model fits obtained in this work are shown in Figure 5.5 for DX NG and DX NG/GO. The values of each component are summarised in Tables 5.1 and 5.2 below. The data were first linearised according to the Langmuir model as stated in the equation below[165, 295]:

$$\frac{C_e}{q_e} = \frac{C_e}{q_{max}} + \frac{1}{q_{max}k_L} \tag{5.2}$$

Where q_{max} is the maximum adsorption capacity and k_L is Langmuir adsorption constant. A plot of C_e/q_e versus C_e gives a straight line with the slope of $1/q_{max}$ and the intercept $C_e/(q_{max})$. The Freundlich model is given by equation 5.3[296]:

$$\ln q_e = \ln k_F + \frac{1}{n} \ln C_e \tag{5.3}$$

Where k_F and $\frac{1}{n}$ are Freundlich adsorption constant and intensity of adsorption.

Based on the analysis in Figure 5.5a, it was found that DX NG and DX NG/GO gels shows good agreement with Langmuir model and q_{max} values obtained for DX NG and DX NG/GO are 204.1 mg/g and 256.4 mg/g. For Freundlich model (Figure 5.5b), the R^2 obtained are less than 0.90. Hence, monolayer like adsorption was found to be a better description for adsorption for both systems. The values obtained also corresponded closely to the isotherm adsorption

plateau (Figure 5.1) which further indicates that the Langmuir modelling is appropriate. It is proposed that the higher q_{max} achieved by DX NG/GO system is due to the presence of GO that possesses -COO^- to bind positively charged Pb^{2+} ions[165].

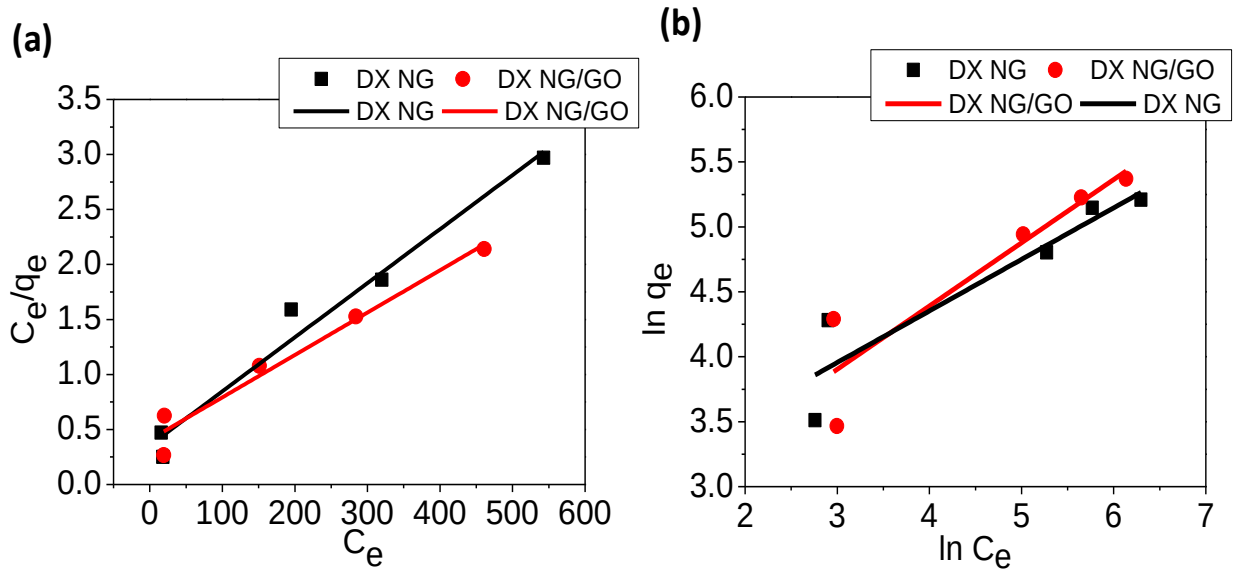

Figure 5.5: (a) Langmuir model fitting of the adsorption data for DX NG/GO and DX NG and (b) Freundlich model fitting for DX NG/GO and DX NG. The line shows linear fitting for DX NG and DX NG/GO.

Table 5.1: Fitting parameters for Langmuir model for DX NG and DX NG/GO. q_{max} is the maximum adsorption capacity, k_L is Langmuir adsorption constant and R^2 is correlation coefficient.

Langmuir	**DX NG**	**DX NG/GO**
q_{max} (mg/g)	204.1 ± 17.1	254.4 ± 15.3
k_L (mg/g) (L/mg)	0.0136	0.0110
R^2	0.976	0.968

Table 5.2: Fitting parameters for Freundlich model for DX NG and DX NG/GO. k_F is Freundlich adsorption constant, n is intensity of adsorption and R^2 is correlation coefficient.

Freundlich	**DX NG**	**DX NG/GO**
k_F (mg/g) (L/mg)	14.8	11.4
n	2.45	2.03
R^2	0.882	0.857

Theoretical calculation for maximum capacity of Pb^{2+} uptake by the gels is shown in appendix and was compared to the experimental values obtained. The theoretical value obtained for maximum uptake of Pb^{2+} for DX NG was 285 mg/g (it was assumed the $-COO^-$ groups bound to Pb^{2+} ions). The value of experimental adsorption capacity of Pb^{2+} determined from the linear Langmuir for DX NG was 204 mg/g indicates the gel managed to adsorb 72% of Pb^{2+} ions. This could be attributed to de-swelling of the gels upon exposure to high concentration of Pb^{2+} which may have restricted ingress. Another reason for lower than expected uptake is that some of $-COO^-$ groups maybe isolated and not be sufficiently close to another $-COO^-$ to enable binding of a Pb^{2+} ion. Therefore, 100% adsorption of Pb^{2+} ions is unfeasible. For DX NG/GO, the gel managed to absorb more Pb^{2+} due to the presence of GO[165]. The implication of GO in DX NG/GO (256.4 mg/g maximum capacity) with 0.2 wt.% has affected the absorption capacity by 20% due to strong complexation between Pb^{2+} and COO^- groups on the surface of DX NG/GO. A larger number of oxygen-containing functional groups such as -COOH and -OH are present on GO, thereby making GO and its nanocomposite effective for capturing heavy metals in aqueous solution[155].

.

5.4.4 Mechanical properties of DX NG and DX NG/GO after Pb adsorption

In this part, the effect Pb^{2+} uptake on the mechanical performance of DX NG/GO and DX NG gels was investigated. The mechanical strength and stability are among the utmost important properties of hydrogels considering the application in wastewater treatment. Figure 5.6a shows that the values of *G'* increased with increase of Pb^{2+} concentration. This behaviour is due to crosslinking of ionic bonding between Pb^{2+} and $–COO^-$ in the gels. The complexation that occurred between Pb^{2+} and functional group that available on the NG gels affected mechanical properties of the hydrogels. The Pb^{2+} caused the gels to collapse (to a hard state) had a major effect on the *G'* after Pb^{2+} uptake. Compared to the as-made gels (Figure 4.16 in Chapter 4), the *G'* values obtained after adsorption are dramatically decreased for the lower initial Pb^{2+} concentration (100 ppm and 200 ppm). Gels at these lower Pb^{2+} concentrations were in swollen state (Figure 5.4) and had low G' values. Interestingly, the GO does not seem to affect G' when Pb^{2+} is present. This is a crucial observation as it means NG ionic crosslinking dominates mechanical properties when Pb^{2+} is present. Figure 5.6b shows *G'* values is proportional with polymer volume fraction (ϕ_p) of the gels (straight line plotted for DX NG and DX NG/GO and the R^2 obtained were 0.967 for DX NG and 0.991 for DX NG/GO) for log-log plots which is greater than the linear behaviour between G and ϕ_p expected from rubber elasticity theory[78]. This departure could be attributed to ionic crosslinking. Table 5.3 shows the values that obtained from the mechanical analysis for DX NG and DX NG/GO before and after adsorption.

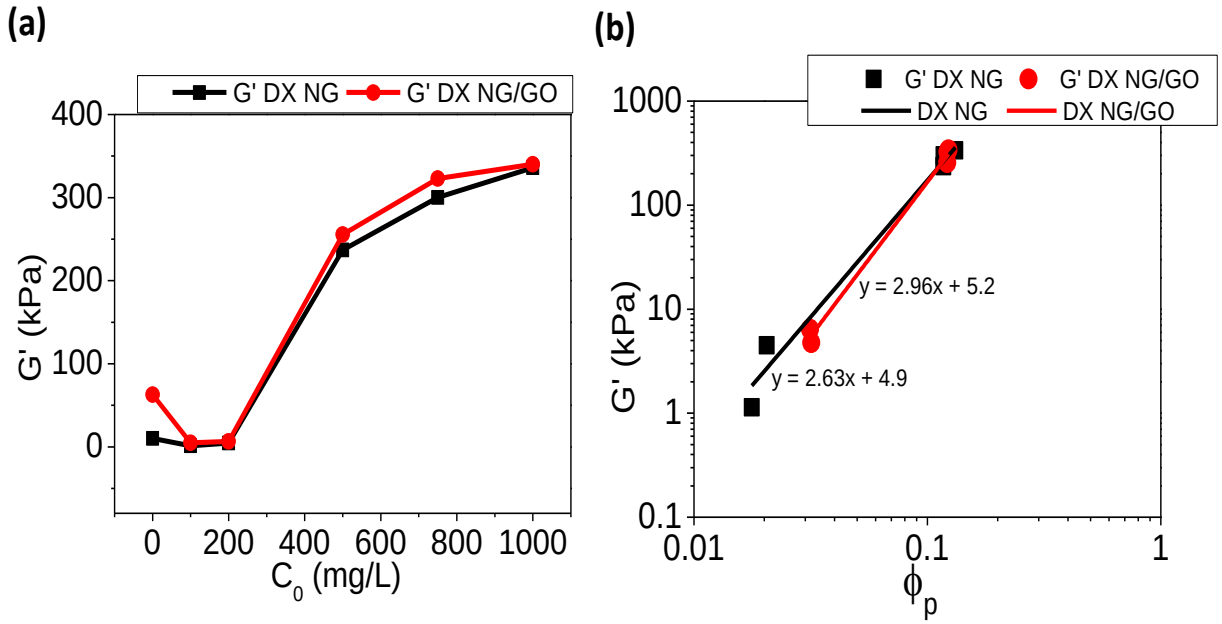

Figure 5.6: Shows the data for G′ as a function of C_0 (a) and G’ as a function of ϕ_p in (b) for DX NG and DX NG/GO.

Table 5.3: Characterisation data for DX NG and DX NG/GO before and after Pb^{2+} adsorption.

Abbreviations	***Q_{DX}*** [a]	***G'/kPa*** [b]	***Φ_p*** [c]	***Breaking δ/%*** [d]	***Breaking σ/kPa*** [e]	***Young's Modulus/ kPa*** [f]
DX NG	19.3	3.50	0.05	63.4 ± 7.4	110 ± 4.6	19.6 ± 0.04
DX NG/GO	11.7	14.30	0.14	42.3 ± 4.4	170 ± 10.6	82.4 ± 0.25
DX NG (1000 ppm)	6.4	334	0.16	56.8 ± 8.05	1045.4 ± 47.5	247 ± 57.9
DX NG/GO (1000 ppm)	7.9	340	0.13	55.4 ± 13.4	1273.2 ± 36.3	336 ± 55.2

[a] Volume swelling ratio at pH 6.8.
[b] Obtained from Frequency sweep at 1% strain.
[c] Volume fraction of the gels.
[d, e, f] Obtained from uniaxial compression using 100 N load.

Uniaxial compression stress strain data for DX NG and DX NG/GO after Pb uptake at 1000 ppm were obtained and are shown in Figure 5.7. The values demonstrated high E values for both systems in comparison to as made gels. The E values obtained for DX NG and DX NG/GO after 1000 ppm Pb uptake are 247 kPa and 336 kPa; respectively (Table 5.3). For the breaking stress, the values obtained for DX NG and DX NG/GO after Pb uptake are 1045 kPa and 1273 kPa. These values are much higher than the as made sample before adsorption takes place; 110 kPa for DX NG and 170 kPa for DX NG/GO. The network structure contained additional ionic crosslinker due to Pb^{2+} ions which tremendously increased mechanical strength of the gels due to ionic crosslinking[297]. It was surprising that the breaking strain increased for DX NG/GO when Pb^{2+} was present.

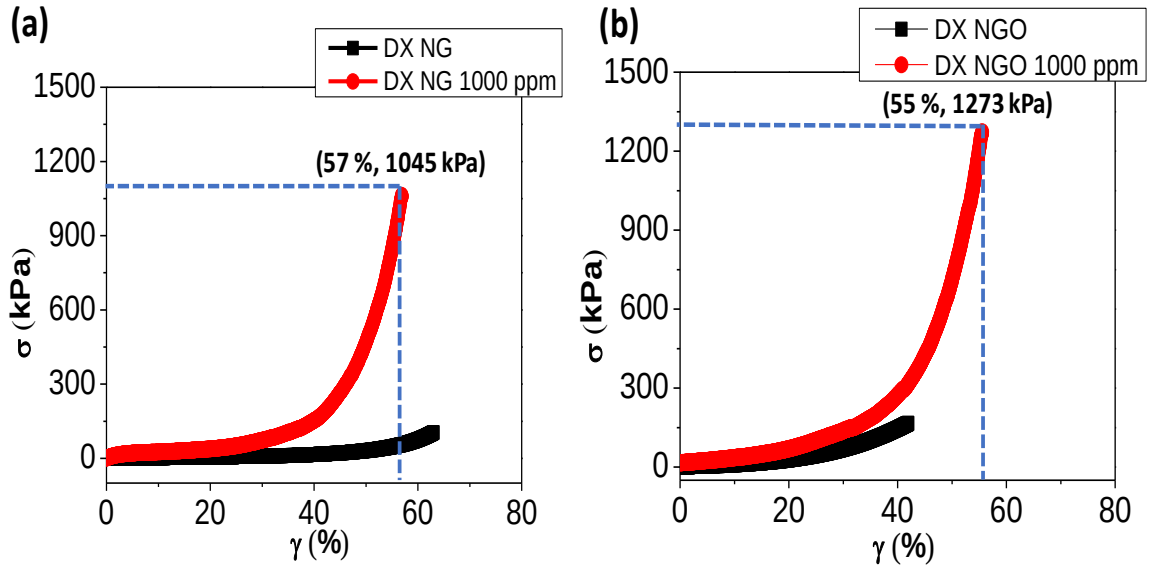

Figure 5.7: Uniaxial compression stress vs strain data for gels after Pb^{2+} adsorption.

5.4.5 FTIR analysis for DX NG and DX NG/GO before and after Pb adsorption

FTIR spectra was conducted for DX NG and DX NG/GO before and after adsorption (for 100 ppm, 200 ppm and 500 ppm. The purpose of FTIR analysis is to investigate any possible interactions between Pb^{2+} ions and functional group. The FTIR spectra are shown in Figure 5.8 and was zoomed-in for the specific wavenumbers. The broad and strong stretching band at 3224 cm^{-1} is attributed to the symmetrical stretching vibration of O−H stretching peak[270]. However, the 1747 cm^{-1} peak was ascribed to the stretching vibration of -COOH. Formation of the coordinate bonds between carboxylate ion groups (COO^-) and Pb^{2+} complexes $Pb(COO^-)_2$ are indicated by this shifting wavenumber[146]. Li et al in his work also investigated on Pb^{2+} adsorption by chitosan granules and poly-acrylic acid (CTS-PAA)[153]. PAA was chosen due to high carboxyl group. In his work, the interaction between Pb^{2+} and CTS-PAA after adsorption was characterised by FTIR. The results obtained showed peak shifted to lower frequency for carbonyl group (coordination between metal ion with COO^-) and shifted to higher vibration frequency for interaction with COOH group (indicate formation of metal ion complexes)[153]. Meanwhile, Park et al in studied on effects of various metal ions on structural changes monodisperse poly (MAA/EGDMA)/Fe_3O_4 hydrogel microspheres. In that work, FTIR analysis was conducted and the stretching vibration of the Fe–O bond was shifted to higher wavenumber indicating Fe_3O_4 was bound to -COO^- on the hydrogel surface[298]. In this work, there is no shift in the wavenumber found and therefore FTIR does not support the complex formation of COO^- groups and Pb^{2+} ions.

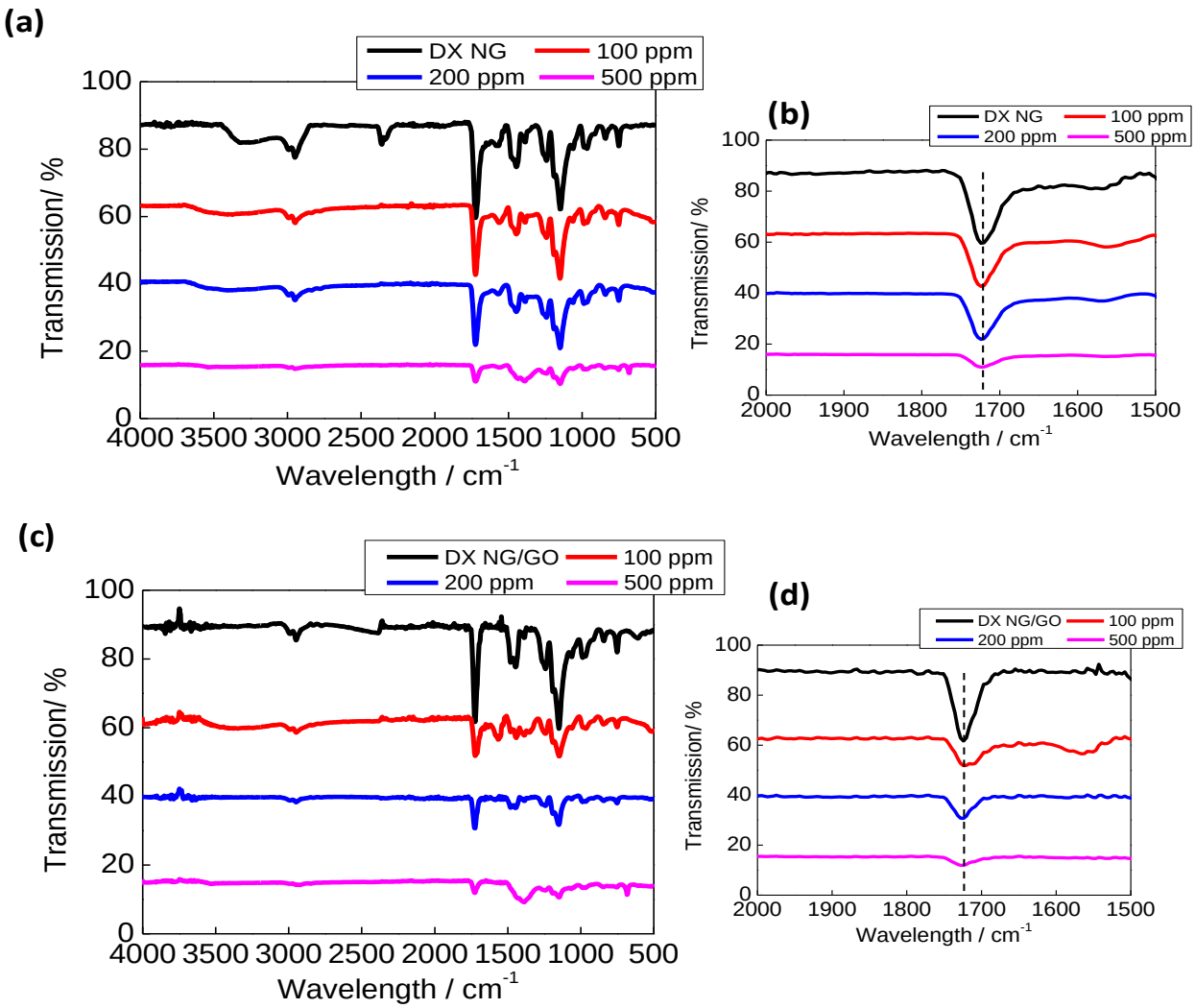

Figure 5.8: FTIR spectra of DX NG and DX NG/GO before and after adsorption of Pb^{2+}.Control samples denoted as DX NG and DX NG/GO.

5.4.6 XPS analysis on DX NG and DX NG/GO before and after Pb adsorption

To support the data obtained above and to enhance understanding on Pb^{2+} adsorption, XPS characterisation was conducted. For Pb analysis, the primary major region is Pb4f. Figure 5.9 shows representative data of DX NG and DX NG/GO after Pb^{2+} adsorption at 1000 ppm for Pb4f core level. These peaks could be assigned to the Pb oxidized state Pb^{2+} [299]. The binding energies of Pb $4f_{7/2}$ and Pb $4f_{5/2}$ are 143.0 and 138.9 eV, respectively[155,300]. The differences in intensities confirm that DX NG/GO gels adsorbed more Pb^{2+} ions in comparison to DX NG. To confirm whether oxygen atoms are involved in Pb^{2+} adsorption, XPS analysis for O1s level

for both gels was conducted before and after Pb^{2+} uptake and shown in Figure 5.10. For this analysis, dominant peak shown at 531.9 eV and a shoulder peak at 533.3 eV for DX NG and for DX NG 1000 ppm, dominant peak is shown at 532.2 eV and a shoulder peak at 533.5 eV. These peaks are attributed to the oxygen atoms in the –C=O and –C–O–H groups in –COOH, respectively[149, 301]. For DX NG/GO, dominant peak is shown at 531.8 eV and shoulder peak at 533.3 and for DX NG/GO 1000 ppm, 532.0 eV is shown at dominant peak and 533.7 eV at shoulder peak. An increase in the values of binding energies after adsorption might suggest coordination between $-COO^-$ and Pb^{2+} [22]. From this XPS analysis, O-Pb species is further ascertained by O1s core level analysis[145]. The changes in O1s core level after Pb^{2+} uptake is assigned to oxygen atom in Pb^{2+} [8]. This may indicate the presence of linkages established between carboxyl groups and Pb^{2+} ions.

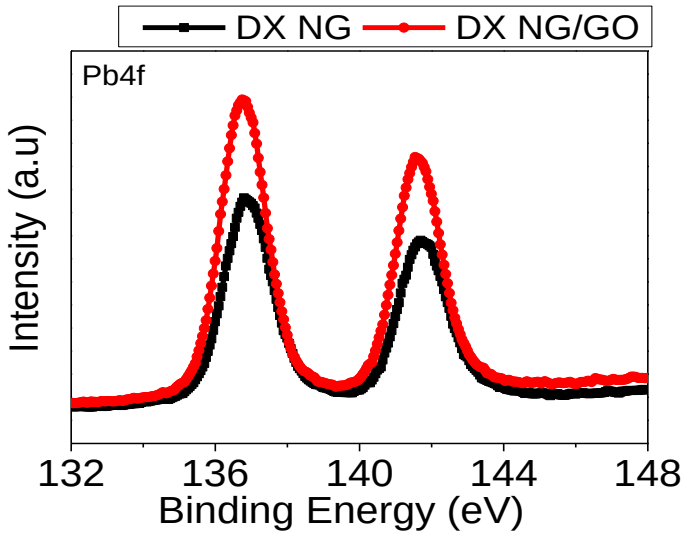

Figure 5.9: XPS Pb4f spectra of DX NG and DX NG/GO after Pb^{2+} adsorption at 1000 ppm.

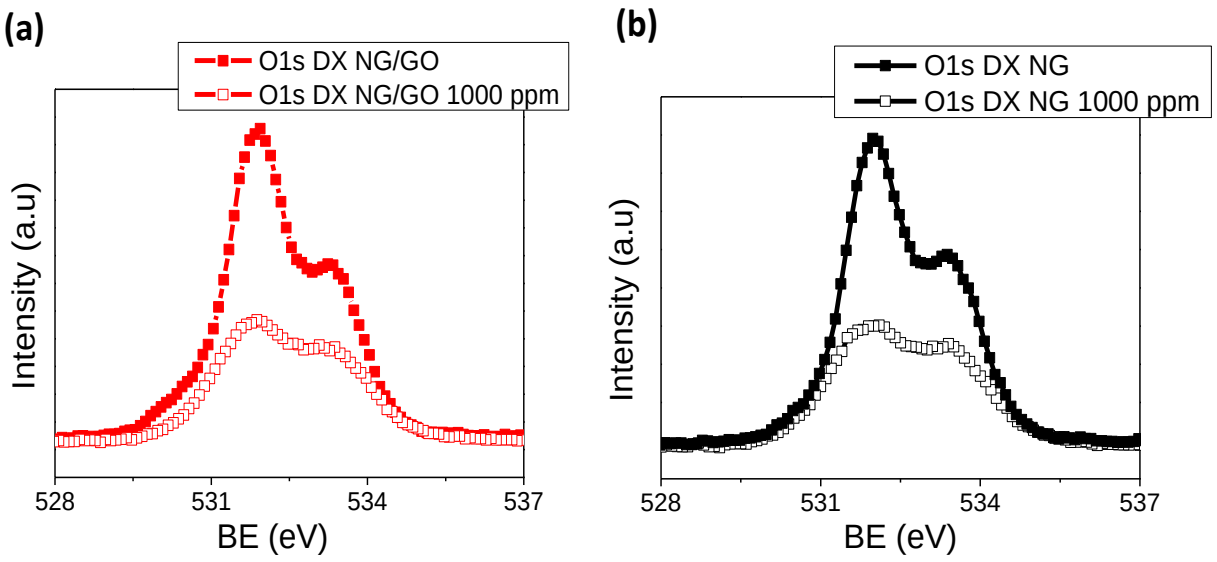

Figure 5.10: XPS O1s spectra for (a) DX NG and (b)DX NG/GO before and after adsorption of Pb^{2+} (1000 ppm).

5.4.7 Reusability test and proposed mechanism.

To access the potential of the gels for reusability, a preliminary study was conducted for DX NG and DX NG/GO after Pb^{2+} adsorption at 750 ppm to investigate the desorption efficiency of the gels. Generally, high desorption efficiency and good reusability are needed for excellent adsorbent to reduce the cost for wastewater treatment[22]. To elute adsorbed Pb^{2+} ions, both gels were placed in 0.1 M HCl at pH 3.5 for 24 hours to observe how quickly Pb^{2+} can be desorbed. As this is only preliminary studies of desorption efficiency, only four data points were measured for DX NG and DX NG/GO gels. As can be seen in Figure 5.11, the final desorption values obtained for DX NG and DX NG/GO after 24 hours were 239 mg/L and 260.9 mg/L, respectively. For DX NG/GO, about 54.8 % of Pb^{2+} was desorbed from the gels and about 55.4 % of Pb^{2+} ions were desorbed from DX NG at 24 hours. Both gels started to elute more Pb^{2+} ions as the time increased (after 4 h). The initial value of Pb^{2+} concentration that was absorbed DX NG and DX NG/GO were 433 mg/L and 476 mg/L at 24 hours. It is anticipated that if the

desorption time is prolonged, all the embedded Pb^{2+} ions in the gels could be removed and the gels might have potential to be reused and recycled. The dilute acid used for desorption caused breaking of coordination bonds between the metal ions and the ligands (–COOH). Therefore, it caused the release of the metal ions from hydrogels into the solution. Easy removal of metal ions (shorter time) from the binding sites suggesting that the hydrogel might be reused for several times without significant loss of its metal ion capacity[293].

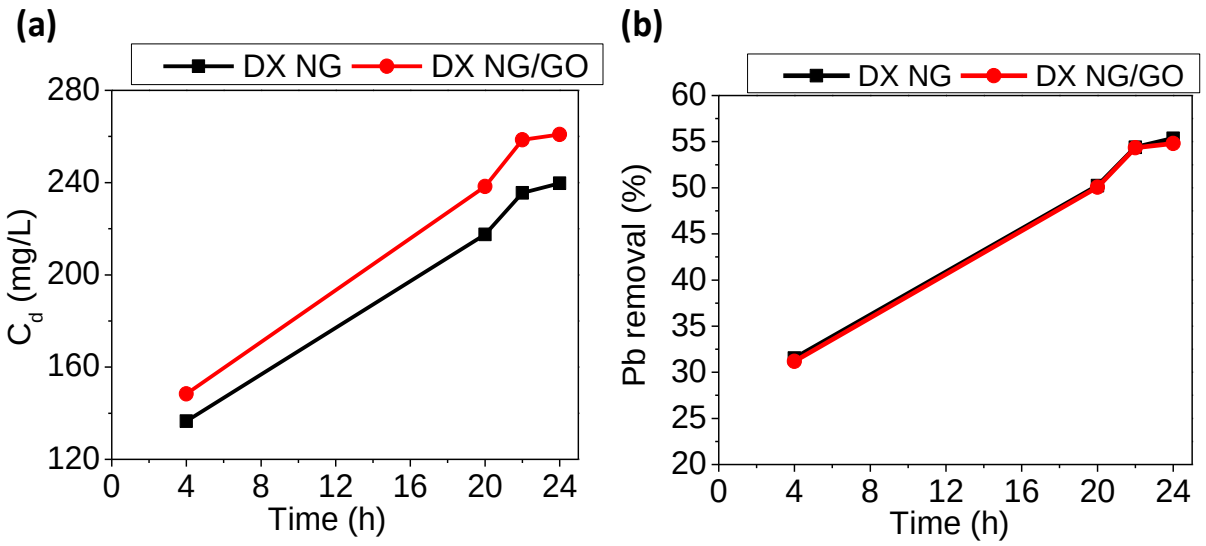

Figure 5.11: (a) Desorption of Pb^{2+} ions of DX NG and DX NG/GO gels after Pb^{2+} adsorption at 750 ppm; C_d is the final desorbed concentration of Pb^{2+}. (b) Graph of Pb removal (%) vs time for 24 h.

The proposed mechanism for Pb^{2+} adsorption is shown in Figure 5.12 and is mainly the complexation between Pb^{2+} ions and $–COO^-$ groups. Pb^{2+} can penetrate the three-dimensional polymeric network due to the electrostatic interaction with negative charged –COO− groups. After entering the network, Pb^{2+} can chelate with the functional groups and adsorption process occurs. Based on the analysis in this chapter, it was inferred that Pb^{2+} ion is adsorbed mainly through chelation and electrostatic interactions to form (reversible) ionic crosslinks.

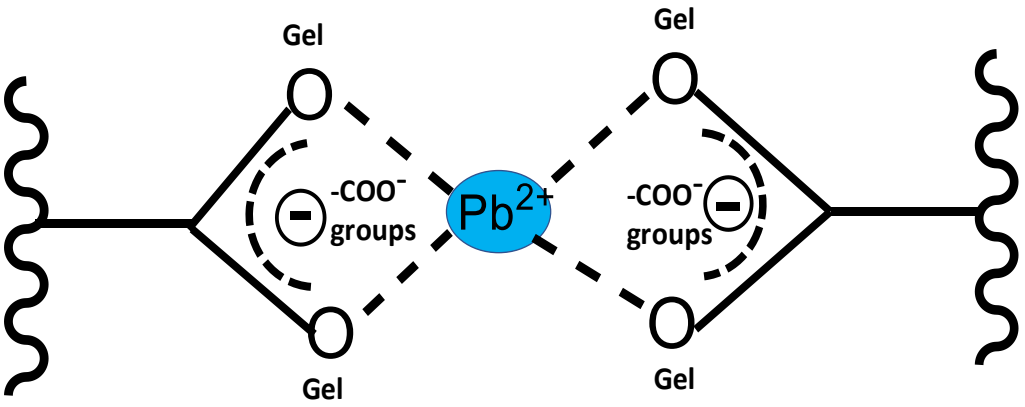

Figure 5.12: Proposed mechanism for Pb^{2+} adsorption by complexation between Pb^{2+} and $–COO^{–}$ groups.

5.5 CONCLUSIONS

The main goal of the current study was to investigate Pb^{2+} adsorption by DX NG and DX NG/GO and the physicochemical properties of the gels after adsorption. The study found that Pb^{2+} removal efficiency was enhanced by the inclusion of GO in the gel network structure. The maximum adsorption capacity of Pb^{2+} obtained by DX NG/GO and DX NG was 254 mg/g and 204 mg/g. The GO role in capturing more Pb^{2+} ions was confirmed by XPS analysis. The results of adsorption isotherm indicate that both systems fitted the Langmuir adsorption isotherm. It was also observed that mechanical properties of DX NG/GO and DX NG greatly increased after Pb^{2+} uptake suggesting crosslinking due to ionic bonding. The proposed mechanism for Pb^{2+} adsorption is mainly through chelation and ionic crosslinking. Desorption tests were conducted to observe gels potential to be reused and recycle. From this analysis, it was found that DX NG/GO managed to desorb about 54.8 % of Pb^{2+} and DX NG/GO managed to desorb 55.4 % of Pb^{2+} ions within 24 hours. This research demonstrates that DX NG/GO and DX NG have potential as effective adsorbents to capture more Pb^{2+} ions in the future. It is suggested that the DX NG/GO may also have potential to trap Pb^{2+} released from perovskite solar cells.

CHAPTER 6 : CONCLUSIONS AND FUTURE WORK

6.1 SUMMARY AND CONCLUSION

This study has involved a thorough investigation of pH-responsive MGs and NGs-based materials specifically for Pb^{2+} ion removal from water. The studies associated to mechanical and physical properties are essential to enhance understanding of the different MGs systems.

In Chapter 3, the data obtained in this study are the first example of DX MGs prepared using a carboxylic acid monomer other than MAA. Further understanding associated to the size of MGs, pK_a and swelling properties are obtained with CEA as a co-monomer. On the other hand, the blending system of CEA was invoked to modulate the mechanical properties of the gels. An improvement in the ductility of DX CEA gel is prominent compared to the established DX MAA gel. The swelling properties of CEA gels were comparable to the control sample and did not plateau until the pH has reached between 8 to 9. Despite the increased amount of GMA in DX CEA28, it did not dominate the swelling properties of this system. The swelling behaviour for the blend system, DX BL-CEA gel was in between of DX CEA21 and DX CEA28. This behaviour shows that the swelling of the DX CEA gels can be tuned by blending between the two components. The Young's modulus value of blend system was remarkably close to that of DX CEA28 which indicated that larger particles from CEA28 distributed more stress within gel. Strong scattering was obtained by the blend gel due to the differences in densities and particle sizes of CEA21 and CEA28**.** These gels were however considered too mechanically weak to pursue as a material for Pb^{2+} capture.

In Chapter 4, low amount of GO (0.2 wt.%) was successfully incorporated into the DX NG network structure and contributed to the remarkable enhancement in the mechanical properties of the gels. The incorporation of GO in the polymer network structure improved the physical and mechanical properties of the gels. From results obtained by rheology and compression, it was found that G' substantially increased for DX NG/GO (60.3 kPa) compared to as-made gel, DX NG (10.2 kPa).The Young's modulus values obtained for DX NG/GO and DX NG were 82.4 kPa and 19.6 kPa, respectively. The strain-at-break values for DX NG/GO and DX NG were 42.3% and 63.7%, respectively. From strain sweep data for DX NG/GO, it was found that additional crosslinking caused the decreased in ductility of the gel. This research also demonstrates that DX NG/GO and DX NG may have potential to be used as an absorbent to capture Pb^{2+} ions due to the presence of GO and improved mechanical properties. These DX NG and DX NG/GO gels had good stability in polar organic solvents (DMSO, DMF, GBL and acetone) which has potential to be used in perovskite solar cells.

In Chapter 5, Pb^{2+} removal efficiency was enhanced by an inclusion of GO (0.2 wt.%) in the gel network structure. From adsorption isotherm analysis, the maximum adsorption capacity obtained for DX NG/GO and DX NG were 254 mg/g and 204 mg/g. From XPS analysis, it was confirmed that the presence of GO enhanced adsorption of Pb^{2+} ions. Additionally, adsorption isotherm obtained for both DX NG/GO and DX NG fitted the Langmuir model. The mechanical properties of DX NG/GO and DX NG were greatly increased after Pb^{2+} adsorption which suggested crosslinking occurred due to ionic bonding. Pb^{2+} was adsorbed mainly through chelation and electrostatic interactions. From reusability test, it was found that DX NG/GO managed to be desorbed about 54.8 % of Pb^{2+} whilst DX NG/GO managed to desorb 55.4 % of Pb^{2+} ions within 24 h. This research demonstrates that DX NG/GO and DX NG have potential to be used as an alternative adsorbent to capture more Pb^{2+} ions in the future.

6.2 RECOMMENDATION FOR FUTURE WORKS

For future studies, experimental work associated to the different types of surfactant and surfactant concentration should be carried out to observe its effect on the formation of CEA-based MGs/NGs by emulsion polymerisation. The potential of CEA based MGs to be used in biomaterials application and Pb adsorption could be explored. In this work, CEA based MGs was produced by emulsion polymerisation, thus CEA based MGs could be produced by using different method such as reversible addition-fragmentation chain transfer (RAFT). This technique has minimal influence on copolymerisation behaviour and hence as an ideal way to control molecular weight and chemical composition. Comparison could be made to the formation of MGs by using these two different methods.

Chapter 4 is associated to the GO effect on the physical and mechanical properties of the gels. Study with higher content of GO should be conducted to observe the effect of GO loadings on the adsorption capacity of Pb^{2+} ions. Preparation of GO by different method should be conducted to obtain more uniform GO sheets. Besides, different form of functionalised graphene such as reduced graphene oxide (RGO) could be used to observe the effect on the NGs. Studies on the NGs with perovskite solar as encapsulating layer to adsorb excess Pb^{2+} generated by perovskite should be carried out due to excellent stability and crosslinked structure. Therefore, it is maybe possible to generate green hybrid solar cells with the presence of DX NG and DX NG/GO.

For the future studies, different dosage of gels to adsorb Pb^{2+} ions should be conducted. Different dosage of the gels would result in difference adsorption capacity. Besides, kinetic studies associated to adsorption isotherm could be explored to validate adsorption mechanism for heavy metal ions. The potential of the gels in capturing multiple ions such as Pb^{2+}, Cu^{2+},

Cd^{2+} simultaneously could be further explored. The recyclability of the gels in capturing multiple heavy metal ions could be investigated.

APPENDIX

The assumption for theoretical calculation of maximum adsorption capacity is stated below:

Mass of polymer = $\frac{\text{(Solid contents of polymer)}}{100}$ x mass of wet gel

Mass of polymer = $\frac{10}{100}$ x 1 g = 0.10 g = 100 mg

MAA concentration = 23.7 wt.% (Section 4.4.1 in Chapter 4)

Mass of MAA= $\frac{\text{(Solid content of MAA)}}{100}$ × mass of polymer

Mass of MAA = $\frac{23.7}{100}$ x 0.1 = 0.0237 g

Mole of MAA = $\frac{\text{Mass of MAA}}{\text{Molecular weight of MAA}}$

Mole of MAA = $\frac{0.0237\ \text{g}}{86\ \text{g/mol}}$

= 2.76×10^{-4}

$Pb^{2+} + 2COO^{-} \rightleftharpoons Pb(COO)_2$

$\frac{n\,(COO^{-})}{n\,(Pb^{2+})} = 2$

Pb^{2+} (optimized) = $\frac{1}{2}\ n\,(RCOO^{-})$

= $\frac{1}{2}$ x 2.76×10^{-4}

= 1.378×10^{-4} mol

Mass of Pb = Mol of Pb^{2+} x atomic mass of Pb

= (1.378×10^{-4}) mol x 207 g/mol

= 0.0285 g

= 28.5 mg

Maximum Pb^{2+} adsorption capacity = $\frac{\text{Mass of Pb}}{\text{Mass of polymer}}$

$= \frac{28.9 \text{ mg}}{0.1 \text{ g}} = 285 \text{ mg/g}$

% of DX NG able to adsorb Pb^{2+} = $\frac{\text{Experimental value}}{\text{Theoretical value}} \times 100$

$= \frac{204}{285} \times 100$

$= 71.6\ \%$

LIST OF REFERENCES

1. Tchounwou, P. B.; Yedjou, C. G.; Patlolla, A. K.; Sutton, D. J., Heavy metal toxicity and the environment. *EXS* **2012,** *101*, 133-164.

2. Suvarapu, L. N.; Baek, S.-O., Determination of heavy metals in the ambient atmosphere:A review. *Toxicol. Ind. Health* **2017,** *33* (1), 79-96.

3. Jaishankar, M.; Tseten, T.; Anbalagan, N.; Mathew, B. B.; Beeregowda, K. N., Toxicity, mechanism and health effects of some heavy metals. *Interdiscip. Toxicol.* **2014,** *7* (2), 60.

4. Güçlü, G.; Al, E.; Emik, S.; İyim, T. B.; Özgümüş, S.; Özyürek, M., Removal of Cu^{2+} and Pb^{2+} ions from aqueous solutions by starch-graft-acrylic acid/montmorillonite superabsorbent nanocomposite hydrogels. *Polymer Bulletin* **2010,** *65* (4), 333-346.

5. Yi, X.; Xu, Z.; Liu, Y.; Guo, X.; Ou, M.; Xu, X., Highly efficient removal of uranium(vi) from wastewater by polyacrylic acid hydrogels. *RSC Adv.* **2017,** *7* (11), 6278-6287.

6. Jaishankar, M.; Tseten, T.; Anbalagan, N.; Mathew, B. B.; Beeregowda, K. N., Toxicity, mechanism and health effects of some heavy metals. *Interdiscip. Toxicol.* **2014,** *7* (2), 60-72.

7. Flora, S. J. S.; Pachauri, V., Chelation in Metal Intoxication. *Int. J. Environ. Res. Public Health* **2010,** *7* (7), 2745-2788.

8. Yuan, S.; Zhang, J.; Yang, Z.; Tang, S.; Liang, B.; Pehkonen, S. O., Click functionalization of poly(glycidyl methacrylate) microspheres with triazole-4-carboxylic acid for the effective adsorption of Pb(ii) ions. *New J. Chem.* **2017,** *41* (14), 6475-6488.

9. Nakata, H.; Nakayama, S. M. M.; Oroszlany, B.; Ikenaka, Y.; Mizukawa, H.; Tanaka, K.; Harunari, T.; Tanikawa, T.; Darwish, W. S.; Yohannes, Y. B.; Saengtienchai, A.; Ishizuka, M., Monitoring Lead (Pb) Pollution and Identifying Pb Pollution Sources in Japan Using Stable Pb Isotope Analysis with Kidneys of Wild Rats. *Int J Environ Res Public Health.* **2017,** *14* (1), 56.

10. Tchounwou, P. B.; Yedjou, C. G.; Patlolla, A. K.; Sutton, D. J., Heavy metal toxicity and the environment. *Exper. Suppl.* **2012,** *101*, 133-164.

11. Bhatia, M.; Rajulapati, S. B.; Sonawane, S.; Girdhar, A., Synthesis and implication of novel poly(acrylic acid)/nanosorbent embedded hydrogel composite for lead ion removal. *Sci. Rep.* **2017,** *7* (1), 16413.

12. Kobya, M.; Demirbas, E.; Senturk, E.; Ince, M., Adsorption of heavy metal ions from aqueous solutions by activated carbon prepared from apricot stone. *Bioresour. Technol.* **2005,** *96* (13), 1518-1521.

13. Abollino, O.; Aceto, M.; Malandrino, M.; Sarzanini, C.; Mentasti, E., Adsorption of heavy metals on Na-montmorillonite. Effect of pH and organic substances. *Water Research* **2003,** *37* (7), 1619-1627.

14. Inglezakis, V. J.; Loizidou, M. D.; Grigoropoulou, H. P., Ion exchange of Pb^{2+}, Cu^{2+}, Fe^{3+}, and Cr^{3+} on natural clinoptilolite: selectivity determination and influence of acidity on metal uptake. *J. Colloid Interface Sci.* **2003,** *261* (1), 49-54.

15. Stylianou, M. A.; Hadjiconstantinou, M. P.; Inglezakis, V. J.; Moustakas, K. G.; Loizidou, M. D., Use of natural clinoptilolite for the removal of lead, copper and zinc in fixed bed column. *J. Hazard. Mater.* **2007,** *143* (1), 575-581.

16. Miretzky, P.; Cirelli, A. F., Cr(VI) and Cr(III) removal from aqueous solution by raw and modified lignocellulosic materials: A review. *J. Hazard. Mater.* **2010,** *180* (1), 1-19.

17. Álvarez-Ayuso, E.; García-Sánchez, A.; Querol, X., Purification of metal electroplating waste waters using zeolites. *Water Research* **2003,** *37* (20), 4855-4862.

18. Lim, A. P.; Aris, A. Z., A review on economically adsorbents on heavy metals removal in water and wastewater. *Rev. Environ. Sci. Bio/Technol.* **2014,** *13* (2), 163-181.

19. Kurniawan, T. A.; Chan, G. Y. S.; Lo, W.-h.; Babel, S., Comparisons of low-cost adsorbents for treating wastewaters laden with heavy metals. *Sci. Total Environ.* **2006,** *366* (2), 409-426.

20. Burakov, A. E.; Galunin, E. V.; Burakova, I. V.; Kucherova, A. E.; Agarwal, S.; Tkachev, A. G.; Gupta, V. K., Adsorption of heavy metals on conventional and nanostructured materials for wastewater treatment purposes: A review. *Ecotoxicol. Environ. Saf.* **2018,** *148*, 702-712.

21. Ma, J.; Zhou, G.; Chu, L.; Liu, Y.; Liu, C.; Luo, S.; Wei, Y., Efficient Removal of Heavy Metal Ions with An EDTA Functionalized Chitosan/Polyacrylamide Double Network Hydrogel. *ACS Sustainable Chem. Eng.* **2017,** *5* (1), 843-851.

22. He, S.; Zhang, F.; Cheng, S.; Wang, W., Synthesis of Sodium Acrylate and Acrylamide Copolymer/GO Hydrogels and Their Effective Adsorption for Pb^{2+} and Cd^{2+}. *ACS Sustainable Chem. Eng.* **2016,** *4* (7), 3948-3959.

23. Li, L.; Scheiger, J. M.; Levkin, P. A., Design and Applications of Photoresponsive Hydrogels. *Adv. Mater.,* **2019,** *31* (26), 1807333.

24. Sahiner, N.; Godbey, W. T.; McPherson, G. L.; John, V. T., Microgel, nanogel and hydrogel–hydrogel semi-IPN composites for biomedical applications: synthesis and characterization. *Colloid Polym Sci.,* **2006,** *284* (10), 1121-1129.

25. Ebara, M.; Kotsuchibashi, Y.; Uto, K.; Aoyagi, T.; Kim, Y.-J.; Narain, R.; Idota, N.; Hoffman, J. M., Smart Hydrogels. In *Smart Biomaterials*, Springer Japan: Tokyo, 2014; pp 9-65.

26. Dai, Z.; Ngai, T., Microgel particles: The structure-property relationships and their biomedical applications. *J. Polym. Sci., Part A: Polym. Chem.,* **2013,** *51* (14), 2995-3003.

27. An, Z.; Qiu, Q.; Liu, G., Synthesis of architecturally well-defined nanogels viaRAFT polymerization for potential bioapplications. *Chem. Commun.,* **2011,** *47* (46), 12424-12440.

28. Neamtu, I.; Rusu, A. G.; Diaconu, A.; Nita, L. E.; Chiriac, A. P., Basic concepts and recent advances in nanogels as carriers for medical applications. *Drug Deliv.* **2017,** *24* (1), 539-557.

29. Zhang, X.; Malhotra, S.; Molina, M.; Haag, R., Micro- and nanogels with labile crosslinks – from synthesis to biomedical applications. *Chemical Society Reviews* **2015,** *44* (7), 1948-1973.

30. Yang, L.; Yang, L.; Ding, L.; Deng, F.; Luo, X.-B.; Luo, S.-L., 1 - Principles for the Application of Nanomaterials in Environmental Pollution Control and Resource Reutilization. In *Nanomaterials for the Removal of Pollutants and Resource Reutilization*, Luo, X.; Deng, F., Eds. Elsevier: 2019; pp 1-23.

31. Kocak, G.; Tuncer, C.; Bütün, V., pH-Responsive polymers. *Polym. Chem.*, **2017,** *8* (1), 144-176.

32. Nicholson, J. W., Polymerisation reactions. In *The Chemistry of Polymers (3)*, The Royal Society of Chemistry: 2006; pp 23-39.

33. Selke, S. E. M.; Culter, J. D., 3 - Polymer Structure and Properties. In *Plastics Packaging (Third Edition)*, Selke, S. E. M.; Culter, J. D., Eds. Hanser: 2016; pp 23-100.

34. Edmondson, S.; Gilbert, M., Chapter 2 - The Chemical Nature of Plastics Polymerization. In *Brydson's Plastics Materials (Eighth Edition)*, Gilbert, M., Ed. Butterworth-Heinemann: 2017; pp 19-37.

35. Wiley-VCH, *Ullmann's Polymers and Plastics, 4 Volume Set: Products and Processes, Volume 1*. Wiley: 2016.

36. Beng Hoon Tan, J. P. K., Kam Chiu Tan, pH-Responsive Nanogels : Synthesis and Physical Properties. In *Hydrogel Micro and Nanoparticles*, L.Andrew Lyon, M. J. S., Ed. Wiley-VCH: Germany, 2012; pp 81-109.

37. Su, W.-F., Radical Chain Polymerization. In *Principles of Polymer Design and Synthesis*, Springer Berlin Heidelberg: Berlin, Heidelberg, 2013; pp 137-183.

38. Distler, D.; Neto, W. S.; Machado, F., Emulsion Polymerization. In *Reference Module in Materials Science and Materials Engineering*, Elsevier: 2017.

39. Daniels, E. S.; Sudol, E. D.; El-Aasser, M. S., Overview of Polymer Colloids: Preparation, Characterization, and Applications. In *Polymer Colloids*, American Chemical Society: 2001; Vol. 801, pp 1-12.

40. Thickett, S. C.; Gilbert, R. G., Emulsion polymerization: State of the art in kinetics and mechanisms. *Polymer* **2007,** *48* (24), 6965-6991.

41. Peacock, A. J.; Calhoun, A., Polymer Chemistry. In *Polymer Science*, Peacock, A. J.; Calhoun, A., Eds. Hanser: 2006; pp 21-43.

42. Bütün, V.; Atay, A.; Tuncer, C.; Baş, Y., Novel Multiresponsive Microgels: Synthesis and Characterization Studies. *Langmuir* **2011,** *27* (20), 12657-12665.

43. Jensen, A. T.; Neto, W. S.; Ferreira, G. R.; Glenn, A. F.; Gambetta, R.; Gonçalves, S. B.; Valadares, L. F.; Machado, F., 8 - Synthesis of polymer/inorganic hybrids through heterophase polymerizations. In *Recent Developments in Polymer Macro, Micro and Nano Blends*, Visakh, P. M.; Markovic, G.; Pasquini, D., Eds. Woodhead Publishing: 2017; pp 207-235.

44. Howe, K. J.; Hand, D. W.; Crittenden, J. C.; Trussell, R. R.; Tchobanoglous, G., *Principles of Water Treatment*. Wiley: 2012.

45. Dukhin, A. S.; Goetz, P. J., Chapter 2 - Fundamentals of Interface and Colloid Science. In *Characterization of Liquids, Dispersions, Emulsions, and Porous Materials Using Ultrasound (Third Edition)*, Dukhin, A. S.; Goetz, P. J., Eds. Elsevier: 2017; pp 19-83.

46. Park, S.-J.; Seo, M.-K., Chapter 1 - Intermolecular Force. In *Interface Sci. Technol.*, Park, S.-J.; Seo, M.-K., Eds. Elsevier: 2011; Vol. 18, pp 1-57.

47. Leclerc, M.; Gauvin, R., *Functional Materials, For Energy, Sustainable Development and Biomedical Sciences*. 2014.

48. Ohshima, H., Chapter 1 - Interaction of colloidal particles. In *Colloid and Interface Science in Pharmaceutical Research and Development*, Ohshima, H.; Makino, K., Eds. Elsevier: Amsterdam, 2014; pp 1-28.

49. Liétor-Santos, J. J.; Fernández-Nieves, A., Motion of microgels in electric fields. *Advances in Colloid and Interface Science* **2009,** *147-148*, 178-185.

50. Butter-worth/Heinemann, D. J. S., Introduction to Colloid and Surface Chemistry, Fourth Edition, , Oxford.

. *Journal of Dispersion Science and Technology* **1994,** *15* (1), 119-119.

51. Shaw, D. J., 8 - Colloid stability. In *Introduction to Colloid and Surface Chemistry (Fourth Edition)*, Shaw, D. J., Ed. Butterworth-Heinemann: Oxford, 1992; pp 210-243.

52. Mo, S.; Shao, X.; Chen, Y.; Cheng, Z., Increasing entropy for colloidal stabilization. *Scientific Reports* **2016,** *6*, 36836.

53. Saunders, B. R.; Laajam, N.; Daly, E.; Teow, S.; Hu, X.; Stepto, R., Microgels: From responsive polymer colloids to biomaterials. *Adv. Colloid Interface Sci.* **2009,** *147-148*, 251-262.

54. Saunders, B. R.; Vincent, B., Microgel particles as model colloids: theory, properties and applications. *Ad¨. Colloid Interface Sci.* **1999,** *80* (1), 1-25.

55. Moreno, R.; Ferrari, B., Nanoparticles Dispersion and the Effect of Related Parameters in the EPD Kinetics. In *Electrophoretic Deposition of Nanomaterials*, Dickerson, J. H.; Boccaccini, A. R., Eds. Springer New York: New York, NY, 2012; pp 73-128.

56. Bonham, J. A.; Faers, M. A.; van Duijneveldt, J. S., Non-aqueous microgel particles: synthesis, properties and applications. *Soft Matter* **2014,** *10* (47), 9384-9398.

57. Chai, Q.; Jiao, Y.; Yu, X., Hydrogels for Biomedical Applications: Their Characteristics and the Mechanisms behind Them. *Gels* **2017,** *3* (1), 6.

58. Dahman, Y., Chapter 3 - Smart Nanomaterials**By Yaser Dahman, Adil Kamil, and Daniel Baena. In *Nanotechnology and Functional Materials for Engineers*, Dahman, Y., Ed. Elsevier: 2017; pp 47-66.

59. Sanson, N.; Rieger, J., Synthesis of nanogels/microgels by conventional and controlled radical crosslinking copolymerization. *Polym. Chem.,* **2010,** *1* (7), 965-977.

60. Creager, S. E.; Clarke, J., Contact-Angle Titrations of Mixed .omega.-Mercaptoalkanoic Acid/Alkanethiol Monolayers on Gold. Reactive vs Nonreactive Spreading, and Chain Length Effects on Surface pKa Values. *Langmuir* **1994,** *10* (10), 3675-3683.

61. Gong, J. P.; Katsuyama, Y.; Kurokawa, T.; Osada, Y., Double-Network Hydrogels with Extremely High Mechanical Strength. *Adv. Mater.* **2003,** *15* (14), 1155-1158.

62. Chen, Q.; Chen, H.; Zhu, L.; Zheng, J., Fundamentals of double network hydrogels. *J. Mater. Chem. B* **2015,** *3* (18), 3654-3676.

63. Zhuang, Y.; Kong, Y.; Han, K.; Hao, H.; Shi, B., A physically cross-linked self-healable double-network polymer hydrogel as a framework for nanomaterial. *New J. Chem.,* **2017,** *41* (24), 15127-15135.

64. Liu, R.; Milani, A. H.; Freemont, T. J.; Saunders, B. R., Doubly crosslinked pH-responsive microgels prepared by particle inter-penetration: swelling and mechanical properties. *Soft Matter* **2011,** *7* (10), 4696-4704.

65. Lillethorup, M.; Shimizu, K.; Plumeré, N.; Pedersen, S. U.; Daasbjerg, K., Surface-Attached Poly(glycidyl methacrylate) as a Versatile Platform for Creating Dual-Functional Polymer Brushes. *Macromolecules* **2014,** *47* (15), 5081-5088.

66. McEwan, K. A.; Slavin, S.; Tunnah, E.; Haddleton, D. M., Dual-functional materials via CCTP and selective orthogonal thiol-Michael addition/epoxide ring opening reactions. *Polym. Chem* **2013,** *4* (8), 2608-2614.

67. Muzammil, Ezzah M.; Khan, A.; Stuparu, M. C., Post-polymerization modification reactions of poly(glycidyl methacrylate)s. *RSC Adv.* **2017,** *7* (88), 55874-55884.

68. Tasfiyati, A. N.; Iftitah, E. D.; Sakti, S. P.; Sabarudin, A., Evaluation of glycidyl methacrylate-based monolith functionalized with weak anion exchange moiety inside 0.5 mm i.d. column for liquid chromatographic separation of DNA. *Anal. Chem. Res.* **2016,** *7*, 9-16.

69. Barbey, R.; Laporte, V.; Alnabulsi, S.; Klok, H.-A., Postpolymerization Modification of Poly(glycidyl methacrylate) Brushes: An XPS Depth-Profiling Study. *Macromolecules* **2013,** *46* (15), 6151-6158.

70. Schroeder, M. E.; Zurick, K. M.; McGrath, D. E.; Bernards, M. T., Multifunctional Polyampholyte Hydrogels with Fouling Resistance and Protein Conjugation Capacity. *Biomacromolecules* **2013,** *14* (9), 3112-3122.

71. Lane, T.; Holloway, J. L.; Milani, A. H.; Saunders, J. M.; Freemont, A. J.; Saunders, B. R., Double network hydrogels prepared from pH-responsive doubly crosslinked microgels. *Soft Matter* **2013,** *9* (33), 7934-7941.

72. Liu, R.; Milani, A. H.; Saunders, J. M.; Freemont, T. J.; Saunders, B. R., Tuning the swelling and mechanical properties of pH-responsive doubly crosslinked microgels using particle composition. *Soft Matter* **2011,** *7* (19), 9297-9306.

73. Muzammil, Ezzah M.; Khan, A.; Stuparu, M. C., Post-polymerization modification reactions of poly(glycidyl methacrylate)s. *RSC Adv.*, **2017,** *7* (88), 55874-55884.

74. Kalal, J.; Švec, F.; Maroušek, V., Reactions of epoxide groups of glycidyl methacrylate copolymers. *J. Polym. Sci.* **1974,** *47* (1), 155-166.

75. Krappitz, T.; Feibusch, P.; Aroonsirichock, C.; Hoven, V. P.; Theato, P., Synthesis of Poly(glycidyl 2-ylidene-acetate) and Functionalization by Nucleophilic Ring-Opening Reactions. *Macromolecules* **2017,** *50* (4), 1415-1421.

76. Richtering, W.; Saunders, B. R., Gel architectures and their complexity. *Soft Matter* **2014,** *10* (21), 3695-3702.

77. Flory, P. J., Molecular Theory of Rubber Elasticity. *Polym. J. (Tokyo, Jpn.)* **1985,** *17*, 1.

78. Treloar, L. R. G., *The Physics of Rubber Elasticity*. Oxford University Press, USA: 1975.

79. Treloar, L. R. G., *The Physics of Rubber Elasticity*. Oxford University Press, USA: 1975; p 322.

80. Vashist, A.; Kaushik, A.; Ghosal, A.; Bala, J.; Nikkhah-Moshaie, R.; A. Wani, W.; Manickam, P.; Nair, M., Nanocomposite Hydrogels: Advances in Nanofillers Used for Nanomedicine. *Gels* **2018,** *4* (3), 75.

81. Zhang, Y.; Liu, Y.; Wang, X.; Sun, Z.; Ma, J.; Wu, T.; Xing, F.; Gao, J., Porous graphene oxide/carboxymethyl cellulose monoliths, with high metal ion adsorption. *Carbohydr. Polym.* **2014,** *101*, 392-400.

82. Thoniyot, P.; Tan, M. J.; Karim, A. A.; Young, D. J.; Loh, X. J., Nanoparticle–Hydrogel Composites: Concept, Design, and Applications of These Promising, Multi-Functional Materials. *Adv. Sci.,* **2015,** *2* (1-2), 1400010.

83. Shang, J.; Theato, P., Smart composite hydrogel with pH-, ionic strength- and temperature-induced actuation. *Soft Matter* **2018,** *14* (41), 8401-8407.

84. Alizadehgiashi, M.; Khuu, N.; Khabibullin, A.; Henry, A.; Tebbe, M.; Suzuki, T.; Kumacheva, E., Nanocolloidal Hydrogel for Heavy Metal Scavenging. *ACS Nano* **2018,** *12* (8), 8160-8168.

85. Cui, Z.; Milani, A. H.; Greensmith, P. J.; Yan, J.; Adlam, D. J.; Hoyland, J. A.; Kinloch, I. A.; Freemont, A. J.; Saunders, B. R., A study of physical and covalent hydrogels containing pH-responsive microgel particles and graphene oxide. *Langmuir* **2014,** *30* (44), 13384-13393.

86. Cong, H. P.; Wang, P.; Yu, S. H., Highly elastic and superstretchable graphene oxide/polyacrylamide hydrogels. *Small* **2014,** *10* (3), 448-453.

87. Haraguchi, K.; Takehisa, T., Nanocomposite Hydrogels: A Unique Organic–Inorganic Network Structure with Extraordinary Mechanical, Optical, and Swelling/De-swelling Properties. *Advanced Materials* **2002,** *14* (16), 1120-1124.

88. Haraguchi, K.; Takehisa, T., Nanocomposite Hydrogels: A Unique Organic–Inorganic Network Structure with Extraordinary Mechanical, Optical, and Swelling/De-swelling Properties. *Adv. Mater.* **2002,** *14* (16), 1120-1124.

89. Sun, X.-F.; Ye, Q.; Jing, Z.; Li, Y., Preparation of hemicellulose-g-poly(methacrylic acid)/carbon nanotube composite hydrogel and adsorption properties. *Polymer Composites* **2014,** *35* (1), 45-52.

90. Adewunmi, A. A.; Ismail, S.; Sultan, A. S., Carbon Nanotubes (CNTs) Nanocomposite Hydrogels Developed for Various Applications: A Critical Review. *J. Inorg. Organomet. Polym.,* **2016,** *26* (4), 717-737.

91. Li, Z.; Liu, Z.; Sun, H.; Gao, C., Superstructured Assembly of Nanocarbons: Fullerenes, Nanotubes, and Graphene. *Chem. Rev* **2015,** *115* (15), 7046-7117.

92. Stankovich, S.; Dikin, D. A.; Dommett, G. H.; Kohlhaas, K. M.; Zimney, E. J.; Stach, E. A.; Piner, R. D.; Nguyen, S. T.; Ruoff, R. S., Graphene-based composite materials. *Nature* **2006,** *442* (7100), 282-286.

93. Kim, H.; Abdala, A. A.; Macosko, C. W., Graphene/Polymer Nanocomposites. *Macromolecules* **2010,** *43* (16), 6515-6530.

94. Bunch, J. S.; Verbridge, S. S.; Alden, J. S.; van der Zande, A. M.; Parpia, J. M.; Craighead, H. G.; McEuen, P. L., Impermeable Atomic Membranes from Graphene Sheets. *Nano Lett.* **2008,** *8* (8), 2458-2462.

95. Dreyer, D. R.; Ruoff, R. S.; Bielawski, C. W., From Conception to Realization: An Historial Account of Graphene and Some Perspectives for Its Future. *Angew. Chem., Int. Ed.* **2010,** *49* (49), 9336-9344.

96. Geim, A. K.; Novoselov, K. S., The rise of graphene. *Nat. Mater.* **2007,** *6*, 183.

97. Dresselhaus, M. S.; Araujo, P. T., Perspectives on the 2010 Nobel Prize in Physics for Graphene. *ACS Nano* **2010,** *4* (11), 6297-6302.

98. Novoselov, K. S.; Geim, A. K.; Morozov, S. V.; Jiang, D.; Zhang, Y.; Dubonos, S. V.; Grigorieva, I. V.; Firsov, A. A., Electric Field Effect in Atomically Thin Carbon Films. *Science* **2004,** *306* (5696), 666-669.

99. Song*, M.; Cai, D., Chapter 1 Graphene Functionalization: A Review. In *Polymer-Graphene Nanocomposites*, The Royal Society of Chemistry: 2012; pp 1-52.

100. Musico, Y. L. F.; Santos, C. M.; Dalida, M. L. P.; Rodrigues, D. F., Improved removal of lead (II) from water using a polymer-based graphene oxide nanocomposite. *Journal of Materials Chemistry A* **2013,** *1* (11), 3789-3796.

101. Islam, A.; Ahmad, H.; Zaidi, N.; Kumar, S., Graphene oxide sheets immobilized polystyrene for column preconcentration and sensitive determination of lead by flame atomic absorption spectrometry. *ACS applied materials & interfaces* **2014,** *6* (15), 13257-13265.

102. Cong, H.-P.; Ren, X.-C.; Wang, P.; Yu, S.-H., Macroscopic multifunctional graphene-based hydrogels and aerogels by a metal ion induced self-assembly process. *ACS nano* **2012,** *6* (3), 2693-2703.

103. Zhuang, Y.; Kong, Y.; Han, K.; Hao, H.; Shi, B., A physically cross-linked self-healable double-network polymer hydrogel as a framework for nanomaterial. *New J. Chem.* **2017,** *41* (24), 15127-15135.

104. Yu, X.; Cheng, H.; Zhang, M.; Zhao, Y.; Qu, L.; Shi, G., Graphene-based smart materials. *Nat. Rev. Mater.* **2017,** *2*, 17046.

105. Dreyer, D. R.; Park, S.; Bielawski, C. W.; Ruoff, R. S., The chemistry of graphene oxide. *Chem. Soc. Rev.* **2010,** *39* (1), 228-240.

106. Fang, M.; Wang, K.; Lu, H.; Yang, Y.; Nutt, S., Covalent polymer functionalization of graphene nanosheets and mechanical properties of composites. *J. Mater. Chem. A* **2009,** *19* (38), 7098-7105.

107. Ferrari, A. C.; Bonaccorso, F.; Fal'ko, V.; Novoselov, K. S.; Roche, S., Science and technology roadmap for graphene, related two-dimensional crystals, and hybrid systems. *Nanoscale* **2015,** *7* (11), 4598-4810.

108. Awad, F. S.; AbouZeid, K. M.; El-Maaty, W. M. A.; El-Wakil, A. M.; El-Shall, M. S., Efficient Removal of Heavy Metals from Polluted Water with High Selectivity for Mercury(II) by 2-Imino-4-thiobiuret–Partially Reduced Graphene Oxide (IT-PRGO). *ACS Appl. Mater. Interfaces*, **2017,** *9* (39), 34230-34242.

109. Huang, Y.; Zhang, M.; Ruan, W., High-water-content graphene oxide/polyvinyl alcohol hydrogel with excellent mechanical properties. *Journal of Materials Chemistry A* **2014,** *2* (27), 10508-10515.

110. Bai, H.; Li, C.; Wang, X.; Shi, G., A pH-sensitive graphene oxide composite hydrogel. *Chemical Communications* **2010,** *46* (14), 2376-2378.

111. Liu, G.; Neoh, K.-G.; Kang, E.-T., Chapter 8 Dispersible Graphene Oxide–Polymer Nanocomposites. In *Polymer-Graphene Nanocomposites*, The Royal Society of Chemistry: 2012; pp 179-210.

112. Dreyer, D. R.; Todd, A. D.; Bielawski, C. W., Harnessing the chemistry of graphene oxide. *Chem. Soc. Rev.*, **2014,** *43* (15), 5288-5301.

113. Wang, T.; Huang, J.; Yang, Y.; Zhang, E.; Sun, W.; Tong, Z., Bioinspired Smart Actuator Based on Graphene Oxide-Polymer Hybrid Hydrogels. *ACS Appl. Mater. Interfaces.* **2015,** *7* (42), 23423-23430.

114. Chen, M.; Zhang, C.; Li, X.; Zhang, L.; Ma, Y.; Zhang, L.; Xu, X.; Xia, F.; Wang, W.; Gao, J., A one-step method for reduction and self-assembling of graphene oxide into reduced graphene oxide aerogels. *J. Mater. Chem. A*, **2013,** *1* (8), 2869-2877.

115. Bourgeat-Lami, E.; Faucheu, J.; Noël, A., Latex routes to graphene-based nanocomposites. *Polym. Chem* **2015,** *6* (30), 5323-5357.

116. Rafiee, M. A.; Rafiee, J.; Wang, Z.; Song, H.; Yu, Z.-Z.; Koratkar, N., Enhanced Mechanical Properties of Nanocomposites at Low Graphene Content. *ACS Nano* **2009,** *3* (12), 3884-3890.

117. Chen, Y.; Zhang, Q.; Chen, L.; Bai, H.; Li, L., Basic aluminum sulfate@graphene hydrogel composites: preparation and application for removal of fluoride. *J. Mater. Chem. A,* **2013,** *1* (42), 13101-13110.

118. Zu, S.-Z.; Han, B.-H., Aqueous Dispersion of Graphene Sheets Stabilized by Pluronic Copolymers: Formation of Supramolecular Hydrogel. *J. Phys. Chem. C,* **2009,** *113* (31), 13651-13657.

119. Bai, H.; Sheng, K.; Zhang, P.; Li, C.; Shi, G., Graphene oxide/conducting polymer composite hydrogels. *J. Mater. Chem.,* **2011,** *21* (46), 18653-18658.

120. Adhikari, B.; Biswas, A.; Banerjee, A., Graphene Oxide-Based Hydrogels to Make Metal Nanoparticle-Containing Reduced Graphene Oxide-Based Functional Hybrid Hydrogels. *ACS Appl. Mater. Interfaces* **2012,** *4* (10), 5472-5482.

121. Ai, W.; Du, Z.-Z.; Liu, J.-Q.; Zhao, F.; Yi, M.-D.; Xie, L.-H.; Shi, N.-E.; Ma, Y.-W.; Qian, Y.; Fan, Q.-L.; Yu, T.; Huang, W., Formation of graphene oxide gel via the π-stacked supramolecular self-assembly. *RSC Adv.,* **2012,** *2* (32), 12204-12209.

122. Jiang, X.; Ma, Y.; Li, J.; Fan, Q.; Huang, W., Self-Assembly of Reduced Graphene Oxide into Three-Dimensional Architecture by Divalent Ion Linkage. *J. Phys. Chem. C,* **2010,** *114* (51), 22462-22465.

123. Xu, Y.; Wu, Q.; Sun, Y.; Bai, H.; Shi, G., Three-dimensional self-assembly of graphene oxide and DNA into multifunctional hydrogels. *ACS nano* **2010,** *4* (12), 7358-7362.

124. Huang, C.; Bai, H.; Li, C.; Shi, G., A graphene oxide/hemoglobin composite hydrogel for enzymatic catalysis in organic solvents. *Chem. Commun* **2011,** *47* (17), 4962-4964.

125. Ramanathan, T.; Abdala, A. A.; Stankovich, S.; Dikin, D. A.; Herrera-Alonso, M.; Piner, R. D.; Adamson, D. H.; Schniepp, H. C.; Chen, X.; Ruoff, R. S.; Nguyen, S. T.; Aksay, I. A.; Prud'Homme, R. K.; Brinson, L. C., Functionalized graphene sheets for polymer nanocomposites. *Nat. Nanotechnol.* **2008,** *3*, 327.

126. Huang, Y.; Zhang, M.; Ruan, W., High-water-content graphene oxide/polyvinyl alcohol hydrogel with excellent mechanical properties. *J. Mater. Chem. A* **2014,** *2* (27), 10508-10515.

127. Xu, Y.; Hong, W.; Bai, H.; Li, C.; Shi, G., Strong and ductile poly(vinyl alcohol)/graphene oxide composite films with a layered structure. *Carbon* **2009,** *47* (15), 3538-3543.

128. Liang, J.; Huang, Y.; Zhang, L.; Wang, Y.; Ma, Y.; Guo, T.; Chen, Y., Molecular-Level Dispersion of Graphene into Poly(vinyl alcohol) and Effective Reinforcement of their Nanocomposites. *Adv. Funct. Mater* **2009,** *19* (14), 2297-2302.

129. Zheng, S. Y.; Ding, H.; Qian, J.; Yin, J.; Wu, Z. L.; Song, Y.; Zheng, Q., Metal-Coordination Complexes Mediated Physical Hydrogels with High Toughness, Stick–Slip Tearing Behavior, and Good Processability. *Macromolecules* **2016,** *49* (24), 9637-9646.

130. Santo, K. P.; Vishnyakov, A.; Kumar, R.; Neimark, A. V., Elucidating the Effects of Metal Complexation on Morphological and Rheological Properties of Polymer Solutions by a Dissipative Particle Dynamics Model. *Macromolecules* **2018,** *51* (14), 4987-5000.

131. Ishiwata, T.; Furukawa, Y.; Sugikawa, K.; Kokado, K.; Sada, K., Transformation of Metal–Organic Framework to Polymer Gel by Cross-Linking the Organic Ligands Preorganized in Metal–Organic Framework. *J. Am. Chem. Soc.* **2013,** *135* (14), 5427-5432.

132. Shao, C.; Chang, H.; Wang, M.; Xu, F.; Yang, J., High-Strength, Tough, and Self-Healing Nanocomposite Physical Hydrogels Based on the Synergistic Effects of Dynamic Hydrogen Bond and Dual Coordination Bonds. *ACS Appl. Mater. Interfaces.*, **2017,** *9* (34), 28305-28318.

133. Yang, Y.; Urban, M. W., Self-healing polymeric materials. *Chem. Soc. Rev.* **2013,** *42* (17), 7446-7467.

134. Auletta, J. T.; LeDonne, G. J.; Gronborg, K. C.; Ladd, C. D.; Liu, H.; Clark, W. W.; Meyer, T. Y., Stimuli-Responsive Iron-Cross-Linked Hydrogels That Undergo Redox-Driven Switching between Hard and Soft States. *ACS Macro* **2015,** *48* (6), 1736-1747.

135. Dong, H.; Snyder, J. F.; Williams, K. S.; Andzelm, J. W., Cation-Induced Hydrogels of Cellulose Nanofibrils with Tunable Moduli. *Biomacromolecules.* **2013,** *14* (9), 3338-3345.

136. Maestri, C. A.; Abrami, M.; Hazan, S.; Chistè, E.; Golan, Y.; Rohrer, J.; Bernkop-Schnürch, A.; Grassi, M.; Scarpa, M.; Bettotti, P., Role of sonication pre-treatment and cation valence in the sol-gel transition of nano-cellulose suspensions. *Sci. Rep.* **2017,** *7* (1), 11129.

137. Kaygusuz, H.; Evingür, G. A.; Pekcan, Ö.; von Klitzing, R.; Erim, F. B., Surfactant and metal ion effects on the mechanical properties of alginate hydrogels. *Int. J. Biol. Macromol.* **2016,** *92*, 220-224.

138. Yang, J.; Chen, S.; Fang, Y., Viscosity study of interactions between sodium alginate and CTAB in dilute solutions at different pH values. *Carbohydrate Polymers* **2009,** *75* (2), 333-337.

139. Mørch, Ý. A.; Donati, I.; Strand, B. L., Effect of Ca^{2+}, Ba^{2+}, and Sr^{2+} on Alginate Microbeads. *Biomacromolecules* **2006,** *7* (5), 1471-1480.

140. Nakagawa, Y.; Ohta, S.; Sugahara, A.; Okubo, M.; Yamada, A.; Ito, T., In Vivo Redox-Responsive Sol–Gel/Gel–Sol Transition of Star Block Copolymer Solution Based on Ionic Cross-Linking. *Macromolecules* **2017,** *50* (14), 5539-5548.

141. Chen, C.-C.; Dormidontova, E. E., Supramolecular Polymer Formation by Metal−Ligand Complexation: Monte Carlo Simulations and Analytical Modeling. *J. Am. Chem. Soc* **2004,** *126* (45), 14972-14978.

142. Zhang, Y.; Hu, C.; Xiang, X.; Diao, Y.; Li, B.; Shi, L.; Ran, R., Self-healable, tough and highly stretchable hydrophobic association/ionic dual physically cross-linked hydrogels. *RSC Adv.* **2017,** *7* (20), 12063-12073.

143. Turhanen, P. A.; Vepsäläinen, J. J.; Peräniemi, S., Advanced material and approach for metal ions removal from aqueous solutions. *Sci. Rep.* **2015,** *5*, 8992.

144. Pu, S.; Ma, H.; Zinchenko, A.; Chu, W., Novel highly porous magnetic hydrogel beads composed of chitosan and sodium citrate: an effective adsorbent for the removal of heavy metals from aqueous solutions. *Environ. Sci. Pollut. Res.* **2017,** *24* (19), 16520-16530.

145. R, S.; A, P.; Balakrishna, G. R.; M. S, J., La activated high surface area titania float for the adsorption of Pb(ii) from aqueous media. *New J. Chem.* **2018,** *42* (2), 1067-1077.

146. Peng, X.-W.; Zhong, L.-X.; Ren, J.-L.; Sun, R.-C., Highly effective adsorption of heavy metal ions from aqueous solutions by macroporous xylan-rich hemicelluloses-based hydrogel. *J. Agric. Food Chem.* **2012,** *60* (15), 3909-3916.

147. Tchounwou, P. B.; Yedjou, C. G.; Patlolla, A. K.; Sutton, D. J., Heavy metal toxicity and the environment. *Experientia supplementum (2012)* **2012,** *101*, 133-164.

148. Baby Shaikh, R.; Saifullah, B.; Rehman, F., Greener Method for the Removal of Toxic Metal Ions from the Wastewater by Application of Agricultural Waste as an Adsorbent. *Water* **2018,** *10* (10), 1316.

149. Yao, Q. X.; Xie, J. J.; Liu, J. X.; Kang, H. M.; Liu, Y., Adsorption of lead ions using a modified lignin hydrogel. *J. Polym. Res.* **2014,** *21* (6), 16.

150. Kireeti, K. V. M. K.; G, C.; Kadam, M. M.; Jha, N., A sodium modified reduced graphene oxide–Fe3O4 nanocomposite for efficient lead(ii) adsorption. *RSC Adv.* **2016,** *6* (88), 84825-84836.

151. Santhosh, C.; Nivetha, R.; Kollu, P.; Srivastava, V.; Sillanpää, M.; Grace, A. N.; Bhatnagar, A., Removal of cationic and anionic heavy metals from water by 1D and 2D-carbon structures decorated with magnetic nanoparticles. *Sci. Rep.* **2017,** *7* (1), 14107.

152. Hailegnaw, B.; Kirmayer, S.; Edri, E.; Hodes, G.; Cahen, D., Rain on Methylammonium Lead Iodide Based Perovskites: Possible Environmental Effects of Perovskite Solar Cells. *J. Phys. Chem. Lett.* **2015,** *6* (9), 1543-1547.

153. Li, N.; Bai, R., Highly Enhanced Adsorption of Lead Ions on Chitosan Granules Functionalized with Poly(acrylic acid). *Ind. Eng. Chem. Res* **2006,** *45* (23), 7897-7904.

154. Pan, B.; Pan, B.; Zhang, W.; Lv, L.; Zhang, Q.; Zheng, S., Development of polymeric and polymer-based hybrid adsorbents for pollutants removal from waters. *Chem. Eng. J.* **2009,** *151* (1–3), 19-29.

155. Musico, Y. L. F.; Santos, C. M.; Dalida, M. L. P.; Rodrigues, D. F., Improved removal of lead(ii) from water using a polymer-based graphene oxide nanocomposite. *J. Mater. Chem. A* **2013,** *1* (11), 3789-3796.

156. Samiey, B.; Cheng, C.-H.; Wu, J., Organic-Inorganic Hybrid Polymers as Adsorbents for Removal of Heavy Metal Ions from Solutions: A Review. *Materials (Basel)* **2014,** *7* (2), 673-726.

157. Zhang, J.; Wang, A., Adsorption of Pb(II) from Aqueous Solution by Chitosan-g-poly(acrylic acid)/Attapulgite/Sodium Humate Composite Hydrogels. *J. Chem. Eng. Data* **2010,** *55* (7), 2379-2384.

158. Setshedi, K.; Ren, J.; Aoyi, O.; Onyango, M. S., Removal of Pb (II) from aqueous solution using hydrotalcite-like nanostructured material. *International Journal of Physical Sciences* **2012,** *7* (1), 63-72.

159. Chen, D.; Wang, L.; Ma, Y.; Yang, W., Super-adsorbent material based on functional polymer particles with a multilevel porous structure. *NPG Asia Mater.* **2016,** *8*, e301.

160. Zhang, B.; Cui, Y.; Yin, G.; Li, X., Adsorption of Copper (II) and Lead (II) Ions onto Cottonseed Protein-PAA Hydrogel Composite. *Polym.-Plast. Technol. Eng.* **2012,** *51* (6), 612-619.

161. Zhu, L.; Liu, P.; Wang, A., High Clay-Content Attapulgite/Poly(acrylic acid) Nanocomposite Hydrogel via Surface-Initiated Redox Radical Polymerization with Modified Attapulgite Nanorods as Initiator and Cross-Linker. *Ind. Eng. Chem. Res* **2014,** *53* (5), 2067-2071.

162. Suja, P. S.; Reshmi, C. R.; Sagitha, P.; Sujith, A., Electrospun Nanofibrous Membranes for Water Purification. *Polym. Rev.* **2017,** *57* (3), 467-504.

163. Han, Z.; Tang, Z.; Shen, S.; Zhao, B.; Zheng, G.; Yang, J., Strengthening of Graphene Aerogels with Tunable Density and High Adsorption Capacity towards Pb^{2+}. *Scientific Reports* **2014,** *4*, 5025.

164. Chen, Y.; Chen, L.; Bai, H.; Li, L., Graphene oxide–chitosan composite hydrogels as broad-spectrum adsorbents for water purification. *J. Mater. Chem. A* **2013,** *1* (6), 1992-2001.

165. Medina, R. P.; Nadres, E. T.; Ballesteros, F. C.; Rodrigues, D. F., Incorporation of graphene oxide into a chitosan–poly(acrylic acid) porous polymer nanocomposite for enhanced lead adsorption. *Environ. Sci.: Nano*, **2016,** *3* (3), 638-646.

166. Bessbousse, H.; Rhlalou, T.; Verchère, J. F.; Lebrun, L., Removal of heavy metal ions from aqueous solutions by filtration with a novel complexing membrane containing poly(ethyleneimine) in a poly(vinyl alcohol) matrix. *J. Membr. Sci.* **2008,** *307* (2), 249-259.

167. Shekinah, P.; Kadirvelu, K.; Kanmani, P.; Senthilkumar, P.; Subburam, V., Adsorption of lead(II) from aqueous solution by activated carbon prepared from Eichhornia. *J. Chem. Technol. Biotechnol.* **2002,** *77* (4), 458-464.

168. Ju, X.-J.; Zhang, S.-B.; Zhou, M.-Y.; Xie, R.; Yang, L.; Chu, L.-Y., Novel heavy-metal adsorption material: ion-recognition P(NIPAM-co-BCAm) hydrogels for removal of lead(II) ions. *J. Hazard. Mater.* **2009,** *167* (1–3), 114-118.

169. Jin, L.; Bai, R., Mechanisms of Lead Adsorption on Chitosan/PVA Hydrogel Beads. *Langmuir* **2002,** *18* (25), 9765-9770.

170. Han, Z.; Tang, Z.; Sun, Y.; Yang, J.; Zhi, L., Controllable Synthesis of Tetraethylenepentamine Modified Graphene Foam (TEPA-GF) for the Removal of Lead ions. *Sci. Rep.* **2015,** *5*, 16730.

171. Zhao, X.; Ma, X.; Zheng, P., The preparation of carboxylic-functional carbon-based nanofibers for the removal of cationic pollutants. *Chemosphere* **2018,** *202*, 298-305.

172. Tripathi, A. K.; Vossoughi, J.; Sundberg, D. C., Partitioning of 2-Carboxyethyl Acrylate between Water and Vinyl Monomer Phases Applied to Emulsion Polymerization: Comparisons with Hydroxy Acrylate and Other Vinyl Acid Functional Monomers. *Ind. Eng. Chem. Res* **2015,** *54* (9), 2447-2452.

173. Tripathi, A. K.; Sundberg, D. C., Partitioning of Functional Monomers in Emulsion Polymerization: Distribution of Carboxylic Acid Monomers between Water and Monomer Phases. *Ind. Eng. Chem. Res* **2013,** *52* (9), 3306-3314.

174. Pietrzak, E.; Wiecinska, P.; Szafran, M., 2-carboxyethyl acrylate as a new monomer preventing negative effect of oxygen inhibition in gelcasting of alumina. *Ceram. Int.* **2016,** *42* (12), 13682-13688.

175. Swift, T.; Swanson, L.; Geoghegan, M.; Rimmer, S., The pH-responsive behaviour of poly(acrylic acid) in aqueous solution is dependent on molar mass. *Soft Matter* **2016,** *12* (9), 2542-2549.

176. Charbonneau, C.; Chassenieux, C.; Colombani, O.; Nicolai, T., Progressive Freezing-in of the Junctions in Self-Assembled Triblock Copolymer Hydrogels during Aging. *Macromolecules* **2012,** *45* (2), 1025-1030.

177. Tripathi, A. K.; Vossoughi, J.; Sundberg, D. C., Partitioning of 2-Carboxyethyl Acrylate between Water and Vinyl Monomer Phases Applied to Emulsion Polymerization: Comparisons with Hydroxy Acrylate and Other Vinyl Acid Functional Monomers. *Ind. Eng. Chem. Res.* **2015,** *54* (9), 2447-2452.

178. Cheng, F.; Yuanyuan, W.; Zhongxiang, L.; S., D. E.; Andrew, K., Partitioning of monobutyl itaconate and β-carboxyethyl acrylate between organic and water phases. *Journal of Applied Polymer Science* **2014,** *131* (19).

179. Milani, A. H.; Bramhill, J.; Freemont, A. J.; Saunders, B. R., Swelling and mechanical properties of hydrogels composed of binary blends of inter-linked pH-responsive microgel particles. *Soft Matter* **2015,** *11* (13), 2586-2595.

180. Kokufuta, E.; Wang, B.; Yoshida, R.; Khokhlov, A. R.; Hirata, M., Volume Phase Transition of Polyelectrolyte Gels with Different Charge Distributions. *Macromolecules* **1998,** *31* (20), 6878-6884.

181. Milani, A. H.; Saunders, J. M.; Nguyen, N. T.; Ratcliffe, L. P. D.; Adlam, D. J.; Freemont, A. J.; Hoyland, J. A.; Armes, S. P.; Saunders, B. R., Synthesis of polyacid nanogels: pH-responsive sub-100 nm particles for functionalisation and fluorescent hydrogel assembly. *Soft Matter* **2017,** *13* (8), 1554-1560.

182. Fang, C.; Wang, Y.; Lin, Z.; Daniels, E. S.; Klein, A., Partitioning of monobutyl itaconate and β-carboxyethyl acrylate between organic and water phases. *J. Appl. Polym. Sci.* **2014,** *131* (19).

183. Paine, A. J.; Luymes, W.; McNulty, J., Dispersion polymerization of styrene in polar solvents. 6. Influence of reaction parameters on particle size and molecular weight in poly(N-vinylpyrrolidone)-stabilized reactions. *Macromolecules* **1990,** *23* (12), 3104-3109.

184. Wang, W.; Sande, S. A., A dynamic light scattering study of hydrogels with the addition of surfactant: a discussion of mesh size and correlation length. *Polym. J.* **2014,** *47*, 302.

185. Costa, E.; Lloyd, M. M.; Chopko, C.; Aguiar-Ricardo, A.; Hammond, P. T., Tuning Smart Microgel Swelling and Responsive Behavior through Strong and Weak Polyelectrolyte Pair Assembly. *Langmuir* **2012,** *28* (26), 10082-10090.

186. Wang, W.; Milani, A. H.; Cui, Z.; Zhu, M.; Saunders, B. R., Pickering Emulsions Stabilized by pH-Responsive Microgels and Their Scalable Transformation to Robust Submicrometer Colloidoisomes with Selective Permeability. *Langmuir* **2017,** *33* (33), 8192-8200.

187. Tillet, G.; Boutevin, B.; Ameduri, B., Chemical reactions of polymer crosslinking and post-crosslinking at room and medium temperature. *Progress in Polymer Science* **2011,** *36* (2), 191-217.

188. Lu, B.; Tarn, M. D.; Pamme, N.; Georgiou, T. K., Microfluidically fabricated pH-responsive anionic amphiphilic microgels for drug release. *J. Mater. Chem. B,* **2016,** *4* (18), 3086-3093.

189. Triftaridou, A. I.; Hadjiyannakou, S. C.; Vamvakaki, M.; Patrickios, C. S., Synthesis, Characterization, and Modeling of Cationic Amphiphilic Model Hydrogels: Effects of Polymer Composition and Architecture. *Macromolecules* **2002,** *35* (7), 2506-2513.

190. Vamvakaki, M.; Patrickios, C. S., Synthesis and characterization of the swelling and mechanical properties of amphiphilic ionizable model co-networks containing n-butyl methacrylate hydrophobic blocks. *Soft Matter* **2008,** *4* (2), 268-276.

191. Hoare, T.; Pelton, R., Titrametric Characterization of pH-Induced Phase Transitions in Functionalized Microgels. *Langmuir* **2006,** *22* (17), 7342-7350.

192. Tillet, G.; Boutevin, B.; Ameduri, B., Chemical reactions of polymer crosslinking and post-crosslinking at room and medium temperature. *Prog. Polym. Sci.* **2011,** *36* (2), 191-217.

193. Lu, M.; Keskkula, H.; Paul, D. R., Toughening of nylon 6 with grafted rubber impact modifiers. *J. Appl. Polym. Sci.* **1995,** *58* (7), 1175-1188.

194. Wang, W.; Milani, A. H.; Carney, L.; Yan, J.; Cui, Z.; Thaiboonrod, S.; Saunders, B. R., Doubly crosslinked microgel-colloidosomes: a versatile method for pH-responsive capsule assembly using microgels as macro-crosslinkers. *Chem. Commun.,* **2015,** *51* (18), 3854-3857.

195. Reis, A. V.; Fajardo, A. R.; Schuquel, I. T. A.; Guilherme, M. R.; Vidotti, G. J.; Rubira, A. F.; Muniz, E. C., Reaction of Glycidyl Methacrylate at the Hydroxyl and Carboxylic Groups

of Poly(vinyl alcohol) and Poly(acrylic acid): Is This Reaction Mechanism Still Unclear? *J. Org. Chem* **2009,** *74* (10), 3750-3757.

196. Milani, A. H.; Freemont, A. J.; Hoyland, J. A.; Adlam, D. J.; Saunders, B. R., Injectable Doubly Cross-Linked Microgels for Improving the Mechanical Properties of Degenerated Intervertebral Discs. *Biomacromolecules* **2012,** *13* (9), 2793-2801.

197. Zhang, Z. P.; Lu, Y.; Rong, M. Z.; Zhang, M. Q., A thermally remendable and reprocessable crosslinked methyl methacrylate polymer based on oxygen insensitive dynamic reversible C–ON bonds. *RSC Adv.,* **2016,** *6* (8), 6350-6357.

198. Yan, C.; Pochan, D. J., Rheological properties of peptide-based hydrogels for biomedical and other applications. *Chem Soc Rev.* **2010,** *39* (9), 3528-3540.

199. Kudo, S.; Kosaka, N.; Konno, M.; Saito, S., Volume-phase transitions of cationic polyelectrolyte gels. *Polymer* **1992,** *33* (23), 5040-5043.

200. Hu, J.; Kurokawa, T.; Hiwatashi, K.; Nakajima, T.; Wu, Z. L.; Liang, S. M.; Gong, J. P., Structure Optimization and Mechanical Model for Microgel-Reinforced Hydrogels with High Strength and Toughness. *Macromolecules* **2012,** *45* (12), 5218-5228.

201. Saunders, B. R.; Vincent, B., Thermal and osmotic deswelling of poly(NIPAM) microgel particles. *J. Chem. Soc., Faraday Trans.* **1996,** *92* (18), 3385-3389.

202. Fan, H.; Lin, N.; Liu, X. Y., 7 - Natural photonic materials for textile coatings. In *Active Coatings for Smart Textiles*, Hu, J., Ed. Woodhead Publishing: 2016; pp 137-156.

203. Tokita, M., Transport Phenomena in Gel. *Gels* **2016,** *2* (2), 17.

204. Everett, D. H., Chapter 7 Some Important Properties of Colloids II Scattering of Radiation. In *Basic Principles of Colloid Science*, The Royal Society of Chemistry: 1988; pp 95-109.

205. Wen, J.; Wilkes, G. L., Organic/Inorganic Hybrid Network Materials by the Sol−Gel Approach. *Chem. Mater.* **1996,** *8* (8), 1667-1681.

206. Seiffert, S., Scattering perspectives on nanostructural inhomogeneity in polymer network gels. *Prog. Polym. Sci.* **2017,** *66*, 1-21.

207. Tummala, G. K.; Rojas, R.; Mihranyan, A., Poly(vinyl alcohol) Hydrogels Reinforced with Nanocellulose for Ophthalmic Applications: General Characteristics and Optical Properties. *J. Phys. Chem. B* **2016,** *120* (51), 13094-13101.

208. Razgoniaev, A. O.; Butaeva, E. V.; Iretskii, A. V.; Ostrowski, A. D., Changing Mechanical Strength in Cr(III)- Metallosupramolecular Polymers with Ligand Groups and Light Irradiation. *Inorg. Chem.* **2016,** *55* (11), 5430-5437.

209. Ozay, O.; Ekici, S.; Baran, Y.; Aktas, N.; Sahiner, N., Removal of toxic metal ions with magnetic hydrogels. *Water Res.* **2009,** *43* (17), 4403-4411.

210. Shen, Y.; Fang, Q.; Chen, B., Environmental Applications of Three-Dimensional Graphene-Based Macrostructures: Adsorption, Transformation, and Detection. *Environ. Sci. Technol.* **2015,** *49* (1), 67-84.

211. Hashemi, A.; Jouault, N.; Williams, G. A.; Zhao, D.; Cheng, K. J.; Kysar, J. W.; Guan, Z.; Kumar, S. K., Enhanced Glassy State Mechanical Properties of Polymer Nanocomposites via Supramolecular Interactions. *Nano Letters* **2015,** *15* (8), 5465-5471.

212. Zhang, J.; Yang, F.; Shen, H.; Wu, D., Controlled Formation of Microgels/Nanogels from a Disulfide-Linked Core/Shell Hyperbranched Polymer. *ACS Macro Lett* **2012,** *1* (11), 1295-1299.

213. Kamerlin, N.; Elvingson, C., Collapse Dynamics of Core–Shell Nanogels. *Macromolecules* **2016,** *49* (15), 5740-5749.

214. Molina, M.; Asadian-Birjand, M.; Balach, J.; Bergueiro, J.; Miceli, E.; Calderón, M., Stimuli-responsive nanogel composites and their application in nanomedicine. *Chem. Soc. Rev.* **2015,** *44* (17), 6161-6186.

215. Guerra, F. D.; Attia, M. F.; Whitehead, D. C.; Alexis, F., Nanotechnology for Environmental Remediation: Materials and Applications. *Molecules* **2018,** *23* (7), 1760.

216. Ferrer, M. C. C.; Ferrier, R. C., Jr.; Eckmann, D. M.; Composto, R. J., A facile route to synthesize nanogels doped with silver nanoparticles. *J Nanopart Res* **2012,** *15*, 1323-1323.

217. Chen, Y.; Zheng, X.; Wang, X.; Wang, C.; Ding, Y.; Jiang, X., Near-Infrared Emitting Gold Cluster–Poly(acrylic acid) Hybrid Nanogels. *ACS Macro Letters* **2014,** *3* (1), 74-76.

218. Sankar, R. M.; Meera, K. M. S.; Samanta, D.; Murali, A.; Jithendra, P.; Baran Mandal, A.; Jaisankar, S. N., The reinforced hydrogel for drug loading: immobilization of single-walled carbon nanotubes in cross-linked polymers via multiple interactions. *RSC Adv.,* **2012,** *2* (32), 12424-12430.

219. Sankar, R. M.; Seeni Meera, K. M.; Samanta, D.; Jithendra, P.; Mandal, A. B.; Jaisankar, S. N., The pH-sensitive polyampholyte nanogels: Inclusion of carbon nanotubes for improved drug loading. *Colloids Surf., B* **2013,** *112*, 120-127.

220. Wu, H.-Q.; Wang, C.-C., Biodegradable Smart Nanogels: A New Platform for Targeting Drug Delivery and Biomedical Diagnostics. *Langmuir* **2016,** *32* (25), 6211-6225.

221. Zhang, Y.; Zhang, J.; Xing, C.; Zhang, M.; Wang, L.; Zhao, H., Protein Nanogels with Temperature-Induced Reversible Structures and Redox Responsiveness. *ACS Biomater. Sci. Eng.* **2016,** *2* (12), 2266-2275.

222. Simpson, M. J.; Corbett, B.; Arezina, A.; Hoare, T., Narrowly Dispersed, Degradable, and Scalable Poly(oligoethylene glycol methacrylate)-Based Nanogels via Thermal Self-Assembly. *Ind. Eng. Chem. Res.* **2018,** *57* (22), 7495-7506.

223. Cinay, G. E.; Erkoc, P.; Alipour, M.; Hashimoto, Y.; Sasaki, Y.; Akiyoshi, K.; Kizilel, S., Nanogel-Integrated pH-Responsive Composite Hydrogels for Controlled Drug Delivery. *ACS Biomater. Sci. Eng.* **2017,** *3* (3), 370-380.

224. Morimoto, N.; Hirano, S.; Takahashi, H.; Loethen, S.; Thompson, D. H.; Akiyoshi, K., Self-Assembled pH-Sensitive Cholesteryl Pullulan Nanogel As a Protein Delivery Vehicle. *Biomacromolecules* **2013,** *14* (1), 56-63.

225. Abd El-Rehim, H. A.; Swilem, A. E.; Klingner, A.; Hegazy, E.-S. A.; Hamed, A. A., Developing the Potential Ophthalmic Applications of Pilocarpine Entrapped Into Polyvinylpyrrolidone–Poly(acrylic acid) Nanogel Dispersions Prepared By γ Radiation. *Biomacromolecules* **2013,** *14* (3), 688-698.

226. Gong, J. P., Why are double network hydrogels so tough? *Soft Matter* **2010,** *6* (12), 2583-2590.

227. Gu, Z.; Chen, L.; Xu, Y.; Liu, Y.; Zhao, Z.; Zhao, C.; Lei, W.; Rong, Q.; Fang, R.; Zhao, T.; Liu, M., General Strategy to Fabricate Highly Filled Microcomposite Hydrogels with High Mechanical Strength and Stiffness. *ACS Appl. Mater. Interfaces* **2018,** *10* (4), 4161-4167.

228. Okay, O.; Oppermann, W., Polyacrylamide−Clay Nanocomposite Hydrogels: Rheological and Light Scattering Characterization. *Macromolecules* **2007,** *40* (9), 3378-3387.

229. Teng, C.; Qiao, J.; Wang, J.; Jiang, L.; Zhu, Y., Hierarchical Layered Heterogeneous Graphene-poly (N-isopropylacrylamide)-clay Hydrogels with Superior Modulus, Strength, and Toughness. *ACS nano* **2015,** *10* (1), 413-420.

230. Voorhaar, L.; Hoogenboom, R., Supramolecular polymer networks: hydrogels and bulk materials. *Chem. Soc. Rev.,* **2016,** *45* (14), 4013-4031.

231. Naficy, S.; Brown, H. R.; Razal, J. M.; Spinks, G. M.; Whitten, P. G., Progress Toward Robust Polymer Hydrogels. *Aust. J. Chem* **2011,** *64* (8), 1007-1025.

232. Teng, C.; Qiao, J.; Wang, J.; Jiang, L.; Zhu, Y., Hierarchical Layered Heterogeneous Graphene-poly(N-isopropylacrylamide)-clay Hydrogels with Superior Modulus, Strength, and Toughness. *ACS Nano* **2016,** *10* (1), 413-420.

233. Sun, L.; Fugetsu, B., Graphene oxide captured for green use: Influence on the structures of calcium alginate and macroporous alginic beads and their application to aqueous removal of acridine orange. *Chem. Eng. J.* **2014,** *240*, 565-573.

234. Carpio, I. E. M.; Mangadlao, J. D.; Nguyen, H. N.; Advincula, R. C.; Rodrigues, D. F., Graphene oxide functionalized with ethylenediamine triacetic acid for heavy metal adsorption and anti-microbial applications. *Carbon* **2014,** *77*, 289-301.

235. Young, R. J.; Kinloch, I. A., Graphene and graphene-based nanocomposites. *Nanoscience: Nanostructures Through Chemistry* **2012,** *1*, 145.

236. Ryu, J.; Lim, J. S.; Ahn, S.; Jo, S. M.; Ko, F. K.; Lee, J. H.; Hwang, J. Y., Structure and properties of graphene oxide/cellulose hybrid fibers via divalent metal ions treatment. *Cellulose* **2018,** *25* (1), 517-525.

237. Khazaei, M.; Nasseri, S.; Ganjali, M. R.; Khoobi, M.; Nabizadeh, R.; Mahvi, A. H.; Nazmara, S.; Gholibegloo, E., Response surface modeling of lead () removal by graphene oxide-Fe3O4 nanocomposite using central composite design. *J Environ Health Sci Eng* **2016,** *14*, 2.

238. Algothmi, W. M.; Bandaru, N. M.; Yu, Y.; Shapter, J. G.; Ellis, A. V., Alginate–graphene oxide hybrid gel beads: An efficient copper adsorbent material. *J. Colloid Interface Sci.* **2013,** *397*, 32-38.

239. Berezkin, A. V.; Kudryavtsev, Y. V., Effect of Cross-Linking on the Structure and Growth of Polymer Films Prepared by Interfacial Polymerization. *Langmuir* **2015,** *31* (44), 12279-12290.

240. Boon, N.; Schurtenberger, P., Swelling of micro-hydrogels with a crosslinker gradient. *Phys. Chem. Chem. Phys.* **2017,** *19* (35), 23740-23746.

241. Sanson, N.; Rieger, J., Synthesis of nanogels/microgels by conventional and controlled radical crosslinking copolymerization. *Polymer Chemistry* **2010,** *1* (7), 965-977.

242. Kimmins, S. D.; Wyman, P.; Cameron, N. R., Amine-functionalization of glycidyl methacrylate-containing emulsion-templated porous polymers and immobilization of proteinase K for biocatalysis. *Polymer* **2014,** *55* (1), 416-425.

243. Parker, R. E.; Isaacs, N. S., Mechanisms Of Epoxide Reactions. *Chem. Rev.,* **1959,** *59* (4), 737-799.

244. Madadrang, C. J.; Kim, H. Y.; Gao, G.; Wang, N.; Zhu, J.; Feng, H.; Gorring, M.; Kasner, M. L.; Hou, S., Adsorption Behavior of EDTA-Graphene Oxide for Pb (II) Removal. *ACS Appl. Mater. Interfaces* **2012,** *4* (3), 1186-1193.

245. Ramesha, G. K.; Sampath, S., Electrochemical Reduction of Oriented Graphene Oxide Films: An in Situ Raman Spectroelectrochemical Study. *J. Phys. Chem. C* **2009,** *113* (19), 7985-7989.

246. Gómez-Navarro, C.; Weitz, R. T.; Bittner, A. M.; Scolari, M.; Mews, A.; Burghard, M.; Kern, K., Electronic Transport Properties of Individual Chemically Reduced Graphene Oxide Sheets. *Nano Lett.,* **2007,** *7* (11), 3499-3503.

247. Low, F. W.; Lai, C. W.; Abd Hamid, S. B., Easy preparation of ultrathin reduced graphene oxide sheets at a high stirring speed. *Ceram. Int.* **2015,** *41* (4), 5798-5806.

248. Sun, L.; Fugetsu, B., Mass production of graphene oxide from expanded graphite. *Mater. Lett.* **2013,** *109*, 207-210.

249. Kudin, K. N.; Ozbas, B.; Schniepp, H. C.; Prud'homme, R. K.; Aksay, I. A.; Car, R., Raman Spectra of Graphite Oxide and Functionalized Graphene Sheets. *Nano Lett.,* **2008,** *8* (1), 36-41.

250. Cao, J.; He, P.; Mohammed, M. A.; Zhao, X.; Young, R. J.; Derby, B.; Kinloch, I. A.; Dryfe, R. A. W., Two-Step Electrochemical Intercalation and Oxidation of Graphite for the Mass Production of Graphene Oxide. *J. Am. Chem. Soc.,* **2017,** *139* (48), 17446-17456.

251. Liu, Y.-T.; Yang, J.-M.; Xie, X.-M.; Ye, X.-Y., Polystyrene-grafted graphene with improved solubility in organic solvents and its compatibility with polymers. *Mater. Chem. Phys.* **2011,** *130* (1–2), 794-799.

252. Rattana; Chaiyakun, S.; Witit-anun, N.; Nuntawong, N.; Chindaudom, P.; Oaew, S.; Kedkeaw, C.; Limsuwan, P., Preparation and characterization of graphene oxide nanosheets. *Procedia Eng.* **2012,** *32*, 759-764.

253. Ferrari, A. C.; Robertson, J., Interpretation of Raman spectra of disordered and amorphous carbon. *Phys. Rev. B* **2000,** *61* (20), 14095-14107.

254. Lee, K. Y.; Rowley, J. A.; Eiselt, P.; Moy, E. M.; Bouhadir, K. H.; Mooney, D. J., Controlling Mechanical and Swelling Properties of Alginate Hydrogels Independently by Cross-Linker Type and Cross-Linking Density. *Macromolecules* **2000,** *33* (11), 4291-4294.

255. Church, R. B.; Hu, K.; Magnacca, G.; Cerruti, M., Intercalated Species in Multilayer Graphene Oxide: Insights Gained from In Situ FTIR Spectroscopy with Probe Molecule Delivery. *J. Phys. Chem. C* **2016,** *120* (40), 23207-23211.

256. Acik, M.; Mattevi, C.; Gong, C.; Lee, G.; Cho, K.; Chhowalla, M.; Chabal, Y. J., The Role of Intercalated Water in Multilayered Graphene Oxide. *ACS Nano* **2010,** *4* (10), 5861-5868.

257. Hu, H.; Wang, X.; Wang, J.; Wan, L.; Liu, F.; Zheng, H.; Chen, R.; Xu, C., Preparation and properties of graphene nanosheets–polystyrene nanocomposites via in situ emulsion polymerization. *Chem. Phys. Lett.* **2010,** *484* (4), 247-253.

258. Fan, J.; Shi, Z.; Lian, M.; Li, H.; Yin, J., Mechanically strong graphene oxide/sodium alginate/polyacrylamide nanocomposite hydrogel with improved dye adsorption capacity. *J. Mater. Chem. A* **2013,** *1* (25), 7433-7443.

259. Wei, X.; Mao, L.; Soler-Crespo, R. A.; Paci, J. T.; Huang, J.; Nguyen, S. T.; Espinosa, H. D., Plasticity and ductility in graphene oxide through a mechanochemically induced damage tolerance mechanism. *Nat. Commun.* **2015,** *6*, 8029.

260. Moghimi, A.; Abdouss, M.; Ghooshchi, G., Preconcentration of Pb (II) by Graphene Oxide with Covalently Linked Porphyrin Adsorbed on Surfactant Coated C 18 before Determination by FAAS. *Int. J. Bio-Inorg. Hybd. Nanomat* **2013,** *2* (2), 355-364.

261. Xie, S.; Zhao, J.; Zhang, B.; Wang, Z.; Ma, H.; Yu, C.; Yu, M.; Li, L.; Li, J., Graphene Oxide Transparent Hybrid Film and Its Ultraviolet Shielding Property. *ACS Appl. Mater. Interfaces.* **2015,** *7* (32), 17558-17564.

262. Gardner, K. L.; Tait, J. G.; Merckx, T.; Qiu, W.; Paetzold, U. W.; Kootstra, L.; Jaysankar, M.; Gehlhaar, R.; Cheyns, D.; Heremans, P.; Poortmans, J., Nonhazardous Solvent Systems for Processing Perovskite Photovoltaics. *Adv. Energy Mater.* **2016,** *6* (14), 1600386.

263. Atanase, L.; Riess, G., Self-Assembly of Block and Graft Copolymers in Organic Solvents: An Overview of Recent Advances. *Polymers* **2018,** *10* (1), 62.

264. Chen, M.; Mokhtar, M. Z.; Whittaker, E.; Lian, Q.; Hamilton, B.; O'Brien, P.; Zhu, M.; Cui, Z.; Haque, S. A.; Saunders, B. R., Reducing hole transporter use and increasing perovskite solar cell stability with dual-role polystyrene microgel particles. *Nanoscale* **2017,** *9* (28), 10126-10137.

265. Dokkhan, C.; Mokhtar, M. Z.; Chen, Q.; Saunders, B. R.; Hodson, N. W.; Hamilton, B., Using microgels to control the morphology and optoelectronic properties of hybrid organic–inorganic perovskite films. *Phys. Chem. Chem. Phys.* **2018,** *20* (44), 27959-27969.

266. Wu, C.; Li, H.; Yan, Y.; Chi, B.; Felice, K. M.; Moore, R. B.; Magill, B. A.; Mudiyanselage, R. R. H. H.; Khodaparast, G. A.; Sanghadasa, M.; Priya, S., Highly-Stable Organo-Lead Halide Perovskites Synthesized Through Green Self-Assembly Process. *Solar RRL* **2018,** *2* (6), 1800052.

267. Chang, C.-Y.; Chu, C.-Y.; Huang, Y.-C.; Huang, C.-W.; Chang, S.-Y.; Chen, C.-A.; Chao, C.-Y.; Su, W.-F., Tuning Perovskite Morphology by Polymer Additive for High Efficiency Solar Cell. *ACS Appl. Mater. Interfaces,* **2015,** *7* (8), 4955-4961.

268. Sun, C.; Guo, Y.; Fang, B.; Yang, J.; Qin, B.; Duan, H.; Chen, Y.; Li, H.; Liu, H., Enhanced Photovoltaic Performance of Perovskite Solar Cells Using Polymer P(VDF-TrFE) as a Processed Additive. *J. Phys. Chem. C,* **2016,** *120* (24), 12980-12988.

269. Luo, J.; Qiu, R. Z.; Yang, Z. S.; Wang, Y. X.; Zhang, Q. F., Mechanism and effect of γ-butyrolactone solvent vapor post-annealing on the performance of a mesoporous perovskite solar cell. *RSC Adv.* **2018,** *8* (2), 724-731.

270. Wang, M.; Ma, Y.; Sun, Y.; Hong, S. Y.; Lee, S. K.; Yoon, B.; Chen, L.; Ci, L.; Nam, J.-D.; Chen, X.; Suhr, J., Hierarchical Porous Chitosan Sponges as Robust and Recyclable Adsorbents for Anionic Dye Adsorption. *Sci. Rep.* **2017,** *7* (1), 18054.

271. Moradi, A.; Najafi Moghadam, P.; Hasanzadeh, R.; Sillanpaa, M., Chelating magnetic nanocomposite for the rapid removal of Pb(ii) ions from aqueous solutions: characterization, kinetic, isotherm and thermodynamic studies. *RSC Adv.* **2017,** *7* (1), 433-448.

272. Javed, R.; Shah, L. A.; Sayed, M.; Khan, M. S., Uptake of heavy metal ions from aqueous media by hydrogels and their conversion to nanoparticles for generation of a catalyst system: two-fold application study. *RSC Adv.* **2018,** *8* (27), 14787-14797.

273. Ahluwalia, S. S.; Goyal, D., Removal of Heavy Metals by Waste Tea Leaves from Aqueous Solution. *Eng. Life Sci.* **2005,** *5* (2), 158-162.

274. Astrini, N.; Anah, L.; Haryadi, H. R., Adsorption of Heavy Metal Ion from Aqueous Solution by Using Cellulose Based Hydrogel Composite. *Macromol. Symp.* **2015,** *353* (1), 191-197.

275. De Gisi, S.; Lofrano, G.; Grassi, M.; Notarnicola, M., Characteristics and adsorption capacities of low-cost sorbents for wastewater treatment: A review. *Sustainable Mater. Technol.* **2016,** *9*, 10-40.

276. Shao, C.; Chang, H.; Wang, M.; Xu, F.; Yang, J., High-Strength, Tough, and Self-Healing Nanocomposite Physical Hydrogels Based on the Synergistic Effects of Dynamic Hydrogen Bond and Dual Coordination Bonds. *ACS Applied Materials & Interfaces* **2017,** *9* (34), 28305-28318.

277. Morris, G. E.; Vincent, B.; Snowden, M. J., Adsorption of Lead Ions ontoN-Isopropylacrylamide and Acrylic Acid Copolymer Microgels. *Adv. Colloid Interface Sci.* **1997,** *190* (1), 198-205.

278. Dai, H.; Wang, N.; Wang, D.; Ma, H.; Lin, M., An electrochemical sensor based on phytic acid functionalized polypyrrole/graphene oxide nanocomposites for simultaneous determination of Cd (II) and Pb (II). *Chem. Eng. J.* **2016,** *299*, 150-155.

279. Kaşgöz, H.; Durmuş, A.; Kaşgöz, A., Enhanced swelling and adsorption properties of AAm-AMPSNa/clay hydrogel nanocomposites for heavy metal ion removal. *Polym. Adv. Technol.* **2008,** *19* (3), 213-220.

280. Hajdu, I.; Bodnár, M.; Csikós, Z.; Wei, S.; Daróczi, L.; Kovács, B.; Győri, Z.; Tamás, J.; Borbély, J., Combined nano-membrane technology for removal of lead ions. *J. Membr. Sci.* **2012,** *409–410*, 44-53.

281. Barakat, M. A., New trends in removing heavy metals from industrial wastewater. *Arabian Journal of Chemistry* **2011,** *4* (4), 361-377.

282. Nakajima, T., Generalization of the sacrificial bond principle for gel and elastomer toughening. *Polym. J. (Tokyo, Jpn.)* **2017,** *49*, 477.

283. Zhang, Y.; Hu, C.; Xiang, X.; Diao, Y.; Li, B.; Shi, L.; Ran, R., Self-healable, tough and highly stretchable hydrophobic association/ionic dual physically cross-linked hydrogels. *RSC Adv.*. **2017,** *7* (20), 12063-12073.

284. Li, X.; Yang, Q.; Zhao, Y.; Long, S.; Zheng, J., Dual physically crosslinked double network hydrogels with high toughness and self-healing properties. *Soft Matter* **2017,** *13* (5), 911-920.

285. Cheng, C.; Deng, J.; Lei, B.; He, A.; Zhang, X.; Ma, L.; Li, S.; Zhao, C., Toward 3D graphene oxide gels based adsorbents for high-efficient water treatment via the promotion of biopolymers. *J. Hazard. Mater.* **2013,** *263*, 467-478.

286. Repo, E.; Warchol, J. K.; Kurniawan, T. A.; Sillanpää, M. E. T., Adsorption of Co(II) and Ni(II) by EDTA- and/or DTPA-modified chitosan: Kinetic and equilibrium modeling. *Chem. Eng. J.* **2010,** *161* (1), 73-82.

287. Peng, W.; Li, H.; Liu, Y.; Song, S., A review on heavy metal ions adsorption from water by graphene oxide and its composites. *J. Mol. Liq.* **2017,** *230*, 496-504.

288. Wan, S.; He, F.; Wu, J.; Wan, W.; Gu, Y.; Gao, B., Rapid and highly selective removal of lead from water using graphene oxide-hydrated manganese oxide nanocomposites. *J. Hazard. Mater.* **2016,** *314*, 32-40.

289. Medina, R. P.; Nadres, E. T.; Ballesteros, F. C.; Rodrigues, D. F., Incorporation of graphene oxide into a chitosan–poly(acrylic acid) porous polymer nanocomposite for enhanced lead adsorption. *Environ. Sci.: Nano* **2016,** *3* (3), 638-646.

290. Mohammadinezhad, A.; Marandi, G. B.; Farsadrooh, M.; Javadian, H., Synthesis of poly(acrylamide-co-itaconic acid)/MWCNTs superabsorbent hydrogel nanocomposite by ultrasound-assisted technique: Swelling behavior and Pb (II) adsorption capacity. *Ultrason. Sonochem.* **2018,** *49*, 1-12.

291. Pal, A.; Majumder, K.; Sengupta, S.; Das, T.; Bandyopadhyay, A., Adsorption of soluble Pb(II) by a photocrosslinked polysaccharide hybrid: A swelling-adsorption correlation study. *Carbohydr. Polym.* **2017,** *177*, 144-155.

292. Katime, I.; Rodríguez, E., ABSORPTION OF METAL IONS AND SWELLING PROPERTIES OF POLY(ACRYLIC ACID-CO-ITACONIC ACID) HYDROGELS. *J. Macromol. Sci., Part A: Pure Appl.Chem.* **2001,** *38* (5-6), 543-558.

293. Wang, J.; Liu, F.; Wei, J., Enhanced adsorption properties of interpenetrating polymer network hydrogels for heavy metal ion removal. *Polym. Bull.* **2011,** *67* (8), 1709.

294. Gupta, N. V.; Shivakumar, H. G., Investigation of Swelling Behavior and Mechanical Properties of a pH-Sensitive Superporous Hydrogel Composite. *Iran J Pharm Res.* **2012,** *11* (2), 481-493.

295. Cheng, C. S.; Deng, J.; Lei, B.; He, A.; Zhang, X.; Ma, L.; Li, S.; Zhao, C., Toward 3D graphene oxide gels based adsorbents for high-efficient water treatment via the promotion of biopolymers. *Journal of hazardous materials* **2013,** *263 Pt 2*, 467-478.

296. Liu, P.; Jiang, L.; Zhu, L.; Wang, A., Novel Covalently Cross-Linked Attapulgite/Poly(acrylic acid-co-acrylamide) Hybrid Hydrogels by Inverse Suspension Polymerization: Synthesis Optimization and Evaluation as Adsorbents for Toxic Heavy Metals. *Ind. Eng. Chem. Res.* **2014,** *53* (11), 4277-4285.

297. Mayumi, K.; Marcellan, A.; Ducouret, G.; Creton, C.; Narita, T., Stress–Strain Relationship of Highly Stretchable Dual Cross-Link Gels: Separability of Strain and Time Effect. *ACS Macro Lett.* **2013,** *2* (12), 1065-1068.

298. Park, S.-J.; Lim, H.-S.; Lee, Y. M.; Suh, K.-D., Facile synthesis of monodisperse poly(MAA/EGDMA)/Fe3O4 hydrogel microspheres with hollow structures for drug delivery systems: the hollow structure formation mechanism and effects of various metal ions on structural changes. *RSC Adv.,* **2015,** *5* (13), 10081-10088.

299. Yuan, L.; Zhi, W.; Xie, Q.; Chen, X.; Liu, Y., Lead removal from solution by a porous ceramisite made from bentonite, metallic iron, and activated carbon. *Environ. Sci.: Water Res. Technol.,* **2015,** *1* (6), 814-822.

300. Liang, X.; Xu, Y.; Sun, G.; Wang, L.; Sun, Y.; Qin, X., Preparation, characterization of thiol-functionalized silica and application for sorption of Pb2+ and Cd2+. *Colloids Surf., A* **2009,** *349* (1), 61-68.

301. Gao, H.; Sun, Y.; Zhou, J.; Xu, R.; Duan, H., Mussel-Inspired Synthesis of Polydopamine-Functionalized Graphene Hydrogel as Reusable Adsorbents for Water Purification. *ACS Appl. Mater. Interfaces.,* **2013,** *5* (2), 425-432.